FEB 12 2004

REPORT DOCUMENTATION PAGE	Form Approved OMB No. 0704-0188

1. AGENCY USE ONLY *(Leave blank)*	2. REPORT DATE	3. REPORT TYPE AND DATES COVERED
	11.Feb.04	DISSERTATION

4. TITLE AND SUBTITLE
"THE APPLICATION OF SECULAR PERTURBATION THEORY TO EXPLAIN WARPING IN THE CIRCUMSTELLAR DISK BETA PICTORIS"

5. FUNDING NUMBERS

6. AUTHOR(S)
MAJ NOVOTNY STEVEN J JR

7. PERFORMING ORGANIZATION NAME(S) AND ADDRESS(ES)
UNIVERSITY OF FLORIDA

8. PERFORMING ORGANIZATION REPORT NUMBER
CI04-102

9. SPONSORING/MONITORING AGENCY NAME(S) AND ADDRESS(ES)
THE DEPARTMENT OF THE AIR FORCE
AFIT/CIA, BLDG 125
2950 P STREET
WPAFB OH 45433

10. SPONSORING/MONITORING AGENCY REPORT NUMBER

11. SUPPLEMENTARY NOTES

12a. DISTRIBUTION AVAILABILITY STATEMENT
Unlimited distribution
In Accordance With AFI 35-205/AFIT Sup 1

DISTRIBUTION STATEMENT A
Approved for Public Release
Distribution Unlimited

12b. DISTRIBUTION CODE

13. ABSTRACT *(Maximum 200 words)*

20040219 092

14. SUBJECT TERMS

15. NUMBER OF PAGES
150

16. PRICE CODE

17. SECURITY CLASSIFICATION OF REPORT	18. SECURITY CLASSIFICATION OF THIS PAGE	19. SECURITY CLASSIFICATION OF ABSTRACT	20. LIMITATION OF ABSTRACT

THE APPLICATION OF SECULAR PERTURBATION THEORY TO EXPLAIN WARPING IN THE CIRCUMSTELLAR DISK OF BETA PICTORIS

By

STEVEN J. NOVOTNY

A DISSERTATION PRESENTED TO THE GRADUATE SCHOOL
OF THE UNIVERSITY OF FLORIDA IN PARTIAL FULFILLMENT
OF THE REQUIREMENTS FOR THE DEGREE OF
DOCTOR OF PHILOSOPHY

UNIVERSITY OF FLORIDA

2003

The views expressed in this article are those of the author and do not reflect the official policy or position of the United States Air Force, Department of Defense, or the U.S. Government

ACKNOWLEDGMENTS

I would never have been able to accomplish what I have if it had not been for my advisor, Dr. Stanley Dermott, and Dr. Charles Telesco. They presented a great opportunity and placed me in a wonderful position to succeed. It was a privilege to work with two scholars who have contributed so much to their respective fields.

Most importantly I thank God for continuing to shower me with opportunities and blessings for which I am undeserving. I am humbly aware of how every opportunity I have had has been given through His grace.

TABLE OF CONTENTS

LIST OF TABLES

Abstract of Dissertation Presented to the Graduate School
of the University of Florida in Partial Fulfillment of the
Requirements for the Degree of Doctor of Philosophy

THE APPLICATION OF SECULAR PERTURBATION THEORY TO EXPLAIN WARPING IN THE CIRCUMSTELLAR DISK OF BETA PICTORIS

By

Steven J. Novotny

December 2003

Chair: Stanley F. Dermott
Major Department: Astronomy

This research is a numerical investigation into the dynamical influences of planets on the dust disks surrounding young main sequence stars. Motivating this research effort are the observations of the Beta Pictoris circumstellar disk made by the UF Department of Astronomy's mid-IR team. These IR images show with unprecedented clarity the features and asymmetries of the inner, $\leq$ 100 AU, portion of the Beta Pictoris disk; the most interesting of which is the dramatic warping of the disk's mid-plane. Analyses of prior observations have suggested that the features are attributed to the presence of a planet or a planetary system. Past dynamic analysis has focused primarily on the presence of a single planet and the resulting perturbations on the dust disk through hydrodynamic or N-body analysis. This research will show that the type of features observed in these images, specifically the warping of the disk, can also be explained with a system of two (or more) planets and secular perturbation theory while using more plausible assumptions than did other models.

CHAPTER 1
INTRODUCTION

1.1 Motivation

As of 18 December, 2002, the discoveries of 102 exosolar planets have been claimed (Schneider, 2002). These planets exist in 88 planetary systems, 11 of which are multiple planet systems. All have been detected through careful observations of dynamical effects with the vast majority detected through stellar radial velocity measurements (Perryman, 2002). Radial velocity measurements are made by observing the doppler shift in the radiated light from a star. The shifts in wavelength result from the gravitational perturbation of a planet on the star around which it orbits. Using indirect methods, such as observing the effect of a planet on its central star instead of the planet itself, is necessary as current technology has not yet allowed direct observation of an exosolar planet. Current direct detection methods with the necessary resolution and sensitivity are not yet in operation.

Several projects are underway to develop the capability to make direct detections of exosolar planets. The most significant of these projects include NASA's Space Interferometry Mission (SIM), the Terrestrial Planet Finder (TPF), and ESAs Infrared Space Interferometry Mission (IRSI). All of these systems will use interferometry to achieve the high angular resolution needed for planetary detection. Interferometry uses the interference of light associated with the observations from two or more different detectors. The goal of designing an interferometer is to have the greatest possible baseline (the distance between the component detectors) as the angular resolution achieved with the instrument is a function of the baseline distance. SIM is a space based optical interferometer with a ten meter baseline and is scheduled for launch in 2009. The final design for TPF will be decided in 2006 and the launch date is somewhere between 2012 and 2015. The IRSI is the most ambitious project and currently plans to utilize six different space telescopes providing an effective baseline of 60 meters and is expected to launch around 2014. Though these projects will provide

great capability, they are all still far from being operational. At this point, the observation of individual planets is still out of reach with current instruments, and thus the indirect methods such as radial velocity measurements and observing brightness variations are still required.

Recent observations of circumstellar disks have provided another possibility for planetary detection. One example is the disk surrounding the star HR4796A which was resolved in the mid-IR (Telesco et al., 2000). The nearly edge-on view of this disk showed a double lobed feature that exhibited a possible overall asymmetry in brightness between the two lobes (Wyatt et al., 1999). This asymmetry was interpreted as the disk being offset from the central star. As will be discussed later, the measurement of this asymmetry was used to make assertions about the possibility of the disk being influenced by the presence of a planet. Another example is Beta Pictoris – the most well studied of all circumstellar disks. Beta Pictoris is an approximately 20 Myr old main sequence star with a disk that is large ($\sim$ 1000 AU), bright, and viewed nearly edge-on. Even more interesting than the size and brightness of the Beta Pictoris disk are the large and small-scale asymmetries and features observed in the morphology of the disk – the most interesting being the warping of the inner disk.

The mid-plane warping of the disk is interesting as it is arguably the distinct signature of gravitational perturbations. Several models have been developed to explain the source of these perturbations. The most in-depth work has been based on the assumption of a close encounter with another star (Kalas et al., 2000), or the presence of a single planet on an orbit inclined to the plane of the disk (Augereau et al., 2001). These models do in fact account for warping in the model disks, but there are several unresolved issues. First, there is no observed star that meets the necessary criteria of proximity and proper motion to match the fly-by star. Second, there is no clear explanation as to why a single planet would be in an orbit with a significant inclination to the disk from which it formed. Current theories of planet formation assert that planets form from the disk material and therefore, without outside perturbations, should be nearly coplanar with the disk.

An alternative approach in investigating the source of the warping is based on a mechanism that explains the observed warping in the zodiacal cloud of our own solar system

– secular perturbations from the planets. Secular perturbations are long term effects that are the result of the combined gravitational perturbations of planets. Secular perturbations manifest themselves as a contribution to the osculating orbital elements of the individual dust particles that comprise the disk. More simply stated, this approach is based on the premise that the cumulative effects of gravitational perturbations, on long timescales, will play a significant role in determining the observed characteristics of a dust particle's orbital trajectory, and hence the morphology of the disk. In this research a second order expansion, in inclination and eccentricity, of the disturbing function is used to calculate these forced components. The theoretical framework for determining these values is provided and discussed in chapter 3.

To support the theory of secular perturbations being the dominant influence on the morphology of a disk, such as that of Beta Pictoris, it necessary to show that the conditions within the disk are conducive to this process. For this research, this is done by determining the timescales associated with each of the physical processes expected to be occurring in a disk with the attributes observed for Beta Pictoris. Some of the physical processes considered include the Poynting-Robertson drag, collisional destruction, and gas drag. These processes are dependent on characteristics of the star/disk system such as the star's luminosity, the particle density within the disk, and the gas content respectively. These effects and the associated analyses are explained further in chapter 2.

The following section provides brief examples of observed asymmetries in circumstellar disks and discusses how secular perturbation theory can be used to explain the observed features.

1.2 Observed Asymmetries in Circumstellar Disks

Indirect methods for determining the presence of a planetary system are still, by far, the most commonly used in the search for exosolar planets. However, when we are able to resolve the disk and characterize the details of the morphology, we have the rare opportunity to probe the dynamics of the material within the disk and the dynamical influences of a planet or planetary system. Two such examples are the disks surrounding the stars HR4796A and Beta Pictoris. These systems are well suited for the application of secular perturbation

theory as the disks surrounding theses stars have arguably existed long enough for secular effects to have influenced the entire disk.

When looking for dynamical influences on secular timescales, there are two key observable features: pericenter glow and mid-plane warping. As will be discussed next, pericenter glow is the result of a disk being offset from the star due to the eccentricity imposed upon the orbits of the disk's dust particles by a perturbing planet. Similarly, warping will be shown to be the result of an imposed inclination.

Essential for understanding secular perturbation theory is the idea that the observable, or osculating, orbital elements of a dust particle within a disk are a combination of forced and proper elements. The forced elements are associated with the gravitational perturbations from the planets and the proper elements are associated with the trajectory of the particles at the time they were created. This will be described in detail in chapter 3.

1.2.1 Pericenter Glow

The phenomenon of pericenter glow was investigated by Wyatt et al. (1999) in an effort to explain the brightness asymmetry in HR4796. This work was motivated by Telesco et al. (1999) who identified the $5.9 \pm 3.2\%$ brightness asymmetry in the double-lobed structure of the disk. This double-lobed structure was considered to be the result of viewing the disk nearly edge on – tilted approximately 13 degrees to the line of sight.

Wyatt et al. proposed that the secular perturbations of a single massive planet imposed a forced eccentricity upon the individual particle orbits, such that the overall disk's center of symmetry was offset from the central star. This offset resulted in one portion of the disk being closer to the star, and thus hotter and brighter. This difference resulted in the observed brightness asymmetry. Detailed modeling showed that a forced eccentricity as small as 0.02 could well account for the $\sim 5\%$ lobe brightness asymmetry.

Another important conclusion from the work of Wyatt et al. is that the observed dust particles are actually a tracer of the larger bodies. By modeling the dust particles as Mie spheres, it was determined that the particles responsible for the mid-IR flux typically have diameters of $2-3$ μm. However, these particles would be quickly removed from the system due to radiation pressure and therefore cannot be primordial. This implies a source for the

smaller particles, arguably large bodies whose dynamics are dominated by secular perturbations over radiation based forces.

1.2.2 Mid-plane Warping

The best example of a directly observed warp in a circumstellar disk is in that of Beta Pictoris. Since its initial IR imaging by Lagage and Pantin (1994), warping of the inner disk (< 100 AU) was apparent. One of the best characterizations of the mid-plane warping was accomplished by Heap et al. (2000) who imaged the disk with the Space Telescope Infrared Spectrograph (STIS) on the Hubble Space Telescope. Their observations indicated warping that extended out to $\sim$80 AU and reached a maximum amplitude of $\sim$1.5 AU. In addition to clearly showing the warping, they quantified the warp by illustrating how it could be well modeled as the superposition of two concentric disk-like components, one inclined to the other by ~ 3 degrees. As will be discussed later, several dynamical explanations were proposed to explain the two component model.

More recent imaging of Beta Pictoris (Weinberger et al. 2003, Wahhaj et al. 2003) indicated additional warping of the inner region of the disk (< 20 AU) which was not observed by Heap et al. Furthermore, the inner disk warping was opposite in direction to the large scale warping observed in the STIS images. As will be discussed later, this additional warping further complicates the models based on a single planet.

Within this work it will be argued that mid-plane warping is the result of a mechanism similar to that which causes pericenter glow. Whereas an imposed forced eccentricity causes the disk to be offset from the central star, an imposed forced inclination causes warping. This phenomenon has been observed and studied for the solar system's zodiacal cloud (Dermott et al., 2001). The general idea behind warping is that a system consisting of multiple planets will impose a forced inclination upon the orbits of dust particles in a way that is dependent on semi-major axis. Furthermore, the forced inclination defines the planes about which the perturbed particle orbits precess. Since the forced inclination defines the dust particles' mean orbital planes and since the forced inclination varies with semi-major axis, warping occurs. Determination of the forced orbital elements arising from planetary perturbations is accomplished through secular perturbation theory. The application of secular

perturbation theory to the mid-plane warping of circumstellar disks is discussed in detail in the following chapters.

1.3 Dissertation Overview

The remainder of this dissertation will discuss the physics associated with the study of the circumstellar environment and application of such models in interpreting the observed characteristics of a complex system such as the disk of Beta Pictoris. Chapter 2 reviews the current theories of circumstellar disk formation and the subsequent planet formation. Also provided within this chapter, is a review of the physical processes that affect the distribution of dust within the disk. Chapter 3 will discuss the theoretical framework for determining the long-term effects of gravity on dust particle trajectories. This is done through a review of secular perturbation theory using a second order expansion of the disturbing function in eccentricity and inclination. The resulting solution in terms of the classical orbital elements is presented. Chapter 4 explains the implications of these results with regard to the effects on disk morphology. Special emphasis is placed on the role that a forced inclination that varies with semi-major axis plays in determining the warping of a disk's mid-plane. Chapter 5 reviews the observational history of Beta Pictoris starting with the initial detection of the disk from the initial IRAS measurements of the spectral energy distribution to the most recent high resolution images of the disk made with the Hubble Space Telescope. Also discussed in this chapter are the theoretical models used to explain the unique features and asymmetries indicated in these observations.

The final three chapters, chapters 7, 8, and 9, present the application of the theoretical tools developed in previous chapters to address the specifics of observed features – not only in the prior observations, but in the most recent high resolution mid-IR images of Beta Pictoris. Also addressed are limitations to the models developed to simulate the observed dust disk. These issues include consideration of a massive disk and the possible effects associated with a non-spherical, or oblate, central star.

CHAPTER 2
THE CIRCUMSTELLAR ENVIRONMENT

2.1 Introduction

The circumstellar environment changes greatly over the lifetime of the star. In particular, the cloud of material surrounding stars, mostly gas and dust, undergoes great transformations in both composition and spatial distribution. Observational evidence suggests that as a normal result of the star formation process that all stars may possibly be born with a distribution of dust and gas in the form of a disk (Beckwith, 1999). However, over time the material is subjected to many influences that may result in the partial or complete destruction of a well structured, easily observable disk. One example of the many changes that occur is in the composition of the disk. When a protostar reaches the main sequence it is estimated that all but one percent of the mass of the disk is in hydrogen and helium gas. The remaining one percent is in the form of dust that is closely coupled with the gas. Over time, the gas is removed and the dust continues to evolve. The dust particles, depending on size, are generally destroyed; blown away by winds or radiation; or are accreted onto larger objects or the central star itself. Observational evidence suggests that most disks effectively disappear by about 10 Myr (Beckwith, 1999).

Many physical processes are involved in the transformation of composition and structure. This chapter first discusses how circumstellar disks are formed during the star formation process and then discusses the processes thought to play the greatest roles in determining the structure and content of disks.

2.2 Formation of Circumstellar Disks

The current paradigm of star formation (described by Shu, Adams, and Lizano 1987) describes a scenario in which stars form from the collapse of slowly rotating molecular cloud cores. The onset of the collapse is a result of a density perturbation within a cloud core.

Perturbations are generally thought to be the result of inhomogeneities within the cloud or the result of an outside disturbance. Recent evidence from analysis of meteorites suggests that the solar system was created when a cloud was perturbed by a nearby supernova (Yulsman 2003). The collapse of a core leads to a protostar and a flattened disk surrounded by an envelope of dust and gas. Theory predicts that the disk forms as a result of the initial rotation of the cloud core and the conservation of angular momentum during the collapse. The material in the envelope is generally removed from the system through an amalgam of processes. These clearing processes include accretion onto the star, stellar winds, radiation pressure, and accretion onto growing planetesimals. The planetesimals that are initially created by mutual collisions of dust grains eventually lead to the large planet sized bodies that populate a planetary system.

The following sections discuss in more detail the processes that lead to the formation of the disk and its structure; the formation of kilometer sized bodies from micron sized dust grains; and finally the formation of terrestrial and giant planets.

2.2.1 Formation and Structure of a Protoplanetary Disk

The star formation process begins in the dense regions of giant molecular clouds (GMCs). In our galaxy, GMCs exist throughout the galaxy but are primarily found in the spiral arms. They are cold clouds of primarily hydrogen gas that have masses $\sim 10^4\ M_\odot$ and are gravitationally bound (Blitz and Williams 1999). Within the GMCs are smaller, but still gravitationally bound, regions known as cores. It is from these cores that the individual stars are likely to form. These cores have typical masses of $\sim 10\ M_\odot$ and typical sizes of ~ 0.1 pc (Shu et al. 1999). They are generally supported through a combination of magnetic fields, turbulence, and gas pressure. When the mass of a core reaches a critical value, known as the Jean's mass, the core begins to contract and the star formation process begins. The Jean's mass is estimated by considering kinetic and potential energy. The magnetic fields, turbulence, and gas pressure also play a role in determining the critical value.

As the irregularly shaped core of dust and gas collapses and begins forming a dense central object, the system must account for the angular momentum associated with the

original rotating core. Some material is accreted onto the central protostar but other material retains enough of its original angular momentum to settle into stable orbits and create a thin protostellar disk. The disk is expected to form roughly 10^5 yrs after the beginning of the initial freefall collapse (Beckwith 1999).

A protoplanetary disk is an example of an accretion disk which is defined as a flattened disk composed of material that is spiraling down onto the surface of a central mass. Through the conservation of angular momentum, the material within an accretion disk is transported inward while the angular momentum is transferred outward. This transport occurs as a result of the viscous effects of the material within the disk (Kenyon 1999). As frictional forces cause heating of material due to differential rotation, some material moves due to net loss of kinetic energy. This motion also results in a decrease in angular momentum and this must be balanced by outward motion of other material to conserve total angular momentum within the disk.

The transport of material inward and angular momentum outward plays a key role in defining the structure and evolution of the protoplanetary disk. As mass is moved inward and accreted on to the star or possibly removed by outflows, the surface density spreads outward (Ruden 1999). This results in a dispersal of the disk material over time.

Since it is not possible to directly image most disks, the general structure of disks has been gleaned through analysis of the spectral energy distributions (SEDs) of star-disk systems. SEDs show the measured flux from a source as a function of wavelength. SEDs associated with a star surrounded by a disk show particular characteristics that clearly confirm both the presence and the details of the disk. The SED for a star is generally that of a black body at the effective temperature of the star. The SED for a star and a disk will show not only the black body curve for the star, but also an excess flux in the infrared region of the SED. This excess is associated with thermal emissions from the dust in the disk that is heated primarily by radiation from the central star.

As the star proceeds through its early evolutionary stages, the SEDs also evolve. In the early stages the SED is actually dominated by the original envelope of dust and gas. As the star evolves material is accreted, is blown out by radiation pressure, or settles into a circumstellar disk. As this occurs, the SED changes to one in which the black body curve

of the star can be seen but is modified by a superposition of black body curves associated with a range of dust particles at lower temperatures.

Mass estimates of disks are most commonly made through long wavelength measurements ($\lambda > 300\mu m$). Typical masses for disks determined from sub-mm observations are on the order of a few percent of a solar mass (Beckwith 1999). This fact is significant as it is considerably higher than the mass thought necessary to form all of the planets within our solar system.

2.2.2 Formation of Planetesimals

The initial protoplanetary disk is almost entirely (~99%) hydrogen and helium gas. However, as the protostar evolves, the gas is removed from the disk primarily by radiation pressure and stellar winds. During this time the dust grains, that make up the remaining ~1% of the disk, begin the process of growth to larger planetesimals.

While gas is still present within the disk, solid particles are affected by gas drag. The effects of gas drag are dependent on the size of the particles. The smaller particles, which are coupled to the gas, move at sub-Keplerian velocities while the larger particles, which are less affected by the gas drag force, continue to move at near Keplerian velocities but experience orbital decay (Ruden 1999). This results in a differential inward drift that increases the frequency of collisions between particles. Many of these particles stick together forming larger particles. This process marks the beginning of the growth to larger objects within the disk.

As particles grow through collisions induced by the inward drift they also begin settling into the mid-plane of the disk. Settling occurs because the mid-plane defines the minimum in the vertical gravitational potential. This is described through the vertical acceleration measured with respect to the disk, and is expressed as

$$g_z = \frac{z}{r}\frac{GM_\star}{r^2} = \Omega^2 z \tag{2.1}$$

where z measures the vertical distance from the mid-plane and Ω is the orbital frequency at a given radius from the star. The above expression implies that the smaller grains, with a longer orbital period due to the gas drag, will take the longest to settle (Ruden 1999).

This leads to a picture in which the larger particles will settle to the disk mid-plane first and begin the process of further growth as the mid-plane density increases. The process is enhanced as the particles get larger and present a larger collisional cross-sectional area. The final result of this process is a thin layer of large particles in the disk's mid-plane.

As the particles become larger, they become less affected by gas drag and eventually reach Keplerian orbits. This occurs when the objects have grown from small dust particles to bodies with diameters $\gtrsim$ 1 km, generally referred to as planetesimals. As the small particles continue to drift inward past the larger planetesimals, they are accreted on to these large bodies and are thought to be capable of producing objects on the scale of $\sim$ 100 km on timescales of $\lesssim 10^6$ years (Ruden 1999).

It is from this distribution of planetesimals scattered throughout the disk that planets begin to grow through the accretion process.

2.2.3 Formation of Planets

Planetesimals distributed through the mid-plane of a disk continue to experience collisions and create larger bodies. As the bodies become more massive the effective collisional cross section increases as gravitational effects begin to become important. This effect can be described by the gravitational focusing factor expressed as $1 + {v_e}^2/V^2$ where V is the relative collisional velocity. The term v_e is the mutual escape velocity and is expressed as

$$v_e = \sqrt{\frac{2G(m_1 + m_2)}{a_1 + a_2}} \tag{2.2}$$

where m_1 and m_2 are the masses of the two bodies and a_1 and a_2 are the radii. Through this gravitational focusing, bodies continue to grow and simultaneously increase their collisional cross section thus enabling them to accelerate their growth.

The idea of runaway growth has been considered as a mechanism which can increase the rate of growth for a protoplanet during the process of planet formation. Runaway growth is the result of an increase in the gravitational focusing factor which occurs because of the increase in mass. This occurs when the ratio of ${v_e}^2/V^2$ becomes very large, $\gg 1$.

This critical ratio is driven both by the size of the planetesimal and by the relative velocity V. The relative velocity is influenced primarily by gravitational scattering, damping due to gas drag, and energy transfer via dynamical friction (Ruden 1999). A planetesimal will continue to grow through this process until it has accumulated all material in what is called the accretion zone. The accretion zone is defined by the Hill sphere which is based on determining the equilibrium point where tidal effects from the star are balanced by the gravity of the planet. The radius of the Hill sphere is given as

$$r_H = r\left(\frac{m_p}{3M_\star}\right)^{\frac{1}{3}} \tag{2.3}$$

where r is the distance from the star, m_p is the mass of the planet, and $M_\star$ is the mass of the star. It is generally thought that the accretion zone is approximately four times the radius of the Hill sphere (Lissauer 1993).

If a reservoir of gas exists near the forming planet, the gas will be accreted. Accretion will occur provided a critical mass of the core is achieved. This critical mass is determined by finding the mass at which gravity precludes hydrostatic equilibrium. This critical mass is generally thought to be $\gtrsim$10-15$M_\oplus$ (Ruden 1999). The accretion of gas onto these rocky, critical mass cores is the process that is thought to lead to the formation of the gas giants.

Other process also occur during the planet formation process that contribute to the structure of the planetary system. These include tidal interactions between the disk and the planets that lead to both gap formation and planetary migration. This will be discussed later in chapters 4 and 8.

2.3 Physical Processes Within a Circumstellar Disk

The primary physical processes which occur within a circumstellar disk that influence the dynamics of the constituent particles are associated with gravitational perturbations, radiation, interaction with gas, and collisions. With each of these processes is an associated time scale that is based on environmental conditions influencing the particular process. An analysis of the timescales is important for two reasons. First, for processes that occur on long time scales, it is necessary to verify that the system has had enough time to fully evolve under the influences of that particular process. Second, the timescales need to be

compared to one another in order to see which process will dominate over others within the disk. In general, the processes that occur on the shortest timescales will have the greatest effect on the disk. For example, if a certain sized particle is quickly destroyed by collisions, such as the case for micron sized particles in Beta Pictoris, the dust particles do not have time to spiral into the star. This implies that the collisional processes will dominate and play a significant role in influencing the distribution of these particular particles.

This section will give a brief description of each of the important processes that occur within a circumstellar disk and discuss their corresponding timescales.

2.3.1 Gravity

The dominant influence in the circumstellar environment is that of gravity associated with the central star. Gravitational perturbations may also come from other planets within the system. These perturbations resulting from the secondary masses are what drive the secular effects and will be discussed in detail in the next section. The timescale associated with the influences of the central star is simply the Keplerian period. This is determined from Kepler's third law that states the square of the orbital period is proportional to the semi-major axis cubed. This law is generally expressed as

$$T^2 = \frac{4\pi}{\mu} a^3 \tag{2.4}$$

where $\mu = G(m_1 + m_2)$. This can also be expressed as a mean rate in terms of solar system parameters, i.e. AUs and years,

$$n = \frac{2\pi}{T} = 2\pi\sqrt{\frac{m_c + m}{a^3}} \tag{2.5}$$

where m_c and m are in units of solar masses, a is in AU, and n is in units of radians per year. This can also be expressed as a characteristic timescale

$$t_{per} = \sqrt{a^3/(m_c + m)} \tag{2.6}$$

where a is again in AUs and m_c and m are in units of solar masses.

These values of frequency and time provide a standard of measure used in evaluating the frequency and timescales of the other processes described below.

2.3.2 Radiative Forces

All particles within a circumstellar disk interact with radiation from the central star. The magnitude of the radiation effects is based on the characteristic cross sectional area of a particle and its mass. For larger particles, gravity dominates over the radiative forces. However, for smaller particles the ratio of radiative forces to gravitational forces approaches or exceeds unity. This ratio can be expressed with the dimensionless quantity β (see for example Gustafson 1994 and references within). The value of β can be expressed as

$$\begin{aligned} \beta(D) &= \frac{F_{rad}}{F_{grav}} = \frac{(S_0/r^2)(Q_{pr}/c)(\sigma/m)}{GM/r^2} \\ &= C_r \left(\frac{L_*}{L_\odot}\right)\left(\frac{M_\odot}{M_*}\right)\left(\frac{\sigma}{m}\right) Q_{PR} \end{aligned} \tag{2.7}$$

where S_0 is the stellar flux density and c is the speed of light. Parameterizing β in terms of solar values uses the constant $C_r = 7.6 \times 10^5\ g\ cm^2$ and defines σ/m as the cross-sectional-area-to-mass ratio for a particle of diameter D and density ρ. The quantity Q_{PR} is the radiation pressure efficiency and is related to the absorption and scattering efficiencies; $Q_{PR} = Q_{abs} + Q_{sca}$. For dust particles assumed to be homogeneous spheres, Q_{PR} is usually calculated from Mie theory (Gustafson 1994). Sample calculations of β as a function of particle diameter are shown in figure 2–1. The optical properties and densities are those of the particles considered to most likely be representative of the dust surrounding Beta Pictoris. This will be discussed further in chapter 7.

Radiation is directed radially away from the star and therefore radiation acts to counter the effect of gravity. This force effectively reduces the mass of the star from the perspective of the dust particle. Equation 2.7 shows that β is dependent on the size of the particle through the σ/m term. This implies an inverse relationship between β and the particle diameter, i.e. $\beta \propto 1/D$. Since β is size dependent, particles of different diameter D, will see a different potential. This means that particles with the same initial conditions of position and velocity, but with different diameters, will move on different orbits.

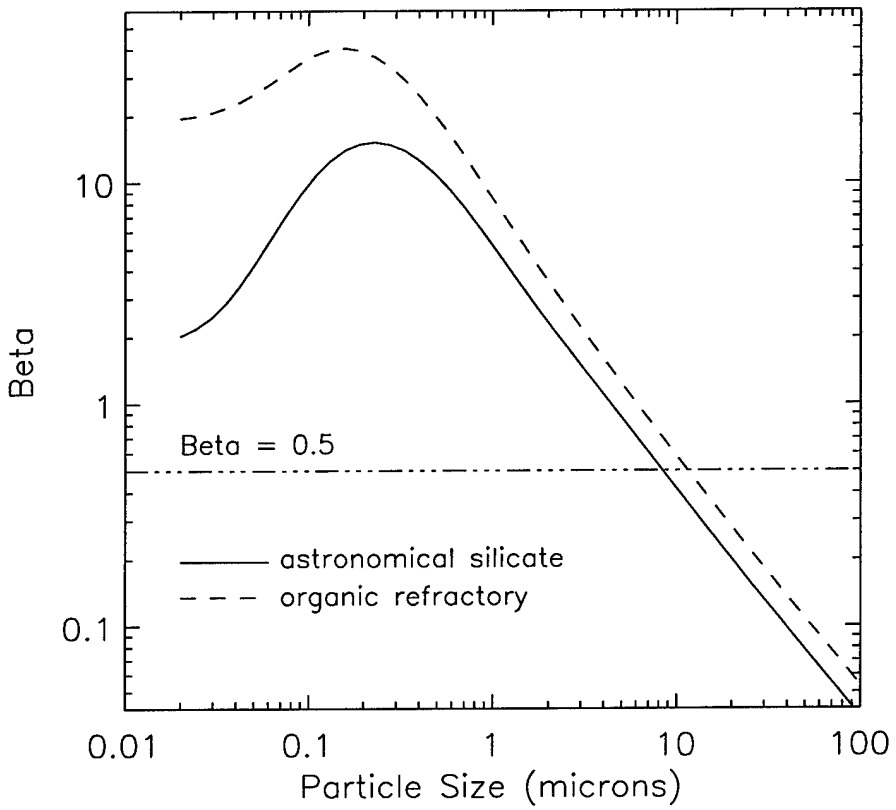

Figure 2–1: The parameter Beta in Beta Pictoris ($M = 1.8M_{\odot}$; $L = 8.7L_{\odot}$) as a function of particle size, calculated using values for Q_{PR} determined from Mie theory. Two different classes of materials are shown: materials described as astronomical silicates (Laor and Draine, 1993) and organic refractory material Li and Greenberg (1997). For this research, these materials are the primary candidates for simulating the dust within Beta Pictoris.

Particles can thus be grouped into different subcategories based on their β value. Large particles have a β value that approaches zero and therefore are relatively unaffected by radiation pressure. The smallest particles, the β meteoroids, have the largest β values, greater than 0.5, and are quickly expelled from the system on hyperbolic orbits. Particles that have intermediate values, $0.0 < \beta < 0.5$, exist on bound but eccentric orbits and are referred to as α meteoroids.

Particles feel another effect of radiation resulting from the component of the radiation force tangential to the particles orbit. This force acts as a dynamic drag force and is referred to as Poynting-Robertson (PR) drag. PR drag acts to decrease both the eccentricity and the semi-major axis in a manner proportional to β (Burns et al. 1979). This drag force causes the particle, initially at r_1, to spiral toward the star and reach a distance r_2 on timescales that are a function of β (Wyatt et al. 1999):

$$t_{PR} = 400 \left(\frac{M_\odot}{M_*}\right) \left[\left(\frac{{r_1}^2}{a_\oplus}\right)^2 - \left(\frac{{r_2}^2}{a_\oplus}\right)^2\right] /\beta \tag{2.8}$$

where t_{PR} is in years. It is important to note that t_{PR} is inversely proportional to β and therefore proportional to the particle size, D, as this effect further differentiates the behavior of particles based on size.

2.3.3 Collisions

Collisions play important roles in the circumstellar environment as they provide mechanisms for both creation and destruction of dust particles. Based on collisional models of dust in disk environments, the size distribution of particles is rather steep, i.e. there are many more small particles than large particles. Due to the steep size distribution expected for particles in the disk environment, the surface area of the disk is dominated by the smaller particles (for a thorough discussion see Wyatt et al. (1999)). These particles, however, may have lifetimes associated with radiation effects that are much shorter than the age of the disk, i.e. these particles cannot be left over from the original formation of the disk. This condition necessitates a source through which these particles can be replenished.

The timescale associated with the destruction of the dust particles is based on the assumption that a typical particle size of the emitting dust can be determined. The typical

size is based on assumptions about the particles responsible for the majority of the cross sectional area observed at a particular wavelength. This is estimated by considering both number density and the physical cross-section of the particle. In terms of this typical particle size, Wyatt et al. (1999) provided an expression for the collisional timescale as

$$t_{coll}(D_{typ}, r) = t_{per}(r)/4\pi\tau_{eff}(r) \tag{2.9}$$

where D_{typ} is the characteristic size of the particles responsible for most of the disk's cross sectional area. The optical depth can be thought of as a measure of the total material in a particular line of sight modulo the effects of absorption and scattering properties of the dust. These optical properties are quantified by the extinction coefficient. The effective optical depth in the above expression is the face-on optical depth of a disk observed if the extinction coefficients for the particles are equal to 1. The face-on optical depth can be estimated observationally by considering the simplified relationship (Wyatt et al. 1999)

$$F_\nu(\lambda, r) \approx \tau_{eff}(r)\Omega_{obs}B_\nu(\lambda, D_{typ}, r)Q_{abs}(\lambda, D_{typ}) \tag{2.10}$$

which relates the flux density received at earth, F_ν, at a given wavelength, λ, from a particle with a Planck function of B_ν, at a distance r from the star, and with characteristic size D_{typ}. The observational solid angle is related to the detector pixel size, $\Omega \sim {d_{pix}}^2$, and the absorption coefficient of the typical particle is Q_{abs}. Since disks are unlikely to be observed directly face-on, projection effects must be considered to transform τ_{eff} into a face-on τ_{eff}. Once the face-on or normal optical depth is determined, the collisional timescales can be estimated.

2.3.4 Other Forces

The circumstellar environment is very complex and has many other factors, besides the ones already mentioned, that influence the dynamics of the dust particles within the disk. The effects that often play significant roles in this environment are briefly described below along with the justification for not emphasizing their impact on the modeling performed in this research.

Stellar wind effects

The stellar wind will interact with the dust particles in two primary ways. First, because the dust particles are charged and because the winds carry with them a magnetic field, a Lorentz force arises. The Lorentz force is a function of the overall charge of the dust particle and the strength of the interacting magnetic field. Second, actual collisions between the dust particles and the protons comprising the wind give rise to an additional drag component (see Gustafson (1994) for example).

Stellar winds are thought to be associated with coronal holes and are thus tied to coronal and possibly chromospheric activity. A-type stars do not possess a deep convective zone from which high speed winds are effectively driven (Panzera et al., 1999). Since Beta Pictoris is an A-type star and since an A-type star is expected to have little chromospheric and coronal activity (Artymowicz 1997) the effects of the stellar winds around Beta Pictoris are neglected in this research.

Gas drag

For very young disks in which the gas to dust mass ratio is significant, the dynamic drag on the dust particles caused by the gas must be considered. However, Liseau and Artymowicz (1997) determined from mm-wavelength observations that the overall gas to dust mass ratio was < 0.003 and that this indicates the disk is effectively gas free (Artymowicz, 1999). Therefore, gas drag within the Beta Pictoris system was assumed to be negligible and this effect was not considered any further in this research.

2.3.5 Conclusions on Timescales

The overall picture that emerges from this analysis for an evolved circumstellar disk is that the smallest particles are quickly removed from the system through radiation pressure. The medium sized particles are either removed by collisions or spiral into the star through the effects of PR drag. The largest particles, which are responsible for the creation of the smaller particles through collisional cascade, are affected by gravitational forces alone. Therefore it can be concluded that, in general, the distribution of larger bodies within a

circumstellar disk is primarily determined by the sum of all gravitational effects within the disk. These gravitational effects can result from the central star, other large bodies, and possibly from the disk itself provided it has a significant mass compared to the other masses within the system. This picture will be discussed further in chapter 7 as it applies to Beta Pictoris.

The following chapter discusses the method of determining the combined effects of gravity in a complex planetary system such as a circumstellar disk with multiple imbedded planets. This will be done through the theoretical framework of secular perturbation theory.

CHAPTER 3
SECULAR PERTURBATION THEORY

3.1 Introduction

The previous chapter began to reveal the many influences that play a part in determining the characteristics of a circumstellar disk. These influences were associated with such things as radiation-particle interaction, collisions, drag forces, etc. This chapter will expand on the discussion by providing a summary of the theory used to describe the effects of gravity from not only the central star, but from other planets in the system.

Generally speaking, a circumstellar disk is a flattened cloud of dust in which each dust particle moves on an its own individual orbit. In order to understand the effects of planets on the disk, a link must be established between the planets and the dust particle orbits. The theoretical framework through which this is accomplished in this research is secular perturbation theory. Secular perturbation theory is a well established approach that has been applied extensively to problems within the solar system. In fact, analysis of the secular perturbations arising from Jupiter and Saturn can be shown to create a forced inclination that varies with semi-major axis, a – see, for example, Dermott et al. (1984, 1985) and Murray and Dermott (1999). This is significant as this characteristic is the source of the mid-plane warping that is the crux of this research.

This chapter will explain how expressions describing particle orbits can be developed by considering the gravitational perturbations from massive bodies. The solutions that result from this approach describe the time evolution of each of the particles orbital elements: eccentricity, longitude of pericenter, inclination, and longitude of ascending node. A very important concept that will be repeated throughout this discussion is that the solutions can be broken down into two components. These components are referred to as the proper and forced orbital elements. The proper elements are related to the initial conditions at

creation of the particle under consideration. The forced elements correspond to the effects of the perturbations and are thus linked to the planets.

The goal of this chapter is to explain the theoretical framework that produces the forced orbital elements from a particular planetary configuration. It is the forced orbital elements that are then used as an input to the modeling process described in the later chapters.

3.2 Second Order Secular Perturbation Theory

Since the many-body problem in dynamics is insoluble analytically, alternatives to an exact solution have been developed. The approach outlined here is to start with the three-body problem and then divide the resulting potential into two components, one of which represents the two-body central mass and the second of which represents the portion of the potential arising from the additional masses. This second component is known as the *Disturbing Function.* A detailed derivation of the disturbing function is presented in Murray and Dermott (1999).

3.2.1 The Disturbing Function

Starting with the three-body equations of motion in cartesian coordinates, the acceleration of the secondary masses with respect to the central mass can be expressed as

$$\begin{aligned} \ddot{r}_i &= \nabla_i(U_i + \mathcal{R}_i) \\ \ddot{r}_j &= \nabla_j(U_j + \mathcal{R}_j) \end{aligned} \tag{3.1}$$

where the potential has been broken up into two components; one describing the two body part, U, where

$$\begin{aligned} U_i &= G\,\frac{(m_c + m_i)}{r_i} \\ U_j &= G\,\frac{(m_c + m_j)}{r_j} \end{aligned} \tag{3.2}$$

and one describing the portion of the potential arising from the gravitational perturbations from the secondary masses, $\mathcal{R}$. This portion of the potential is referred to as the *Disturbing*

Function. For the three body problem, the disturbing function for the individual masses can be expressed as

$$\begin{aligned} \mathcal{R}_i &= G\frac{m_j}{\mathbf{r}_j - \mathbf{r}_i} - Gm_j\frac{\mathbf{r}_i \cdot \mathbf{r}_j}{r_j^3} \\ \mathcal{R}_j &= G\frac{m_i}{\mathbf{r}_i - \mathbf{r}_j} - Gm_i\frac{\mathbf{r}_i \cdot \mathbf{r}_j}{r_i^3}. \end{aligned} \tag{3.3}$$

In order to handle the $\mathbf{r}_i - \mathbf{r}_j$ terms analytically, the disturbing function is usually expanded in terms of Legendre polynomials. Furthermore, the disturbing function can be transformed from a form based on positions and velocities to a form expressed in terms of the osculating orbital elements, a, e, I, λ, ϖ, and Ω which represent the semi-major axis, eccentricity, inclination, mean longitude, longitude of pericenter, and longitude of the ascending node respectively, i.e.

$$\mathcal{R} = f(m, m', a, a', e, e', I, I', \cos\phi)$$

where the argument of the cosine function is a linear combination of the mean longitudes, longitude of pericenter, and longitude of ascending node. This term is expressed as

$$\phi = j_1\lambda' + j_2\lambda + j_3\varpi' + j_4\varpi + j_5\Omega' + j_6\Omega \tag{3.4}$$

where the unprimed quantities represent the inner mass and the primed quantities represent the outer mass.

3.2.2 The Secular Portion of the Disturbing Function

The terms within the disturbing function can be grouped together by characteristic timescales. The three categories are short period terms, mean motion resonance terms, and secular terms. The short period terms are dependent on the mean longitude λ, and represent effects that occur on the scale of orbital periods. The terms associated with mean motion resonances represent effects that are also dependent on the mean longitude and would only effect certain locations within a disk, generally at radii where the corresponding period has a commensurability with one of the planets. The secular terms produce effects that are felt throughout the disk and are independent of mean longitude. The independence

of mean longitude implies that the instantaneous positions of the masses have no effect on large timescales. For this research, long term effects that are felt throughout the disk will be considered as the source of perturbations leading to large scale warping, and thus only the secular part of the disturbing function will be retained.

The time variation of the orbital elements can be expressed through the use of *Lagrange's Planetary Equations*:

$$\dot{e}_j = -\frac{1}{n_j a_j^2 e_j}\frac{\partial \mathcal{R}_j}{\partial \varpi_j} \tag{3.5a}$$

$$\dot{\varpi}_j = -\frac{1}{n_j a_j^2 e_j}\frac{\partial \mathcal{R}_j}{\partial e_j} \tag{3.5b}$$

$$\dot{I}_j = -\frac{1}{n_j a_j^2 I_j}\frac{\partial \mathcal{R}_j}{\partial \Omega_j} \tag{3.5c}$$

$$\dot{\Omega}_j = -\frac{1}{n_j a_j^2 I_j}\frac{\partial \mathcal{R}_j}{\partial I_j}. \tag{3.5d}$$

This particular form of Lagrange's equations assumes low inclination and eccentricity.

This research will consider massless test particles disturbed by an arbitrary number of planets and the resulting effects on the large scale structure of a disk. In this case, the disturbing function can be expressed as

$$\begin{aligned}\mathcal{R} &= na^2\Big\{\frac{1}{2}Ae^2 + \frac{1}{2}BI^2 \\ &+ \sum_{j=1}^{N} A_j e e_j \cos(\varpi - \varpi_j) + \sum_{j=1}^{N} B_j I I_j \cos(\Omega - \Omega_j)\Big\}\end{aligned} \tag{3.6}$$

where the values of A and B are functions of mass and semi-major axis only, and are given by

$$A = -n\frac{1}{4}\sum_{j=1}^{N}\frac{m_j}{m_c}\alpha_j\bar{\alpha}_j b_{3/2}^{(2)}(\alpha_j) \tag{3.7a}$$

$$A_j = -n\frac{1}{4}\frac{m_j}{m_c}\alpha_j\bar{\alpha}_j b_{3/2}^{(2)}(\alpha_j) \tag{3.7b}$$

$$B = -n\frac{1}{4}\sum_{j=1}^{N}\frac{m_j}{m_c}\alpha_j\bar{\alpha}_j b_{3/2}^{(1)}(\alpha_j) \tag{3.7c}$$

$$B_j = -n\frac{1}{4}\frac{m_j}{m_c}\alpha_j\bar{\alpha}_j b_{3/2}^{(1)}(\alpha_j) \tag{3.7d}$$

The value of α is determined through the ratios of semi-major axes of the test particle and the perturbing mass. More precisely $\alpha_j = a_j/a$ if $a_j < a$ and a/a_j if $a_j > a$. Similarly, $\bar{\alpha}_j = a_j/a$ if $a_j < a$ and a/a_j if $a_j > a$. The quantities $b^{(1)}_{3/2}(\alpha)$ and $b^{(2)}_{3/2}(\alpha)$ are the Laplace coefficients and are given by the following expressions

$$b^{(1)}_{3/2}(\alpha) = \frac{1}{\pi}\int_0^{2\pi} \frac{\cos\psi d\psi}{(1-2\alpha\cos\psi+\alpha^2)^{\frac{3}{2}}} \tag{3.8a}$$

$$b^{(2)}_{3/2}(\alpha) = \frac{1}{\pi}\int_0^{2\pi} \frac{\cos 2\psi d\psi}{(1-2\alpha\cos\psi+\alpha^2)^{\frac{3}{2}}}. \tag{3.8b}$$

The form of the disturbing function presented here is to second order in inclination and eccentricity – e^2, I^2, ee_j, and II_j. The truncation of the disturbing function limits the analysis to small eccentricities and inclinations.

3.3 Solutions to Lagrange's Equations

The form of Lagrange's planetary equations shown in the previous section has obvious difficulties when the eccentricity, e, and inclination, I, are small. To remove the singularities when e and I are small, the different components can be used together in a vector representation with the following components

$$h = e\sin\varpi \tag{3.9a}$$

$$k = e\cos\varpi \tag{3.9b}$$

$$p = I\sin\Omega \tag{3.9c}$$

$$q = I\cos\Omega. \tag{3.9d}$$

These variables define the components of the eccentricity and inclination vectors and are functions of the osculating orbital parameters – the instantaneous parameters determined for a specific particle trajectory. Using these components of the eccentricity and inclination

vectors the disturbing function takes the form

$$\begin{aligned}\mathcal{R} &= na^2\Big\{\frac{1}{2}A(h^2+k^2)+\frac{1}{2}B(p^2+q^2) \\ &+ \sum_{j=1}^{N} A_j(hh_j+kk_j)+\sum_{j=1}^{N} B_j(pp_j+qq_j)\Big\}\end{aligned} \tag{3.10}$$

Likewise, Lagrange's planetary equations take on the form

$$\dot{h} = -\frac{1}{n_j a_j^2}\frac{\partial \mathcal{R}}{\partial k} \tag{3.11a}$$

$$\dot{k} = -\frac{1}{n_j a_j^2}\frac{\partial \mathcal{R}}{\partial h} \tag{3.11b}$$

$$\dot{p} = -\frac{1}{n_j a_j^2}\frac{\partial \mathcal{R}}{\partial q} \tag{3.11c}$$

$$\dot{q} = -\frac{1}{n_j a_j^2}\frac{\partial \mathcal{R}}{\partial p}. \tag{3.11d}$$

Solving these equations provides solutions to the equations of motion in terms of the components h, k, p, and q. The solutions to these equations are

$$h = e_{proper}\sin(At+\beta)+h_0(t) \tag{3.12a}$$

$$k = e_{proper}\cos(At+\beta)+k_0(t) \tag{3.12b}$$

$$p = I_{proper}\sin(Bt+\gamma)+p_0(t) \tag{3.12c}$$

$$q = I_{proper}\cos(Bt+\gamma)+q_0(t) \tag{3.12d}$$

where e_{proper} and I_{proper} are the proper eccentricity and proper inclination, or the eccentricity and inclination associated with the initial conditions of the test particles. The quantities $At+\beta$ and $Bt+\gamma$ are equal to ϖ_{proper} and Ω_{proper}, the test particles proper pericenter and longitude of ascending node respectively. As was stated earlier in the discussion, the two components of the solutions are related to the two primary aspects of the problem. The first term is related to the initial conditions of the massless particle under consideration. The second term in each equation is associated with the perturbation and can be expressed

as

$$h_0(t) = -\sum_{i=1}^{N} \frac{\nu_i}{A - g_i} \sin(g_i t + \beta_i) \tag{3.13a}$$

$$k_0(t) = -\sum_{i=1}^{N} \frac{\nu_i}{A - g_i} \cos(g_i t + \beta_i) \tag{3.13b}$$

$$p_0(t) = -\sum_{i=1}^{N} \frac{\mu_i}{B - f_i} \sin(f_i t + \gamma_i) \tag{3.13c}$$

$$q_0(t) = -\sum_{i=1}^{N} \frac{\mu_i}{B - f_i} \cos(f_i t + \gamma_i) \tag{3.13d}$$

where g_i and f_i are system eigenfrequencies. Eigenfrequencies are characteristic frequencies associated with all dynamical systems possessing internal periodicity. It is the eigenfrequencies of a system that determine at which frequencies the secular resonances will occur. It is important to remember that the form of the disturbing function considered here is truncated. The resonances implied from equations 3.13a through 3.13d cause behavior that exceeds the limitations of the second order theory. The values ν and μ are functions of the systems eigenvectors and have the form

$$\nu_i = \sum_{j=1}^{N} A_j e_{ji} \tag{3.14a}$$

$$\mu_i = \sum_{j=1}^{N} B_j I_{ji}. \tag{3.14b}$$

Once again, these relationships imply that the vector components h, k, p, and q consist of two parts – the proper component and the forced component:

$$h = e_p \sin \varpi_p + e_f \sin \varpi_f \tag{3.15a}$$

$$k = e_p \cos \varpi_p + e_f \cos \varpi_f \tag{3.15b}$$

$$p = I_p \sin \Omega_p + I_f \sin \Omega_f \tag{3.15c}$$

$$q = I_p \cos \Omega_p + I_f \cos \Omega_f. \tag{3.15d}$$

The solutions for h, k, p, and q can be used to determine the components of the osculating orbital elements – the orbital elements associated with the observable dynamics of

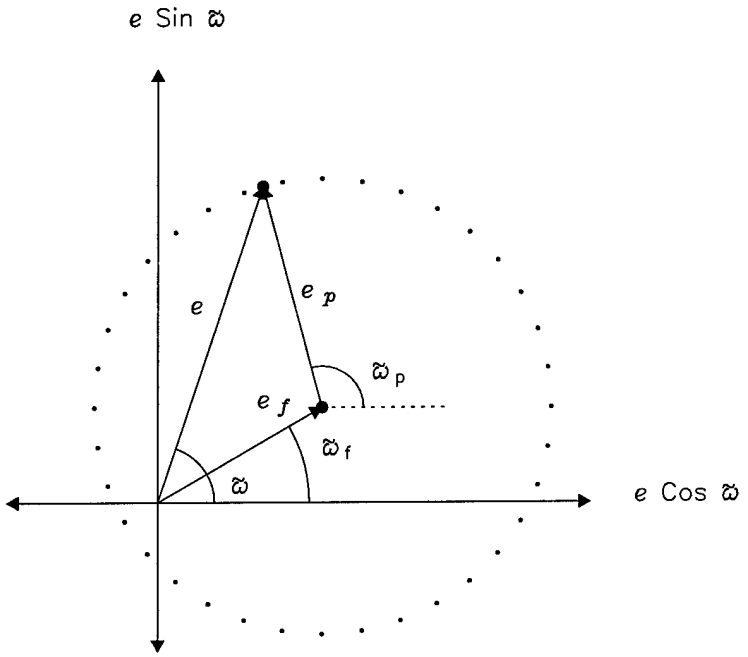

Figure 3–1: Vector relationship between the components of the osculating orbital elements.

the particle. The relationship between these components are best thought about as vector components. This relationship can be depicted graphically through the use of a vector diagram such as that shown in figure 3–1. This particular diagram illustrates the relationship between the osculating, forced, and proper elements of eccentricity and longitude of pericenter. A similar diagram can be constructed for inclination and longitude of ascending node as well.

To understand the vector illustration, two important points must be understood. First, the forced elements are a function of the perturbing planets' masses and osculating elements. Since the osculating elements evolve, the forced elements are also a function of time. However, for a given planetary system at a given time, the forced elements are a function of semi-major axis alone, and therefore the vector diagram depicts the relationship between components of the orbital elements for a particular value of semi-major axis. Second, though the forced elements are constant for the particular value of semi-major axis, all of the proper elements are not that simple. Though the proper inclination and eccentricity may be constant for a particular semi-major axis value, the proper pericenter and node are actually a distribution of values over 2π resulting from the randomization of these elements after initial creation.

The forced orbital elements represent the influence of the perturbation by the secondary masses and are the result of performing the calculations outlined in this section. By determining the values for the forced orbital elements, the instantaneous trajectory of a particle can be determined provided the proper elements can be determined from the initial conditions. From the relationships shown in equations 3.15a through 3.15d, and the solutions shown in equations 3.13a through 3.13d, the forced elements can be expressed as

$$e_f = \sqrt{h_0^2 + k_0^2} \tag{3.16a}$$

$$I_f = \sqrt{p_0^2 + q_0^2} \tag{3.16b}$$

$$\varpi_f = \arctan\ (h_0/k_0) \tag{3.16c}$$

$$\Omega_f = \arctan\ (p_0/q_0) \tag{3.16d}$$

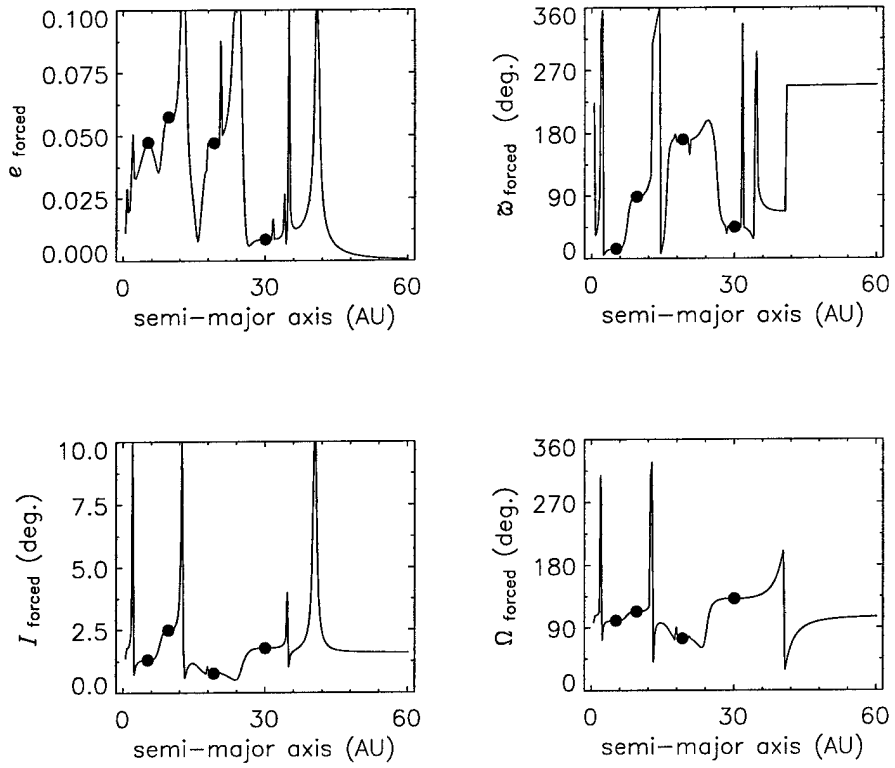

Figure 3–2: Forced orbital elements as a function of semi-major axis for a massless test particle perturbed by the four Jovian planets. The filled circles represent the osculating elements of the planets. a) forced eccentricity b) forced longitude of pericenter c) forced inclination d) forced longitude of ascending node.

Examples of the calculated forced orbital elements for a massless test particle are shown in figure 3–2, for the J2000 orbital elements given in the appendix. This set of forced elements is based on perturbations of the four Jovian planets in the solar system. The osculating elements associated with each planet are shown as filled circles on the plots. An important result of the calculations is that the forced parameters are equal to the osculating elements of the perturbing planets at the semi-major axis of the planets. Further discussion of the physical implications of the results from secular perturbations is presented in the following chapter. The discussion will emphasize the role the forced inclination plays on dust particle orbits within a disk and the resulting overall morphology.

Though orbital parameters define a particle's trajectory, a trajectory defined by the forced orbital parameters alone does not define a true physical particle orbit. As stated

above, the forced elements are only one part of the story. However, by examining the forced orbital elements and trajectories determined by the forced elements alone, insight to a system's dynamics can be gleaned. If the forced elements are defined as a function of semi-major axis and trajectories based on the forced elements are plotted for a range of semi-major axes, the planes about which the particles will precess can be visualized.

The following chapter discusses the role played by the calculated proper and forced orbital elements on the morphology of a simulated disk.

CHAPTER 4
RESULTS FROM PERTURBATION THEORY

The previous chapter discussed the formalism of secular perturbation theory. Within the solutions presented in equations 3.15a through 3.15d the behavior of the osculating orbital elements can be gleaned. However, the goal of this research is to understand, both quantitatively and qualitatively, the role that the perturbations, and hence the planets, play in defining the morphology of a circumstellar disk. The goal of this chapter is to develop a more intuitive understanding about how the secular perturbations affect a disk, specifically observed warping. This is pursued by first studying the details of the results presented in the previous chapter and then by considering the results in the context of the angular momentum of dust particle and planetary orbits.

4.1 Effects of Forced Elements on Disk Morphology

As shown in the previous chapter, the forced orbital elements for a test particle are determined by solving the differential equations describing the long term gravitational perturbations from massive bodies. It was also shown that the forced elements are a function of semi-major axis. This dependency on semi-major axis results in several important characteristics that influence the morphology of a model disk that is based on these parameters. An example of the forced orbital parameters for a massless test particle under the influence of two planets is illustrated in figure 4–1. This particular calculation considered perturbations by a planetary configuration based on Jupiter and Saturn. Figure 4–1 illustrates the dependence of the forced elements as a function of semi-major axis. Of particular interest for this research are the characteristics of the forced elements that cause the warping of a circumstellar disk. This chapter will discuss in physical terms how the variations in the forced parameters, particularly the forced inclination, are manifested into a warped disk.

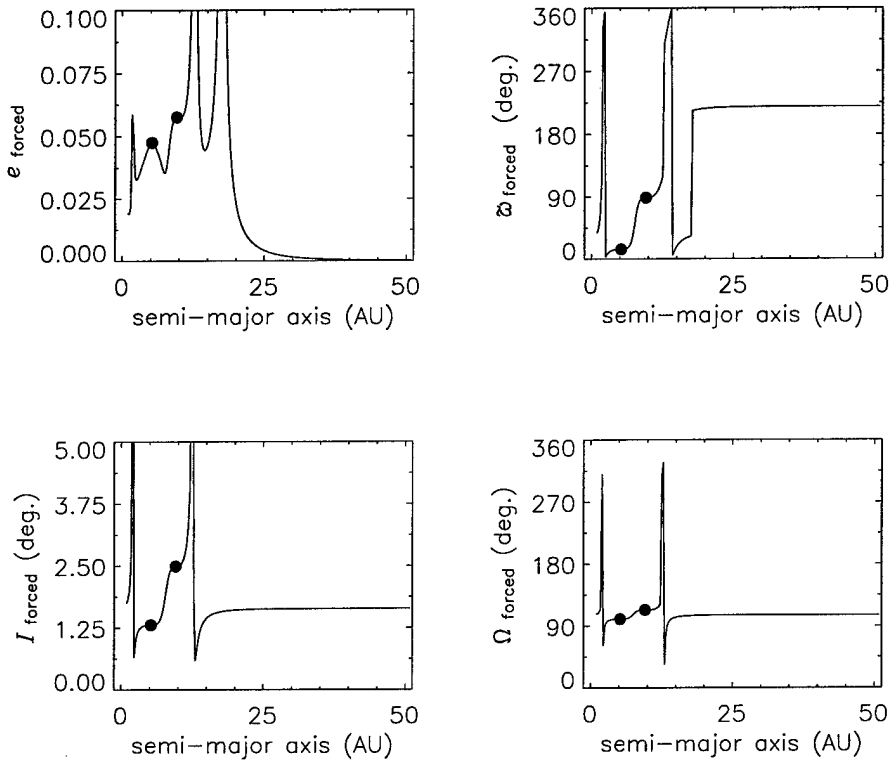

Figure 4–1: Forced orbital elements as a function of semi-major axis for massless test particles perturbed by a two planet system. The filled circles represent the osculating orbital elements of the perturbing planets.

4.2 Solutions from Secular Perturbation Theory

The solutions to Lagrange's equations of planetary motion in secular perturbation theory show that a particle's osculating orbital elements can be broken down into two components: the forced and proper orbital parameters. The forced elements are based on the perturbations by the other masses within the system and the proper orbital parameters are based on the problem's boundary conditions. More specifically, the proper elements are related to the orbital elemenents of the massless test particles at the moment of their creation. In general, this is determined by considering the origin of the particles. If the test particles are assumed to come from the break up of larger bodies, the proper elements are related to the characteristics of those original bodies.

In evolved circumstellar disks, the type considered in this research, the material is not primordial but is indeed created through the break-up of larger parent bodies, either asteroids or comets. Evolved disks are disk systems in which planetesimal formation has already occurred or is in the process of occurring. Furthermore, radiation effects have already had the opportunity to remove material via PR drag or radiation pressure. In these types of systems, the characteristics of the parent bodies' orbits determine the proper orbital elements for the dust particles. This is based on the idea that the most probable collision in which a large body is broken up, is one in which the colliding particle has just enough mass and energy to do so. Therefore, the relative velocity between the resulting fragments is low. This results in the fragments and dust having essentially the same orbital parameters as the original parent body for inclination, eccentricity, and semi-major axis. However, since the particles have a wide range of sizes they have differing values of β. This essentially causes each size of particle to exist in a unique potential. In other words, it makes each particle see a star of a different mass. The net effect of these differences is that the particles have slightly different orbits and in turn disperse. The way in which this is incorporated into disk models is by randomizing the proper pericenter and longitude of ascending node over 2π radians.

In the models created in this research, the proper orbital elements of the source particles are based on distributions consistent with the main belt asteroids within the solar system. Though it is conceivable that multiple reservoirs of source bodies could exists at different

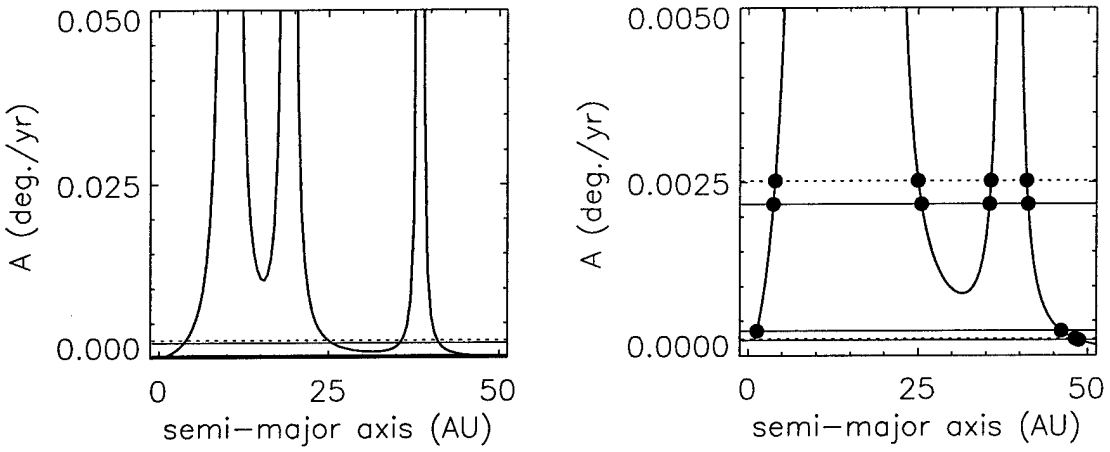

Figure 4–2: Proper precessional rate as a function of semi-major axis. The horizontal lines indicate the eigenfrequencies associated with the system: the solid lines are eccentricity/pericenter eigenfrequencies and the dashed are inclination/node eigenfrequencies. The intersections between the eigenfrequencies and precessional frequency determine the locations of secular resonances.

radii from a star and have distributions of orbital elements that are significantly different, this alone would not produce warping in the disk. It will be shown in this chapter that varying the distributions of proper inclination affects the morphology of a disk by changing the observed opening angle of the disk, but not by creating a warp.

On the other hand, the variation in forced inclination with semi-major axis does cause warping of the disk. If it is accepted that the forced inclination defines, in part, the plane about which particle orbits will precess, this is obvious.

By examining the plot of the forced inclination in figure 4–1, several key features should be noted. The first are the regions associated with the singularity in the secular solutions; these are the large spikes observed in the function. These singularities occur at locations where the system eigenfrequencies are equal to the local precessional rates of the proper elements and represent the location of secular resonances. Recall that eigenfrequencies are characteristics of a dynamic system and define the frequencies at which secular resonances occur. An example of how this is determined is shown in figure 4–2. This plot shows the proper precessional rate, A, as a function of semi-major axis. Plotted as horizontal lines are

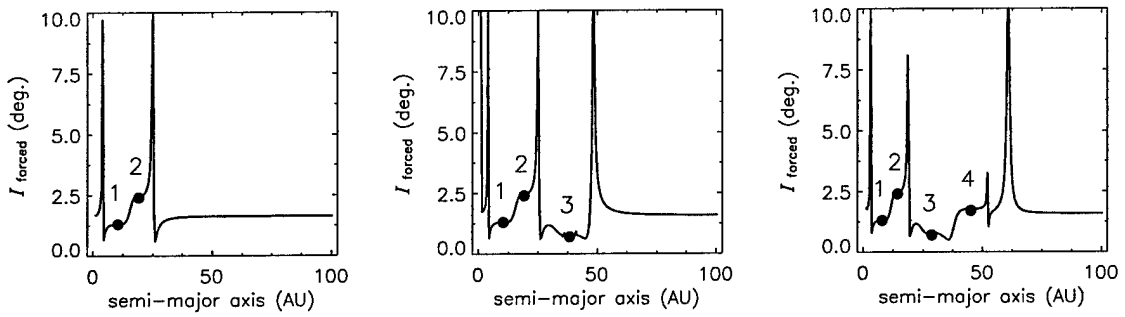

Figure 4–3: Forced inclination as a function of semi-major axis for massless test particles perturbed by a two, three, and four planet system. The numbers indicate the inclination as a function of semi-major axis for the perturbing planets.

the the system's eigenfrequencies. As seen in the equations 3.13a-3.13d, singularities exist where the eigenfrequencies intersect with the proper precessional rate. The second important characteristic is that the values of the forced elements at the semi-major axis values associated with the perturbing planets are equal to the corresponding planets' osculating orbital elements. This is illustrated in the lower left panel of figure 4–1 by plotting the inclinations of the perturbing planets as a function of their respective semi-major axes. As will be discussed in the next section, this correlation between the forced parameters and the parameters associated with the perturbing planets seems reasonable based on arguments made in terms of angular momentum.

The same characteristics appear when the analysis is performed for three or more planets. Plots of the forced inclination for two, three, and four planets are shown in figure 4–3. The number of resonances increase as the number of planets increase because of the additional eigenfrequencies. Important for the following section is the fact that the forced parameters are still equal to the osculating orbital parameters of the planets at the semi-major axis values corresponding to the semi-major axis of the planets.

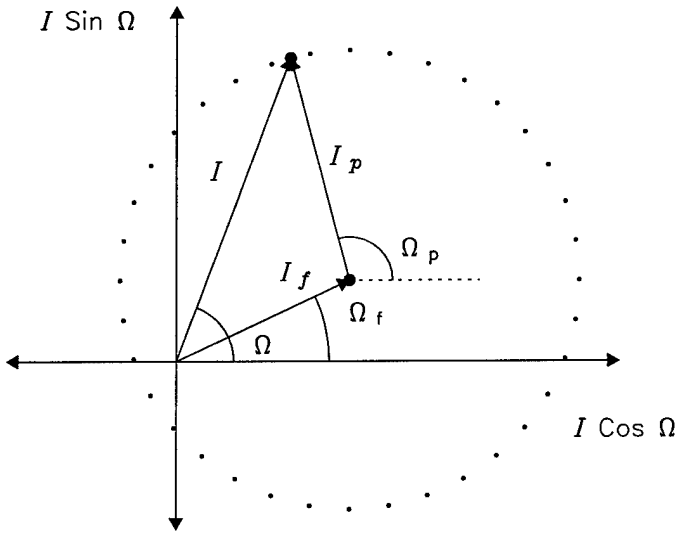

Figure 4–4: Vector relationship between the components of the osculating orbital elements.

4.3 Defining a Section of Disk

4.3.1 General Characteristics

The solutions for h, k, p, and q can be used to determine the components of the osculating orbital elements – the orbital elements associated with the observable dynamics of the particle. The relationship between these components is best considered as vector components. The relationship between components can be depicted graphically through the use of a vector diagram such as that shown in figure 4–4. This particular diagram illustrates the relationship between the osculating, forced, and proper elements of inclination and longitude of ascending node. This figure is similar to the diagram constructed for eccentricity and pericenter as shown in the previous chapter.

To understand the vector illustration, two important points must be understood. First, for a given planetary system at a given time the forced elements are a function of semi-major axis alone, and therefore the vector diagram depicts the relationship between components of the orbital elements for that particular value of semi-major axis. Second, though the forced elements are single valued for a particular value of semi-major axis, the proper elements are not. The proper pericenter and node, for a particular semi-major axis value, are actually a distribution of values over 2π resulting from the randomization of these elements after initial creation. As mentioned earlier, this results from phase mixing - the dispersal of particles within an ensemble due to slight differences in orbital periodicity.

Figure 4–5 shows the relationship between the components of the forced and proper orbital elements and the section of disk which they define. Because the proper pericenter and node are randomized over 2π, particles at a given value of semi-major axis will create a distribution of orbits, each with slightly different osculating elements. This distribution will result in a torus that is responsible for defining that particular section of disk. These plots show the distribution of orbits having the same semi-major axis, and thus the same forced eccentricity and the same forced pericenter. The top-left panel has a forced inclination of zero while the other panels show disks with a nonzero forced inclination. The filled circle represents the geometric center of the torus and and the empty circle represents the central star.

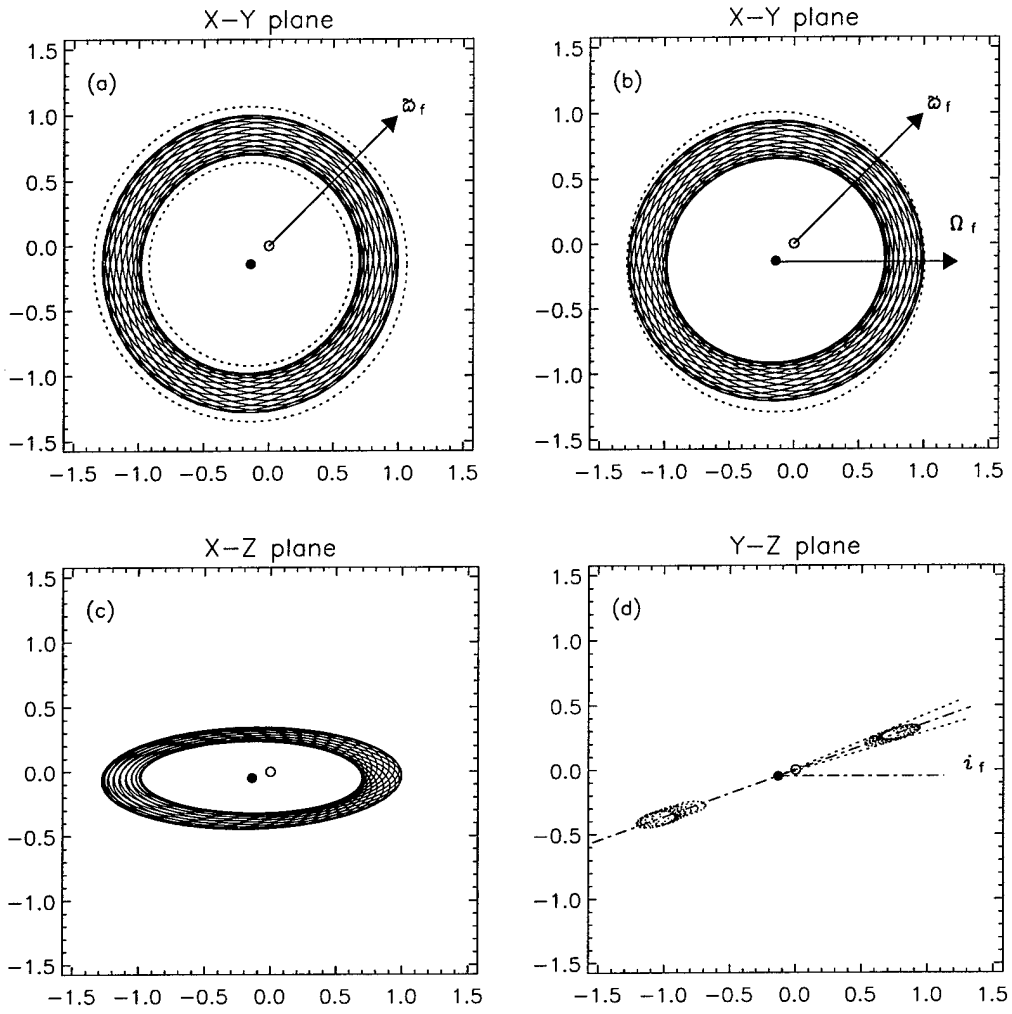

Figure 4–5: The distribution of test particle orbital trajectories representing the influence of forced elements. Panel a shows the torus resulting from a disk with a nonzero forced and proper eccentricity. The Other panels show different views of (a) the same disk but with nonzero values of forced and proper inclination with respect to the X-Y plane. The forced eccentricity determines the offset of the disks center of symmetry from the central star and the proper eccentricity determines the width of the tauri. Similarly the forced inclination determines the angle of the orbital plane to a reference plane and the proper inclination determines the disk opening angle.

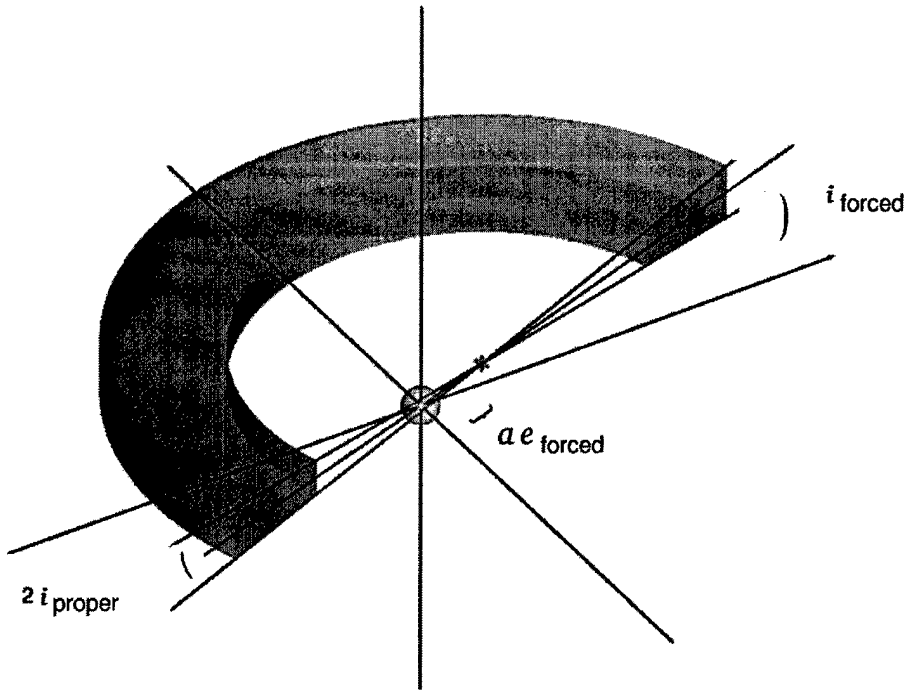

Figure 4–6: Visualization of a section of disk. The offset of the disk section's center of symmetry is $\sim ae_f$. The angular thickness is $\sim 2i_p$ and the angle of the section's symmetry plane with respect to the system's reference plane is $\sim i_{forced}$.

All of the characteristics of the torus representing the distribution of dust particle orbits can be related to the forced and proper elements. Generally speaking, the proper elements define the geometric size of the torus while the forced elements define the orientation of the torus with respect to the central star and an associated reference plane and direction – such as the ecliptic plane and the vernal equinox for our solar system.

The dimensions of the torus are related to the proper elements of eccentricity and inclination. The inner radius of the torus is equal to $a(1-e_p)$ and the outer radius is equal to $a(1+e_p)$. The center of symmetry is offset from the central star by a distance ae_f in the direction opposite to ϖ_f (Dermott et al. 1985; Dermott et al. 1998).

Likewise, the proper inclination determines the angular thickness of the disk. As has been shown for the solar system dust bands (Dermott et al. 2001), the angular thickness

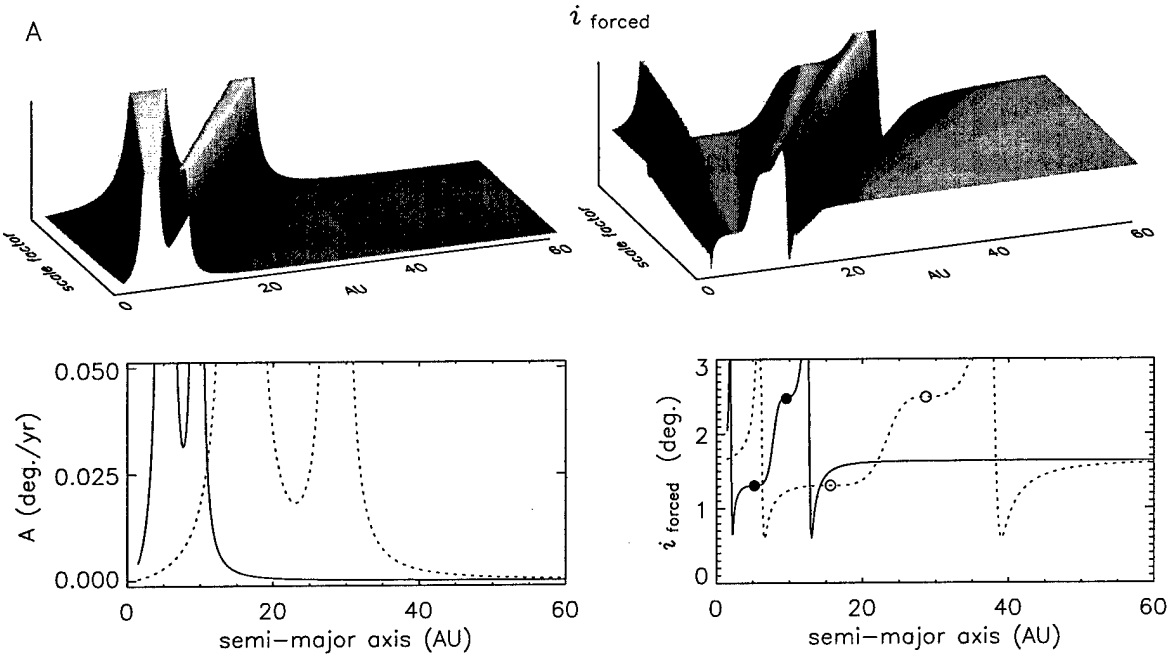

Figure 4–7: Proper precessional rates and forced inclination for a system modeled after Jupiter and Saturn. The top illustrations show how the precessional rate/ inclination vary with radial distance from the central star and with an increase in the mass and semi-major axes of the planets. The bottom plots show the same for the first and last values of mass and semi-major axes scale factor.

$\sim 2I_p$. The forced inclination determines the plane of symmetry or the disk section's mid-plane. This is illustrated in panel (d) of figure 4–5 which shows a cross-sectional view of the torus representing the contributions of dust particles with a common semi-major axis to the overall disk. An actual disk could be though of as a superposition of many such tori, each characterized by a set of forced parameters associated with a particular value of semi-major axis. Figure 4–6 shows another view of a disk section and illustrates the relationships between the geometry and the forced and proper elements.

4.3.2 Determining the Radial Extent of the Influence of Perturbing Planets

Analysis of the forced orbital elements determined from secular perturbation theory show an invariant value is approached at large vales of semi-major axis. The region through which the elements begin to approach this invariant value define the extent of observable effects from the secular perturbations.

Figure 4–7 provides an illustration of how the range of influence for a given planetary configuration is altered by modifying both the planetary masses and the semi-major axis of the planets by an increasing scale factor. The top surface plots show the changes to the proper precessional rate, A, and the forced inclination, I_f. The diagram shows the amplitude of A and I_f with semi-major axis and increasing values of the mass and semi-major axis scale factor. The bottom plots show a two dimensional version of the same, with only the first and last values of the scale factor plotted.

The increase in mass and the increase in semi-major axis have unique effects on the elements. The semi-major axis scale factor determines the location of the important features in the plots including the locations of the singularities as well as the location of the invariant plane for the forced elements.

Increasing the mass scale factor has a different effect in that it extends the region over which an individual planet exerts an influence. For example, the width of the singularities associated with the proper precessional rates are widened as the masses of the planets increase. Since the proper precessional rate also determines the timescales of secular effects, this effect highlights how more massive systems have shorter secular timescales.

An important characteristic of the forced elements is that they match the osculating elements of the perturbing planets when the particle's semi-major axis matches that of the corresponding planet. As can be seen in the plot of inclination, a small plateau exists in the vicinity of the planet. For more massive planets, this plateau is increased in its semi-major axis range. This implies that a more massive planet will impose its orbital elements on a test particle over a larger region of a disk.

By developing intuition on how these elements behave when scaling parameters such as semi-major axis and planetary mass, and by understanding how these elements ultimately affect the morphology of a disk, developing an initial planetary configuration for a model disk becomes much less of a process based solely on trial and error.

4.4 Planes Defined by the Angular Momentum Vector

As stated in the previous section, a warped disk is the result of the forced inclination varying as a function of semi-major axis. This variation in forced inclination, as is the

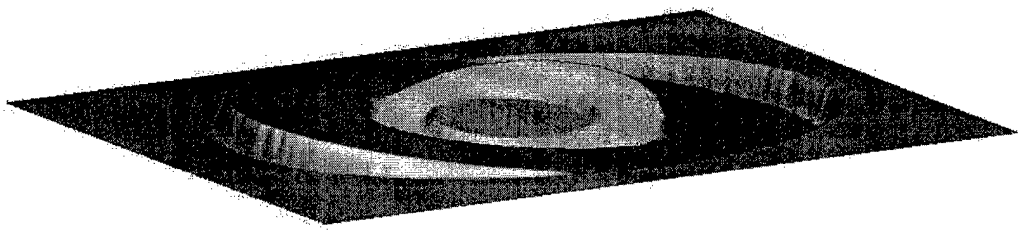

Figure 4–8: Planes defined by angular momentum of individual planets in a multi-planet system. The reference plane represents the invariant plane; that plane perpendicular to the system's total angular momentum vector.

case with the other orbital parameters as well, is the result of the gravitational perturbations associated with the presence of planets. Another way to consider why this occurs is by considering the planes associated with angular momentum vectors; both the angular momentum associated with each planet and the total angular momentum of the system.

Warps in circumstellar disks have been indicated in both observations of real disks and theoretical models. In both cases, the warping has been described as the edge on view of a multi-component disk in which the components are inclined to one another. The origin of these multiple components are generally attributed to the presence of planets. One of the more thorough analyses argues that the multiple component configuration results from a single planet having an orbit inclined to the plane of the disk. The general idea is that through interaction between the planet and the disk material, the dust becomes, over time, coplanar with the orbital plane of the planet. Furthermore, the presence of the planets cause differential rotation throughout the disk. If the system is relatively young, material at outer radii, whose orbits precess more slowly, has not yet become coplanar. This scenario results in two planes of symmetry and satisfies the premise for the multi-component theory.

However, there exists a more evolved system in which a warp is present as well: the solar system dust bands. Therefore, there must be another mechanism to create the multiple symmetry planes or components. If one considers the angular momentum associated with individual planetary orbits as well as with the entire multi-planet system, the multiple components naturally arise.

Arguments made considering the influence of a single planet on a circumstellar disk, describe a situation in which, through torquing, particle orbits will slowly become coplanar with the plane defined as being perpendicular to the angular momentum vector of the planet's orbit. This can be extended to, but becomes more complicated for, a multi-planet system as each planetary orbit has associated with it an angular momentum vector. Furthermore, there exists a total angular momentum vector for the system which defines the plane at large distances from the system, where the radii of the individual masses are comparatively small. To state more succinctly, multiple planes or components will naturally arise through the angular momentum in a multi-planet system.

Determination of the orbital angular momentum is based on the mass of the planet and the planet's orbital parameters: semi-major axis, mean rate, inclination, and longitude of ascending node. Therefore, two bodies with angular momentum vectors oriented in the same direction will have, at the very least, the same orbital plane. Using the orbital parameters of a three planet system, the planes perpendicular to the individual angular momentum vectors have been calculated and are shown in figure 4–8. The reference plane is the invariant plane associated with the system's total angular momentum vector. The values used in this plot are the same as those used in creating the middle panel of figure 4–3.

By carefully considering the information in figure 4–8 and the corresponding panel in figure 4–3. relationships can be discerned. First, if the forced orbital elements match those of one of the perturbing planets at the same semi-major axis of that planet, the test particle orbits necessarily will be precessing around a plane that is in fact perpendicular to that specific planet's orbital angular momentum vector; i.e. one of the planes shown in figure 4–8. Second, on large scales, the particle orbits will precess around an invariant plane that is perpendicular to the systems total angular momentum vector; i.e. the reference plane shown in figure 4–8.

As should be expected, other permutations of this model showed that the number of components increases with the number of planets. This is consistent with the results illustrated in figure 4–9 which show how each planet has associated with it a plane defined by its angular momentum vector.

It should be noted that, though these models have been designed to highlight the potential for warping, it could easily be imagined that a system could be composed of many planets and still show little sign of a multiple component configuration if the corresponding nodes were not aligned and the mutual inclination was low.

4.5 Model Disks

Simulations of model dust disks were created to support the suggestions made within the previous sections that the variation of forced inclination with semi-major axis is capable of producing observable warping of the type identified in the Beta Pictoris disk. These simulations involved first calculating the forced orbital parameters for a particular planetary configuration. Second, using assumed values for the proper orbital elements, a model dust disk was generated. The resulting models, shown in figure 4–9 are three dimensional mappings of surface area. The primary significance of these diagrams is in showing the symmetry planes for a disk perturbed by a particular configuration of planets.

Different views of three model disks are shown in figure 4–9. The top row depicts a disk perturbed by two planets; the second row depicts a disk perturbed by three planets; and the bottom row depicts a disk perturbed by four planets. The first column shows a face-on view of the model disks. The second column shows a nearly edge-on view, ~ 3 degrees of tilt to the line of sight. The third column shows the same image presented in the second column but stretched vertical by a factor of four. Furthermore, the images in the third column have had each vertical cut in the disk image normalized to the peak value of that particular cut. The calculated forced inclinations for each planetary configuration used in developing each disk model are shown in figure 4–3.

Warping is clearly seen in each model, especially in the stretched and normalized images. Within each image, one can easily visualize a configuration of multiple components which are offset to one another. Furthermore, the inclusion of additional planets seem to add more components and additional structure to the disk. As was explained in an earlier section, this seems intuitive if one considers this problem in terms of angular momentum.

Comparisons can also be made between the four planet simulations and the plot of angular momentum planes illustrated in figure 4–8, which are both based on the same

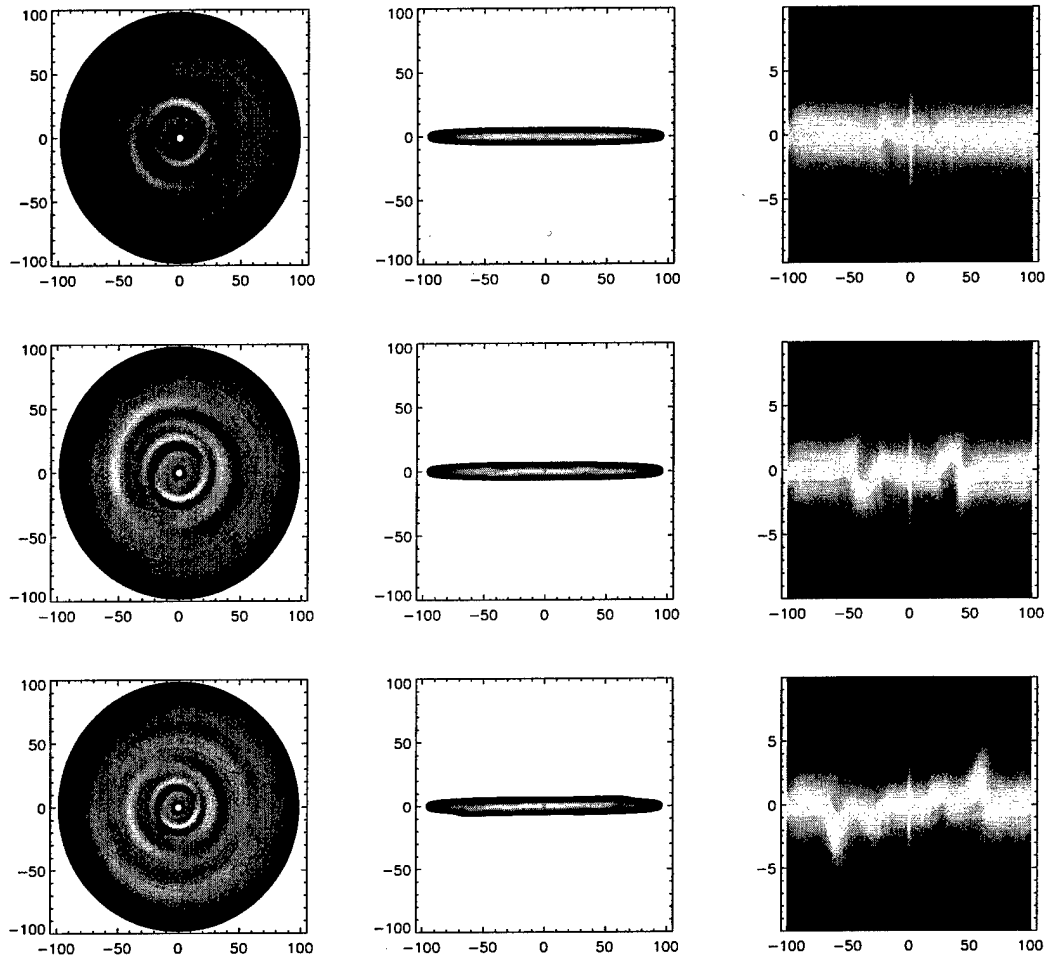

Figure 4–9: Various views of simulated dust disks. The top row is a disk perturbed by two planets, the second by three, and the bottom row by four. The first column is a face-on view, the second column is an near edge-on view (3 degrees), and the third column is normalized version of the edge-on view.

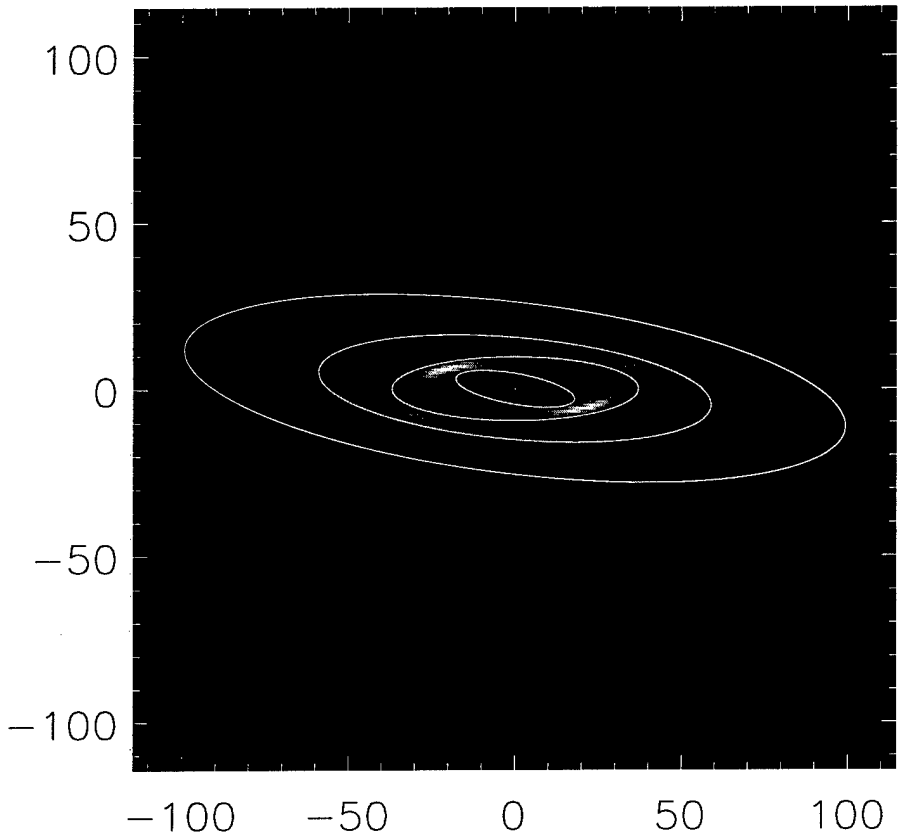

Figure 4–10: Planes defined by angular momentum of individual planets in a multi-planet system. The reference plane represents the invariant plane; that plane perpendicular to the system's total angular momentum vector.

orbital parameters. In the simulations shown in figure 4–9, multiple components can be identified. Furthermore, the number of components increases with the number of planets. This is consistent with the results illustrated in figure 4–10, which show how each planet has associated with it a plane defined by its angular momentum. This figure is a simulated disk with orbital trajectories of the perturbing planets superimposed over the disk. This illustrates how the orbital planes are coplanar to the major symmetry planes of the model dust disk.

4.6 Inclination Excitation

4.6.1 Introduction

The previous sections have discussed how the mid-plane of a circumstellar disk can be warped due to the presence of a multi-planet system. One of the requirements for producing the mid-plane warping is a relatively large mutual inclination between the planets within the system. In the first chapter, it was asserted that previous models of the disk morphology were questionable due to their unclear explanation of exactly how a single planet would become highly inclined to the disk from which it formed. If the model of the disk presented in this research is indeed more plausible, then the origin of the high mutual inclination between the constituent planets must be addressed.

Fortunately, theoretical work on orbital element excitation has already been well studied. Dermott, Malhorta, and Murray (1988) illustrated how inclination and eccentricity can be increased dramatically by the temporary capture of a satellite into a resonance. In this work it was shown that for two satellites moving on a converging orbit, the evolution that occurs during capture will increase the orbital elements. This is based on tidal interactions that work to transfer angular momentum from the inner to the outer body. Chiang (2003) discussed how this can occur in exosolar planets that are migrating in a circumstellar disk. Presented in this section is summary of the mathematics behind these theories and a discussion of the applicability to planetary systems on a scale similar to that of Beta Pictoris.

4.6.2 Excitation of Orbital Elements by Capture into Resonance

After protoplanets have formed and accretion has stopped due to the clearing of a gap in the disk, a protoplanet continues to interact with disk through tidal forces. This interaction can lead to an evolution of the protoplanet's orbit through eccentricity excitation and/or orbital migration (Lin and Papaloizou 1993).

The evolution of the orbital elements associated with planets orbiting a central star can be described through the use of Lagrange's planetary equations. Lagrange's equations for the mean rate, eccentricity, and inclination are given below:

$$\dot{n} = -\frac{3}{a^2}\frac{\partial \mathcal{R}}{\partial \lambda} \tag{4.1a}$$

$$\dot{e} = -\frac{\sqrt{1-e^2}}{na^2 e}(1-\sqrt{1-e^2})\frac{\partial \mathcal{R}}{\partial \lambda} - \frac{\sqrt{1-e^2}}{na^2 e}\frac{\partial \mathcal{R}}{\partial \varpi} \tag{4.1b}$$

$$\dot{I} = -\frac{\tan\frac{1}{2}I}{na^2\sqrt{1-e^2}}\left(\frac{\partial \mathcal{R}}{\partial \lambda} + \frac{\partial \mathcal{R}}{\partial \varpi}\right) - \frac{1}{na^2\sqrt{1-e^2}\,\sin I}\frac{\partial \mathcal{R}}{\partial \Omega} \tag{4.1c}$$

where a, e, I, ϖ, Ω, and λ are the semi-major axis, eccentricity, inclination, longitude of pericenter, longitude of ascending node, and mean longitude respectively.

The disturbing functions for m and m' were given in the previous chapter and were expressed as

$$\begin{aligned} \mathcal{R} &= G\frac{m'}{\mathbf{r}-\mathbf{r}'} - Gm'\frac{\mathbf{r}\cdot\mathbf{r}'}{r'^3} \\ \mathcal{R}' &= G\frac{m}{\mathbf{r}-\mathbf{r}'} - Gm\frac{\mathbf{r}\cdot\mathbf{r}'}{r^3}. \end{aligned} \tag{4.2}$$

From the approach of Dermott et al. (1988) these expressions can be expanded in a Fourrier series and expressed as

$$\mathcal{R} = \mu' S\cos\phi \tag{4.3}$$

$$\mathcal{R}' = \mu S\cos\phi \tag{4.4}$$

where $\mu = Gm$ and $\mu' = Gm'$. The S term can be thought of as the 'strength' of a particular term in the expansion and, to lowest order, can be given as

$$S = \frac{f(\alpha)}{a'} e^{|q_1|} e'^{|q_2|} s^{|q_3|} s'^{|q_4|} \tag{4.5}$$

where $f(\alpha)$ can be expressed as a function of Laplace coefficients and $s = \sin \frac{1}{2} I$. The values of q represent the commensurability between the periods of the planets' orbits, in the form of $p : p + q$. Using these variables, the term ϕ is given as

$$\phi = p\lambda - (p+q)\lambda' + q_1 \varpi + q_2 \varpi' + q_3 \Omega + q_4 \Omega' \tag{4.6}$$

where the value q is given as

$$q = \sum_{i=1}^{4} q_i \tag{4.7}$$

the time rate of change of the mean rate, n, can be considered to be changing due to resonance and tidal effects. Using equation 4.1a, the change in mean rate can be written as

$$\begin{aligned} \dot{n} &= -\frac{3}{a^2} \frac{\partial}{\partial \lambda} \left(\mu' S \cos \phi \right) + \dot{n}_t \\ &= -\frac{3}{a^2} p \mu' S \sin \phi + \dot{n}_t \end{aligned} \tag{4.8}$$

and likewise

$$\dot{n}' = -\frac{3}{a'^2} p \mu S \sin \phi + \dot{n}'_t \tag{4.9}$$

An expression for $S \sin \phi$, can be found by taking the second time derivative of ϕ

$$\ddot{\phi} = p\ddot{\lambda} - (p+q)\ddot{\lambda}' + q_1 \ddot{\varpi} + q_2 \ddot{\varpi}' + q_3 \ddot{\Omega} + q_4 \ddot{\Omega}' \tag{4.10}$$

Since the second derivatives of the orbital elements are generally small, they can be ignored. This allows $\ddot{\phi}$ to be expressed as

$$\begin{aligned} \ddot{\phi} &= p^2 \frac{3}{a^2} \mu' S \sin \phi + p \dot{n}_t - (p+q)^2 \frac{3}{a'^2} \mu S \sin \phi - (p+q) \dot{n}'_t \\ &= 3gS \sin \phi + F \end{aligned} \tag{4.11}$$

where the values of g and F are given by

$$g = p^2\frac{\mu'}{a^2} + (p+q)^2\frac{\mu}{a'^2} \tag{4.12}$$

$$and\ F = p\dot{m}_t - (p+q)\dot{m}'_t \tag{4.13}$$

where F is determined from the drag forces on the body. An expression for the average value of $S\sin\phi$ can be found by assuming that the $< \ddot{\phi} >= 0$ which leads to

$$\langle S\sin\phi\rangle = -\frac{F}{3g} \tag{4.14}$$

The average values for $\dot{I}$ can be expressed using the equation

$$\langle\dot{I}\rangle = -\frac{\tan\frac{1}{2}I}{na^2\sqrt{1-e^2}}\left(\left\langle\frac{\partial\mathcal{R}}{\partial\lambda}\right\rangle + \left\langle\frac{\partial\mathcal{R}}{\partial\varpi}\right\rangle\right) - \frac{1}{na^2\sqrt{1-e^2}\ \sin I}\left\langle\frac{\partial\mathcal{R}}{\partial\Omega}\right\rangle \tag{4.15}$$

(4.16)

If the problem is constrained to low inclinations and eccentricities

$$\left\langle\frac{\dot{I}}{I}\right\rangle = -\frac{\mu'}{na^2\sqrt{1-e^2}}\frac{1}{\sin^2 I}\{(p+q_1)\sin^2\frac{1}{2}I + q_3\}\frac{F}{3g} \tag{4.17}$$

similarly, the expression for the time rate of change of orbital eccentricity can be written as

$$\left\langle\frac{\dot{e}}{e}\right\rangle = -\frac{1}{na^2e^2}q_1\frac{F}{3g} \tag{4.18}$$

It needs to be pointed out that though equations 4.17 and 4.18 may seem to indicate that higher order resonances play bigger roles, through the q_i terms, this is not the whole story. The probability of capture into a resonance must be considered and this is smaller for the higher order resonances (Dermott et al., 1988).

Equations 4.17 and 4.18 show how the inclination and eccentricity can grow if there exists tidal interactions and a commensurability between the periods of the orbits. It is generally believed that planets may migrate during the planet forming epoch and are thus likely to pass through resonances. This leads to the conclusion that planets should, provided they are able to interact tidally, experience excitation to some extent. This supports the argument that a non-mutual inclination should be expected in a multi-planet system.

4.7 Conclusions

This is an investigation motivated by the observations of mid-plane warping in real circumstellar disks. Based on the idea that an observed warp is actually the edge-on projection of a multi component disk, in which the components are inclined to one another, the goal was to determine what mechanism was responsible for creating the multi-component configuration. It is suggested here that multiple planes of symmetry, or components, naturally arise in a multi-planet system due to the differences in angular momentum between the constituent planets. Material within the disk at the same radii as a planet, behaves in such a way as to precess around the plane defined by that planets' angular momentum; between the planets the behavior is more complicated as the dynamics become influenced by a combination of gravitational effects from different planets.

This qualitative argument is complimentary to the conclusions reached through perturbation theory. The results from secular perturbation theory illustrate how the forced orbital elements of the test particles are equal to the osculating elements of the perturbing planet when the orbits have a common semi-major axis. Additionally, the mass of the planets play a role in defining the region over which they impose their orbital parameters on a near-by particle.

CHAPTER 5
PRIOR OBSERVATIONS AND MODELING OF BETA PICTORIS

Though the observation of individual planets is still out of reach, recent observations of circumstellar disks have provided another possibility for planetary detection. The most well studied of the circumstellar disks is that of Beta Pictoris. Beta Pictoris is a $\sim$ 20 Myr old main sequence star with a disk that is large (extending out to $\sim$1000 AU from the central star) , bright, and viewed nearly edge-on. Even more interesting than the size and brightness of the Beta Pictoris disk are the asymmetries and features observed in the morphology of the disk - the most interesting being the warping of the inner disk.

This chapter will provide a general review of the observations made of scattered light and thermal emissions originating from the Beta Pictoris circumstellar disk. The major asymmetries observed in the disk on both large and small scales are discussed and quantified when possible. The stellar properties of Beta Pictoris, as determined through analysis of Hipparcos data, are also reviewed. These properties are important in determining characteristics like age and luminosity which play an important role in the dynamics of the material within the disk.

Past approaches to modeling the Beta Pictoris circumstellar disk are also discussed. The two primary approaches of modeling, a close stellar encounter or the presence of a single planet on an inclined orbit, are reviewed and their limitations are discussed.

The goal of this chapter is to provide the observational constraints that will be applied to the simulated circumstellar disks to be discussed in the following chapters.

5.1 The Discovery of the Beta Pictoris Disk

In 1984 Aumann presented a sample of stars with infrared fluxes measured at 12 and 25 μm from the Infrared Astronomical Survey (IRAS). Approximately 18 percent of the 280 stars in the survey showed fluxes in the infrared beyond what was appropriate

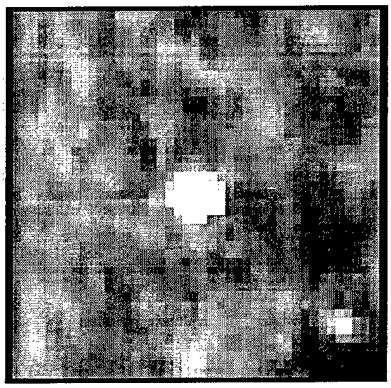

Figure 5–1: 60 μm point source image of Beta Pictoris acquired during the IRAS survey (Aumann, 1984)

for an isothermal blackbody (Aumann, 1984). The infrared excess was interpreted as the superposition of the blackbody curves of the star and the dust component or components each with a different effective temperature. Aumann further suggested that the infrared excess was the result of the star being surrounded by a cloud of cold, solid material possibly in the form of a circumstellar disk (Aumann, 1984b).

The stars possessing the brightest infrared excess were Vega (α-Lyrae), Fomalhaut, Epsilon Eridani, and Beta Pictoris. These stars are at a distance of 7.75, 7.69, 3.22, and 19.28 pc respectively. Of the three, Beta Pictoris, despite being the farthest, possessed the brightest excess (Aumann, 1985). Based on the assertion that a significant fraction of stars (approximately 30% of all F and G type stars) in the solar neighborhood were surrounded by circumstellar disks and the fact that Beta Pictoris was the best example, Beta Pictoris became a very well studied object. The 60 μm image of Beta Pictoris taken during the IRAS survey is shown in figure 5–1.

When the disk was first imaged in scattered light by Smith and Terrile (1984), the observation showed a nearly edge on disk that was resolved out to 25 arcsec ($\sim$ 500 AU). Later, higher resolution observations of the scattered light and the thermal emission from the dust disk showed structures and asymmetries that were argued to be related to the presence of a planet or a planetary system.

The remainder of this chapter will review many of the observations made describing the features, structures, and asymmetries of the Beta Pictoris dust disk. The following section

reviews the stellar properties of Beta Pictoris determined from Hipparcos measurements and analysis of the Beta Pictoris moving group. The next few sections will discuss the specific attributes of the disk and how they are determined through different observational methods. Certain features are seen only at certain wavelengths due to the differences in the sources of light – i.e. scattering of optical light verses the thermal emission of infrared radiation. Section 5.3 reviews and highlights first the scattered light images and then the thermal emission observations. Also discussed are spectroscopic observations and measurements of the photometric variations of Beta Pictoris and the associated implications to the structure of the dust disk.

5.2 Stellar Properties

Based on data gained from the Hipparcos mission, Beta Pictoris was determined to be at a distance of 19.28 $\pm$ 0.19 pc (Crifo et al, 1997) . From the distance measurements, the ratio of stellar to solar luminosity, $L/L_{\odot}$, was estimated to be 8.7. Based on analysis of the Hγ line profile, the effective temperature of Beta Pictoris was estimated to be 8200 K (Crifo et al, 1997). Furthermore, using models of main sequence and pre-main sequence tracks, Crifo et al. used the effective temperature and the luminosity to suggest that Beta Pictoris fell very close to the zero age main sequence (ZAMS) and had a mass of 1.7-1.9 $M_{\odot}$. All of the conclusions reached by Crifo et al. based on Hipparcos data were consistent with a prior spectrophotometric study (Alekseeva et al., 1996) of Beta Pictoris which found T_{eff}=7950 K, $L \approx 8\ L_{\odot}$, and a minimum age of $\sim$ 20 Myr.

The accurate determination of distance determined by Hipparcos changed prior conclusions based on an assumed distance of $\sim$16 pc for Beta Pictoris. For example, a break in the power law describing the radial surface brightness distribution determined by the observations of Golimowski et al. (1993) to be at 100 AU for a distance of 16.4 pc became 120 AU for 19.28 pc. In addition, the inner radius of the central hole of the disk, usually estimated as being at 30 AU, became 35 AU. Within this chapter, all distance measurements are based on the currently accepted distance of 19.28 pc as determined from Hipparcos.

A separate determination of the age of Beta Pictoris was made based on a study of the Beta Pictoris moving group (Navascues et al., 1999). This study was based on determining

the stellar properties of several observed stars deemed dynamically related to Beta Pictoris. The mean age of the group was estimated as 20±10 Myr. Assuming all of the stars within the group to be coeval, this age is applicable to Beta Pictoris as well.

5.3 Observations

Following the initial measurement of the infrared excess associated with Beta Pictoris and the interpretation that the excess was associated with a disk of material surrounding the star, a direct image of the disk became a goal of the astronomical community. The first images were obtained through observations of scattered light using the technique of coronagraphy. This approach observed the dust disk by blocking out the light from the star that would, in normal circumstances, overwhelm the light scattered from material within the disk. As will be discussed in the following sections, early observations using this method showed a debris disk extending out nearly 48 arcsec ($\sim$ 900 AU). Also seen in these images were asymmetries in the disk that began the debate over the possibility of a planetary perturbation being the source of the observed structure.

Observations of the thermal emissions of the debris disk, particularly around 10 μm, precluded the need for techniques such as coronagraphy, as the intensity of the thermal emissions of the dust was comparable to that of the photosphere of the star. Thermal images of the debris disk were acquired later and also showed asymmetries. However, the features associated with the thermal emissions were not the same as those seen in scattered light. The asymmetries occurred on different scales and were, in some instances, reversed from the scattered light images.

Other observations were also taken that provided more clues to the composition and dynamics of the dust disk. For instance, spectroscopic variations were used to argue the presence of cometary bodies which were evaporating. Also, measurements of photometric variations were used to validate the idea that the the Beta Pictoris disk possessed significant asymmetries in the azimuthal distribution of dust.

This section gives a brief discussion of several of the significant observations made with the above techniques and discusses their significance in terms of providing constraints to a

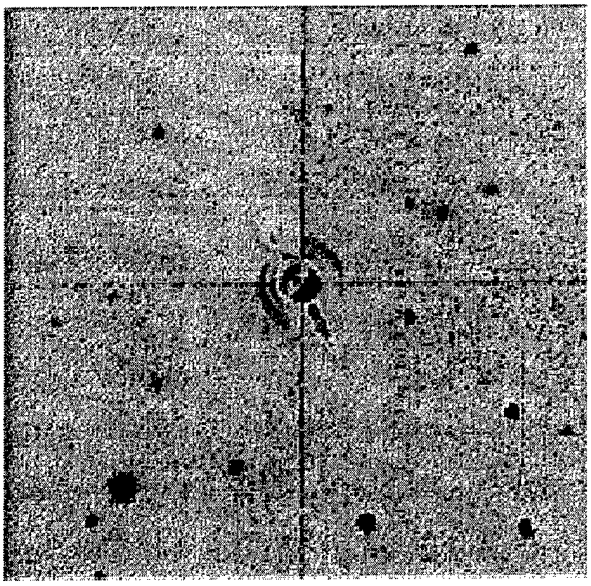

Figure 5–2: 890 nm coronagraphic image of Beta Pictoris in scattered light (Smith and Terrile, 1984).

complete dynamic model of the dust disk.

5.3.1 Scattered Light

In 1984 Smith and Terrile produced the first direct image of the Beta Pictoris disk using a coronagraph at 890 nm. The image showed what was interpreted as an edge-on disk extending to 25 arcsec ($\sim$ 500 AU). Their coronagraphic image is shown in figure 5–2. The mask within the coronagraph covered the central 7 arcsec ($\sim$ 135 AU) of the image and therefore the central region of the disk was not imaged. However, it was inferred from extrapolation of the optical thickness that there exists a central hole within the inner 35 AU. The optical thickness was estimated using the observed brightness distribution and assumptions about the physical properties and size distribution of the scattering particles. The argument for the hole was based on the fact that if the optical depth continued to increase at the estimated rate, a disk approaching closer than 35 AU would be inconsistent with observed attenuation of the star's radiation. Smith and Terrile also claimed that the disk was wedge-shaped, having a width that increased with radius; measurements of the angle associated with the wedge indicated that the particles within the disk were inclined at 5° or less. It was also inferred that because no reddening was observed in multicolored

photometry, the size of the emitting particles must be much larger that the wavelength of the light observed; $\lambda \ll d \sim$ few μm. Smith and Terrile argued that the Beta Pictoris disk was likely in the process of planetary formation due to the presence of the inner hole, which is best explained through clearing mechanisms associated with the presence of planets, and the fact that the circumstellar disk takes the form of a flattened disk, which is consistent with theories of planetary formation.

Table 5–1: Index for Radial Brightness Profile

Authors	Range(AU)	Band	NE slope	SE slope	FWHM
Smith and Terrile (1984)	120-480	R	-4.3	-4.3	...
Parsce and Burrows (1987)	120–960	BVRI			
Artymowicz et al. (1989)			-3.6	-3.6	increasing with r
Lecavalier des Etangs (1993)	48–360	BVRI	-3.6	-3.6	...
Golimowski et al. (1993)	48–120	R	-2.38 ± 0.72	-1.91 ± 0.89	...
	120–360		-3.7 ± 0.1	-4.0 ± 0.2	increasing with r
Kalas and Jewitt (1995)	60–120	R	-2.4 ± 0.24	-2.47 ± 0.36	43 AU
Moulliet et al. (1997)	30–48	K'	-1.0 ± 0.8	-1.0 ± 0.8	24 AU
	48–77		-1.3 ± 0.2	-1.2 ± 0.2	24 AU
	77–120		-2.5 ± 0.4	-2.9 ± 0.5	24 AU
Heap et al. (2000)	32–74		-1.28 ± 0.04	-1.12 ± 0.01	$\sim$ 20 AU
	56–120		-1.79 ± 0.01	-1.74 ± 0.04	$\sim$ 20 AU

The above distances were corrected to reflect the Hipparcos distance to Beta Pictoris of 19.28 pc

The surface brightness profile measured by Smith and Terrile decreased as a power law with radius with an index of -4.3 over the range of 120 to 480 AU. Additional measurements (Parsce and Burrows, 1987; Artymowicz et al., 1989; Lecavalier des Etangs, 1993) were made that further refined the power law index for the brightness profile beyond 120 AU. The later measurements showed an asymmetry between the extensions in both total brightness and in the power law describing the brightness profile. A summary of the indices for the power laws describing the radial brightness distribution as determined in different observations is given in table 5–1

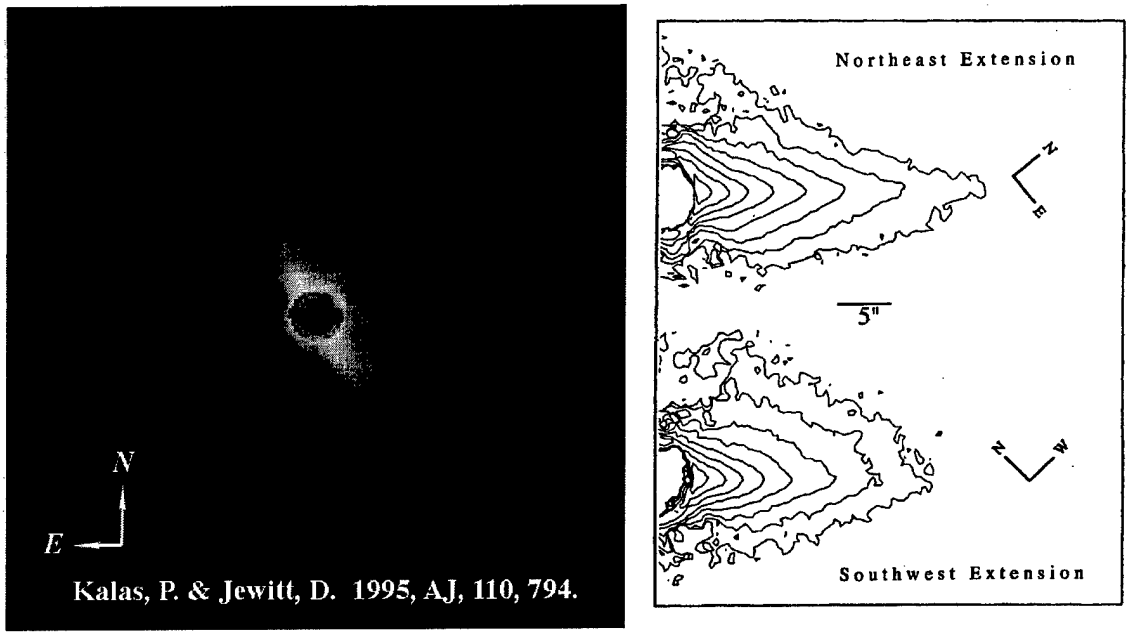

Figure 5–3: Kalas and Jewitt (1995): (left) Coronagraphic image of Beta Pictoris in scattered light. (right) Contour plot of surface brightness of the NE and SW extensions. The 'butterfly' asymmetry can be seen as the asymmetry in width perpendicular to the mid-plane.

The first images of the disk within 6 arcsec (120 AU) were produced using observations made with the Adaptive Optics Coronagraph (AOC) by Golimowski et al. (1993). The *R*-band images showed a transition in the power law describing the surface brightness of the mid-plane at 6 arcsec (120 AU). The change in surface brightness indicated a change in the nature of the disk at this distance. This change was either in the form of the optical properties of the material and/or a change in the number density. This conclusion was consistent with models developed earlier (Backman et al., 1993) describing the Beta Pic disk as having two components; the inner disk (the region within $\sim$ 100 AU) having lower density and either smaller particles or a less steep spatial gradient.

The break in the power law describing the radial surface brightness distribution was further verified by Kalas and Jewitt (1995) using an *R*-band coronagraph on the University of Hawaii 2.2 m telescope on Mauna Kea. Their image is shown in figure 5–3 along with a contour plot of the surface brightness. Once again, a transition in the disk at 6 arcsec was observed. Furthermore, five major asymmetries were highlighted. The first was the overall size of the NE and SW extensions of the disk. The NE extension was measured out

to 48 arcsec (925 AU) and the SW to only 40 arcsec (770 AU) indicating an asymmetry of approximately 20%. The second was an asymmetry in the overall brightness as measured along the mid-plane. At distances greater than 20 arcsec from the star, the NE extension is brighter along the mid-plane than is the SW for the same distance from the star. The third asymmetry is in the width of the extensions. At distances greater than 7 arcsec, the FWHM increases with radius. The fourth asymmetry was described as the 'butterfly asymmetry' and referred to the extensions being fatter on one side of the mid plane than on the other. The fifth asymmetry was described as the 'wing-tilt asymmetry' and referred to the fact that the mid-planes of the NE and SW extensions were inclined to one another by $\sim$ 1.3 degrees. Each of the asymmetries were scrutinized to determine whether they were associated with a true physical asymmetry in the disk, or if they represented an optical effect. Kalas and Jewitt concluded that all were true physical asymmetries except for the wing-tilt asymmetry which was found to be consistent with observing light scattered from a disk inclined to the line of sight. It was also determined, based on integrated brightness, that the overall number of scattering particles in each extension were comparable. This implied that the asymmetries represented a difference in the spatial distribution of dust rather than a depletion. Kalas and Jewitt also stated that the cause of the asymmetries remained a mystery. This conclusion was based on considering two possible sources: a planetary perturbation or a close stellar encounter. The planetary scenario did not seem reasonable because a planetary perturbation was unlikely to cause asymmetries on such large scales (out to $\sim$ 1000 AU). The stellar encounter seemed unlikely based on a statistical analysis of the probability associated with such an event and the fact that no candidate star has been observed.

High resolution observations were reported by Heap et al. (2000) using data obtained by the Space Telescope Imaging Spectrograh (STIS) on HST. The observations were made using a filter that covered 200 to 10000 Å, and achieved a resolution of $\sim$ 0.1". The circumstellar disk was detected as close to 0.75" which corresponds to $\sim$ 15 AU. The STIS images showed a warped disk with a maximum amplitude of $\sim$ 1.5 AU at $\sim$ 3.6 arcsec (70 AU) as seen in figure 5–4. It was shown that the observations could be matched by modeling the overall disk image as the projection of two disks, one inclined to the other. This was

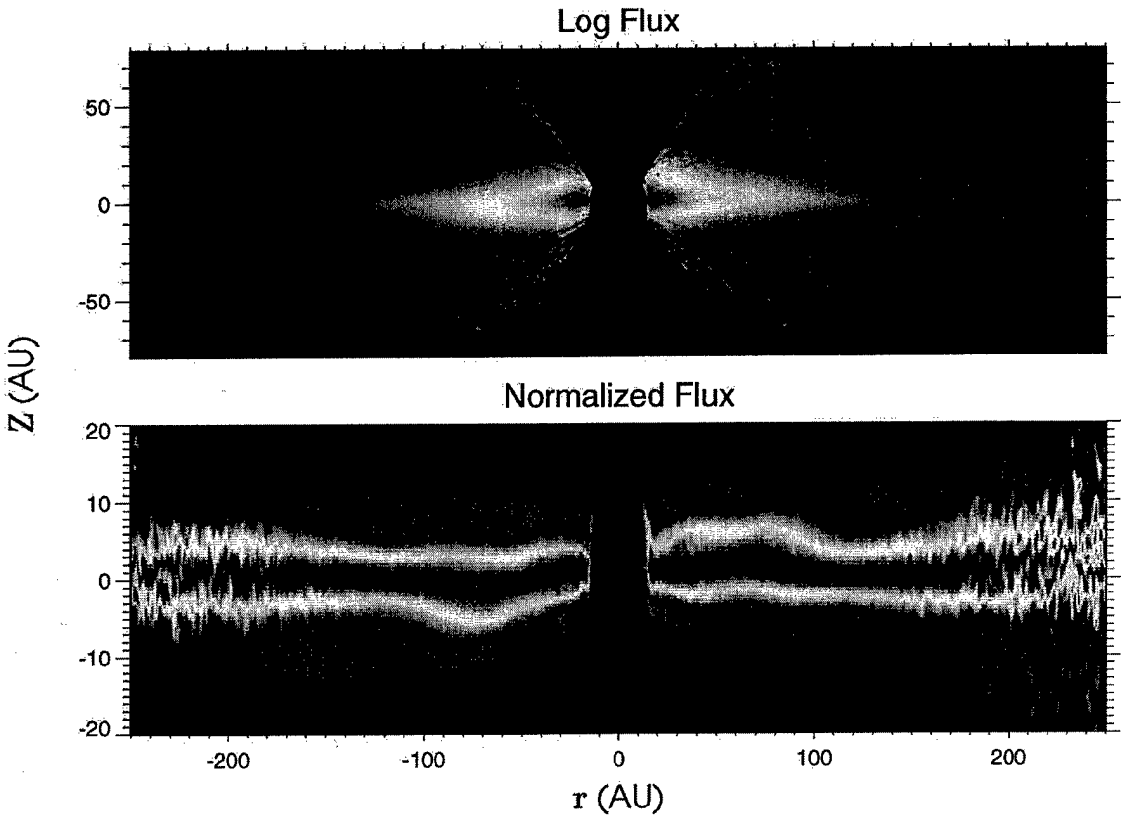

Figure 5–4: HST visible light image from the Space Telescope Imaging Spectrograph (STIS) clearly showing the warping of the inner disk (Heap et al., 2000). The bottom image shows the same data as the top, but each vertical slice of the image has been normalized to the peak value of that slice.

illustrated by decomposing the vertical brightness profile of the overall disk images into two symmetric profiles corresponding to a brighter main component and a fainter inclined component. This is illustrated in figure 5–5. The best fit corresponded to the inner, fainter, disk being inclined to the main component by 4.6 degrees. Heap et al. also suggested that the warp is associated with the presence of a planet and the radial extent of the warp depends on the orbital parameters of the planet (Larwood and Papaloizou, 1997). The analysis showed that the warp scaled with the mass of the planet, the semi-major axis or the planetary orbit, and the age of the system. Using the estimated age of 20 Myr, the planet ranged from 17.4 M_J at 5 AU to 0.17 M_J at 50 AU. The analysis was constrained by the fact that stellar radial velocity variations are not observed which implies $M_P/M_\star \leq 0.01$.

5.3.2 Thermal Emissions

The disk of Beta Pictoris was first resolved in the mid-infrared by Telesco et al. (1988) using a 20-pixel bolometer array on the Infrared Telescope Facility (IRTF) on Mauna Kea. The measurements made at 10 and 20 μm suggested sub-micron particle sizes and an inner hole with radius of $\sim$ 40 AU. A later observation (Telesco and Knacke, 1991) clearly identified the presence of the silicate feature. Furthermore, it was suggested that the disk could also include particles with radii greater than 1 μm. An extension of this work (Knacke et al., 1993) used extensive spectroscopic data to constrain a model of the disk. The results suggested a two component disk with inner radius of 30 AU and a transition region at 80 AU. It was also concluded that the silicates in the disk consisted of a mixture of materials similar to that observed in comets.

Lagage and Pantin (1994) presented an infrared image of the inner part of the Beta Pictoris dust disk by observing the thermal emissions at 11.9 μm using the 3.6 m ESO telescope. The image is shown in figure 5–6. They achieved a spatial resolution of 0.3 arcsec which corresponds to $\sim$ 5 AU. The observations showed the dust was asymmetrically distributed around the star and depleted within 2.5 arcsec (48 AU). Their analysis showed the dust density distribution experienced a transition at 6 arcsec (120 AU) which was attributed to the sublimation of ice particles. They suggested that the inner region, $\leq$ 48 AU, experienced a significant depletion in dust, but no strict void. This inner depletion was

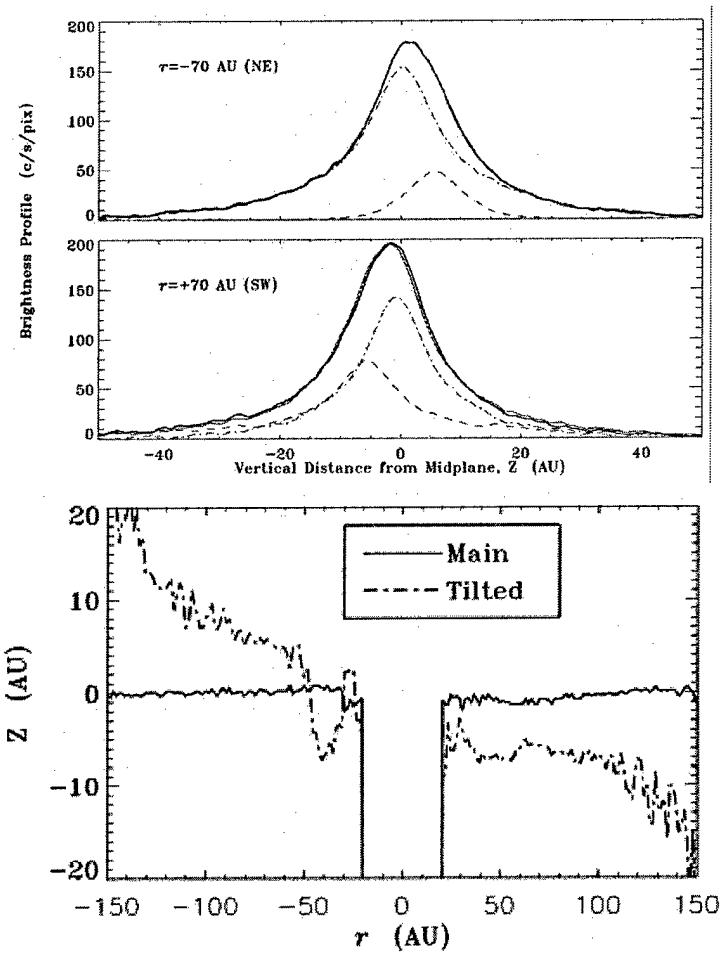

Figure 5–5: (top) Decomposition of the vertical brightness profile in to two symmetric profiles associated with the faint inner disk and the main disk. (bottom) Plot illustrating the inclination of the inner disk relative to the outer main disk (Heap et al., 2000).

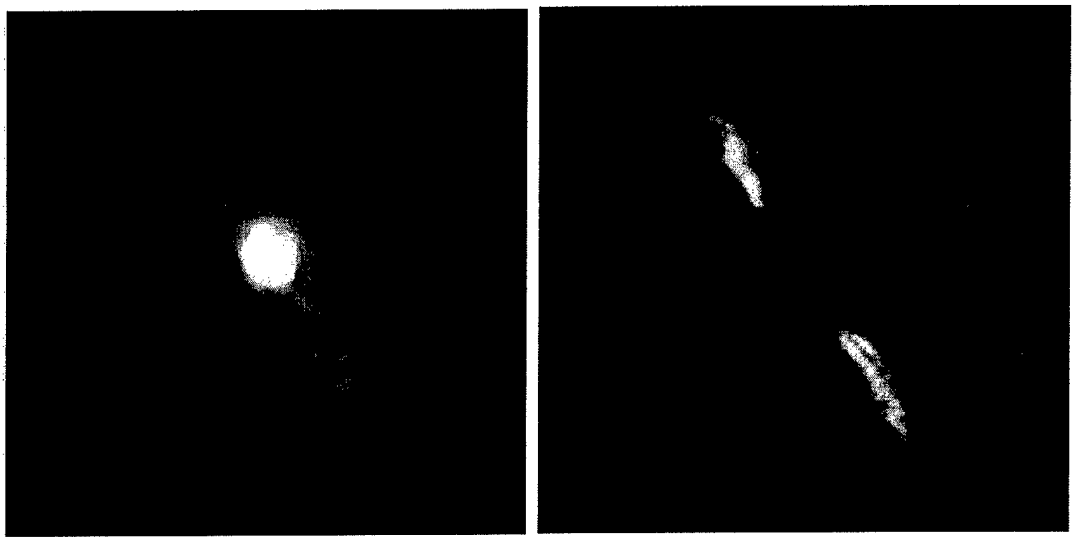

Figure 5–6: (left) 11.9 μm image of thermal emissions from Beta Pictoris (Lagage and Pantin, 1994). (right) 2.120 μm coronagraphic image using the ESO 3.6 m telescope with adaptive optics (Moulliet et al., 1997).

attributed to the dust being trapped in gravitational resonances or being swept up by a planet. They also provided a qualitative argument that a planet with a modest eccentricity could produce the asymmetries observed.

The inner disk was later detected down to 1.5 arcsec from the star and extending out to 6 arcsec using a coronagraph at 2.120 μm on the ESO 3.6 m with adaptive optics (Moulliet et al., 1997). Previous observations showed that the radial surface brightness began a transition at $\sim$ 120 AU, but Mouillet et al. showed that the distribution not only experienced a transition at 120 AU but another at $\sim$ 65 AU such that a single power law could not reasonable fit the entire radial distribution. The power law developed to fit the observations indicated that at 6 arcsec (120 AU) the distribution becomes flatter as it approaches the star. It was also shown that the FWHM of the vertical profile stayed constant over 2 arcsec to 5 arcsec.

Pantin et al. (1997) reported mid-infrared observations of the inner disk which they used to derive the 0-120 AU density profile. The observations were made using the Thermal Infrared Multi Mode Instrument (TIMMI) mounted on the ESO 3.6 m telescope at 11.9 μm. The image is shown in figure 5–7. The density profile was calculated by assuming the composition of the dust material and in turn developing a thermal model of the disk. The

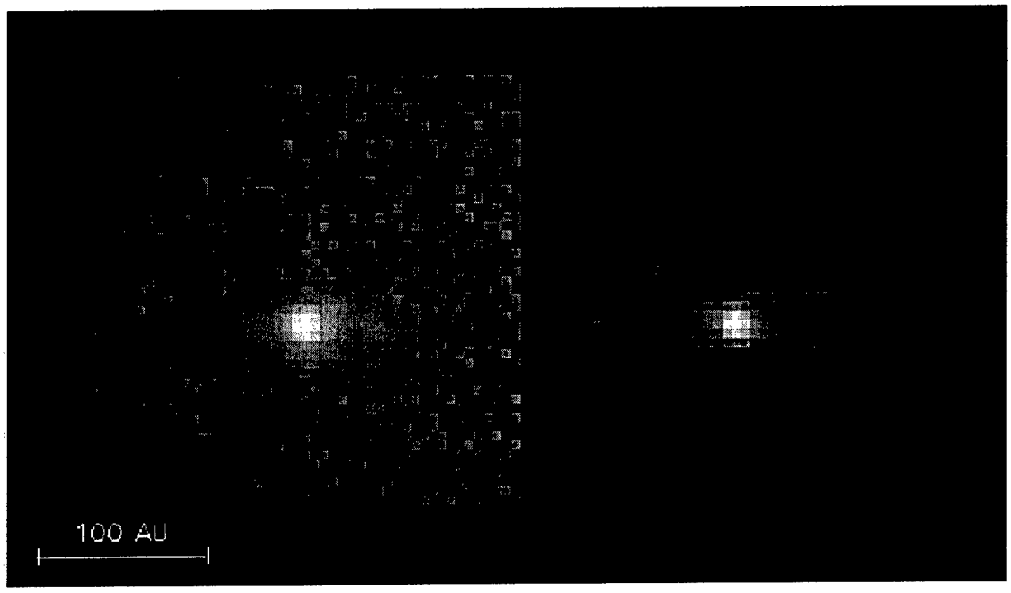

Figure 5–7: 12 μm image of Beta Pictoris using the Thermal Infrared Multi Mode Instrument (TIMMI) on ESO 3.6 m (Pantin et al., 1997).

material composition was based on prior observations (Telesco et al., 1988; Knacke et al., 1993; Aitken et al., 1993) mostly related to detection of the silicate feature. A model based on a single grain composition proved unable to make a good fit to the data, but a model with two components was more successful. The transition between the components was defined by the ice boundary estimated to be at $\sim$ 90 AU beyond which the particles contain some ice.

5.3.3 Spectroscopic Observations

An effort to combine ground and space based spectroscopic observations of the Beta Pictoris disk was performed by Lagrange et al. (1996) to test the Falling Evaporating Body (FEB) scenario. The FEB theory proposes that comet sized bodies on near circular orbits become star-grazers due to planetary perturbations. These bodies are generally thought to be asteroid-like with an icy nucleus rather than fully icy comets (Karmann et al., 2001). As these bodies move near the star they begin to evaporate. If this occurs during a transit across the line of sight, it will produce observable absorption lines with short timescale variations.

Velocities and timescales for variability were determined by looking at absorption lines associated with Ca II, Mn II, Fe II, Al III, and Al II. Their approach was based on correlating

the observed red-shift with variability timescales, line width, and line depth. Two regimes were reported: 1) low velocity, slowly varying lines and 2) high velocity, rapidly varying lines. The high velocity lines were determined to be consistent with and well explained by the evaporation of single bodies within 10 stellar radii. The low velocity lines were best explained by the evaporation of families of bodies crossing the line of sight at large distances, $\sim$ 20 - 30 stellar radii, from the star. Therefore the conclusion reached by Lagrange et al. was that the variable features could be interpreted as signs of km-sized solid bodies on star grazing orbits evaporating near periastron - the FEB scenario. It was also argued that, because all of the variability was seen on relatively short time scales, mean motion and not secular resonances were the dominant factor (Lagrange et al., 1996).

It was also noted that the ratio between red-shifted and blue-shifted events was not 1:1. In fact, for every one blue-shifted event observed, nine red-shifted events were recorded. It was suggested (Artymowicz, 1997) that this was indicative of a preferential orientation for the orbits of the solid bodies.

5.3.4 Photometric Variations

Photometric variations of Beta Pictoris were studied (Lecavalier des Etangs et al., 1995) using data compiled from near-continuous observations made between 1975 and 1992. A variation was detected with a timescales of $\sim$ 1000 days and an amplitudes of $\sim$ 0.01 magnitudes. It was suggested that this variation was attributed to inhomogeneities in the azimuthal distribution of dust possibly caused by the presence of a planet or planetesimals. Another short term variation was observed in November of 1981. The timescale associated with this variation was $\sim$ 30 days and reached a maximum amplitude of 0.04 magnitudes. It was proposed that this short time scale variation was the result of a passage of a planet – an occultation of Beta Pictoris by a planet roughly the size of Jupiter. The region around the planet was considered to be relatively clear of dust due to accretion or ejection of the particles and this resulted in the brightness enhancement.

5.4 Dust Properties

This section provides a brief review of the properties of the dust comprising the Beta Pictoris circumstellar disk. It is these properties, based on observation, that will be used in the models described in the following chapters.

5.4.1 Dust optical properties

The presence of the silicate feature first identified by Telesco and Knacke (1991) indicated that the particles were likely similar to material common within the solar system. Prior to 1998 the material was generally modeled as Mie spheres of astronomical silicates whose optical material properties were described by Draine and Lee (1984). However, Li and Greenberg (1998) performed a more detailed analysis of the optical properties of the dust within the Beta Pictoris system and concluded that the dust had a more complicated structure and hence interacted with light in a way much different than what would be expected for homogeneous spheres.

Li and Greenberg (1998) proposed that the dust material within Beta Pictoris is cometary in origin and consisted of aggregates of particles with silicate cores and an organic refractory mantle. Furthermore, these particles are highly porous, $\sim P \geq 0.95$. It was also suggested that in the outer regions, the particles possessed a water dominated ice-mantle. In general Li and Greenberg asserted that the material is created near the central star due to the evaporation of the comets and distributed throughout the disk via radiation pressure.

5.4.2 Dust Particle Size

Typical particle sizes determined from past observations and analysis are thought to have a radius of ≈ 1 to 3 μm (Artymowicz, 1997). This estimate was based on both dynamical considerations and constraints from the 10 μm emissions. Artymowicz suggested that particles smaller than ~ 1 μm are quickly removed from the system by radiation pressure. Furthermore, the particles must be $\sim$2 μm to stay in orbit long enough to produce the 10 μm emissions. Further analysis of the typical particle size is addressed in chapter 7.

Figure 5–8: HST WFPC2 and UH images after subtraction of a smooth model disk. The lines show the corresponding brightness enhancements located at $\sim$ 750 AU (Kalas et al., 2000).

5.5 Models

The most extensive numerical modeling done on the dust disk of Beta Pictoris has been based on the presence of a single planet inclined to the plane of the disk or due to the close encounter with another star. An alternative approach was based on considering a driving force produced by stellar radiation (Armitage and Pringle, 1996). In this theory, stars with luminosities greater than $10L_{\odot}$ are expected to produce warps in circumstellar disks. However, when the Hipparcos data determined a new distance to Beta Pictoris, and thus a new value for luminosity, this theory no longer seemed applicable (Heap et al., 2000).

This section discusses first the theory of a close stellar encounter and then the models based on a single planet on an inclined orbit.

5.5.1 Close Stellar Encounter

Kalas et al. (2000) compiled images from three different telescopes using four different instruments: Las Campanas 2.5 m, University of Hawaii 2.2 m, HST Planetary Camera, and HST Wide Field Camera. After subtracting a smooth, symmetric model disk, bright features located $\sim$ 3.9 arcsec ($\sim$ 750) AU from the star in the NE extension were identified in

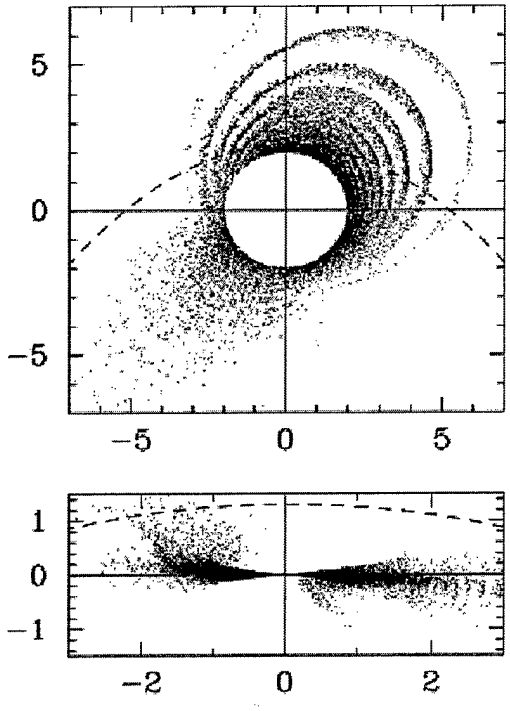

Figure 5–9: Results of a numerical simulation of a close stellar encounter with a disk of planetesimals. (Kalas et al., 2000).

all four images. These brightness enhancements were interpreted as signs of a ring system. Furthermore, since the features were not seen in the SW extension, it was proposed that the rings were not centered on the star. Therefore, it was suggested that these features were the edge-on view of an asymmetric ring system within the disk. Two of the images used for the analysis are shown in figure 5–8.

To explain the nature of the ring system, numerical simulations were performed to study the effect of a close stellar encounter with a quiescent disk of planetesimals (Kalas et al., 2000; Larwood and Kalas, 2001). The model included 10^6 collisionless particles initially in circular orbits about a point-mass potential. The stellar flyby consisted of a secondary point mass, $M \sim 0.3M_\star$, on a parabolic orbit which was not coplanar to the original plane of the disk.

The encounter resulted in the planetesimals being scattered outward several times the initial disk radius but maintaining a well defined disk structure. Large scale ring structures formed but dissolved after about 10^5 years, or 10 orbital periods at 500 AU, due to phase mixing – the dispersal of particles based on differences in their periodicity. It was suggested

that the observed ring structure was a tightly wound spiral pattern resulting from the induced motion of the primary star by the perturber (Larwood and Kalas, 2001). The results of one simulation are shown in figure 5–9.

Multiple simulations were performed and artificial isophotes were created and compared to observations of Beta Pic. The best fit occurred for an encounter distance of $\sim$ 700 AU. For this value the probability of such an encounter is very low, $\sim$ 0.01% in 10^6 years (Kalas et al., 2000). Furthermore, no suitable candidate has been identified. Kalas et al. (2000) suggested that if Beta Pic formed with a bound companion that the probability increased by an order of magnitude. However, no companion for Beta Pictoris has been identified.

Kalas et al. (2000) also suggested that a close stellar encounter could provide an explanation for the observed warp in the disk. It was argued that a non-coplanar flyby would increase the inclination and eccentricity of the planetesimal orbits. This would create a second plane whose edge on projection, when coupled with the main disk, would create the appearance of a warp.

5.5.2 Single Planet on an Inclined Orbit

Based on the observation of a possible occultation of Beta Pictoris (Lecavalier des Etangs et al., 1995) and the observed high rate of cometary infall (Lagrange et al., 1996), Moulliet et al. (1997b) suggested that a planet was likely present and performed numerical simulations to illustrate the effects of a single planet on a circumstellar disk. The model was based on smoothed particle hydrodynamics with pressure and viscous forces removed. They also made the assumption that the disc shape, observed through the small particles, was driven by gravitational effects on larger, longer lived particles.

The disk model consisted of 15,000 particles initially on circular orbits populated in such a manner as to be consistent with an assumed matter distribution. A planet was introduced with an eccentric orbit inclined to the disk mid-plane. Moulliet et al. (1997) suggested that as a result of the break in symmetry, a deformation in the disk occurs that is directly related to the planets inclination. The results of one simulation are shown in figure 5–10.

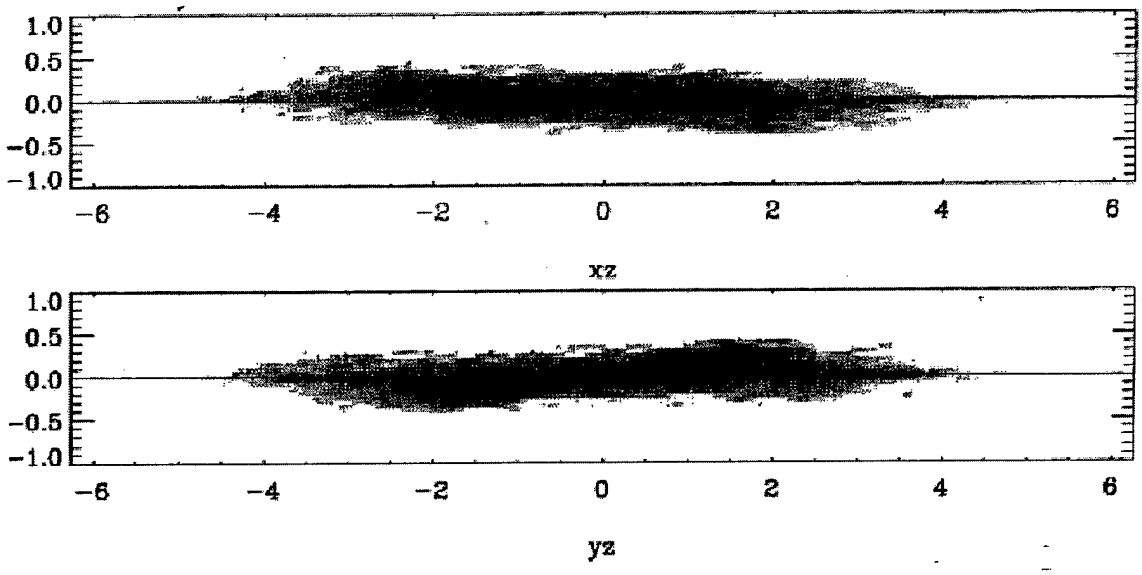

Figure 5–10: Results of a numerical model involving 15,000 particles in a disk perturbed by a planet on an inclined orbit (Moulliet et al., 1997).

By calculating the flux due to stellar light being scattered from the dust in the disk and integrating along a line of sight, Moulliet et al. (1997b) determined an apparent surface brightness distribution which they compared to previous coronagraphic observations (Moulliet et al., 1997). Using the constraints associated with the observations and the fact that no radial velocity variations have been observed for Beta Pictoris, it was determined that a planet should be located between 1 and 20 AU, be inclined at $3-5°$, and have a mass between 10^{-2} and $10^{-5}M_{\star}$. It was also suggested that the planet should have a significant eccentricity to explain the high rate of cometary infalls.

Augereau et al. (2001) presented a 'complete model' of the Beta Pictoris disk that successfully accounted for the major asymmetries seen in both scattered light and thermal emissions. The model was based on a disk of planetesimals extending out to 150 AU perturbed by a single planet on an inclined orbit. The small scale asymmetries, $\leq$ 120 AU, were explained through the gravitational perturbation of the planet. The large scale asymmetries were explained by radiation pressure extending the distribution of small particles, created by collisional processes, far beyond that of the parent body disk.

The modeling approach was to construct a parent disk from 100 concentric rings each composed of 10^4 particles. The disk was allowed to phase mix for 20 orbital periods. The

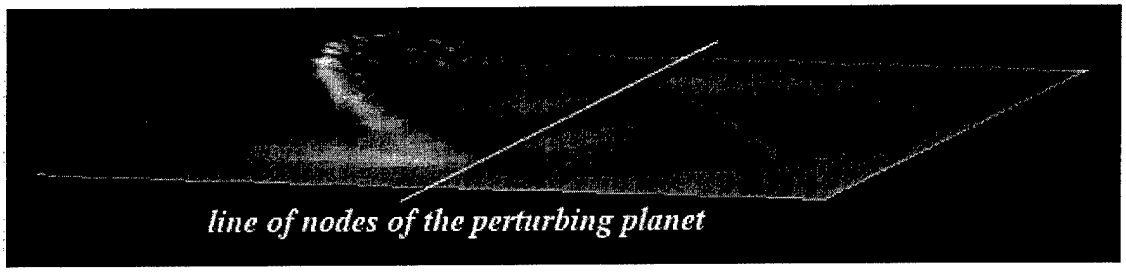

Figure 5–11: A plot of the vertical position of the mean parent body disk mass (Augereau et al., 2001). The maximum is at a distance corresponding to $\sim$ 75 AU.

orbital planes were precessed based on the local precession rate determined by the dynamical influence of the planet. The disk was then allowed to phase mix again. It was then assumed that each parent body produced a distribution of grains each with a specific value of β, the ratio between the force due to radiation pressure and the force due to gravity from the star. The spatial distribution of small particles was determined for 11 different values of β running between 0.001 and 0.45. Simulated images were made for each value of β. The final image was a superposition using weighting factors based on the assumed grain size distribution.

Augereau et al. (2001) claimed that the presence of the planet causes the parent body disk to precess differentially. The inner region of the disk becomes coplanar with the planet due to its more rapid rate of precession. This means that the extent of the warp is based on the precessional rate and the age of the system, suggesting that the warp propagates outward. A plot illustrating how the mass of the parent body disk was distributed is shown figure 5–11.

The best fit to observations occurred with a perturbing planet of mass $M/M_\star = 10^{-3}$, semi major axis, $a = 10$ AU, $e = 0.0$, and $I = 3°$.

5.5.3 Limitations of Models

The modeling of the Beta Pictoris disk that has been discussed in this chapter has been based on a single planet with an inclination relative to the disk. However, these models do not address the issue of how such a configuration could arise. An alternative approach is to consider a system of two or more planets that could produce secular perturbations.

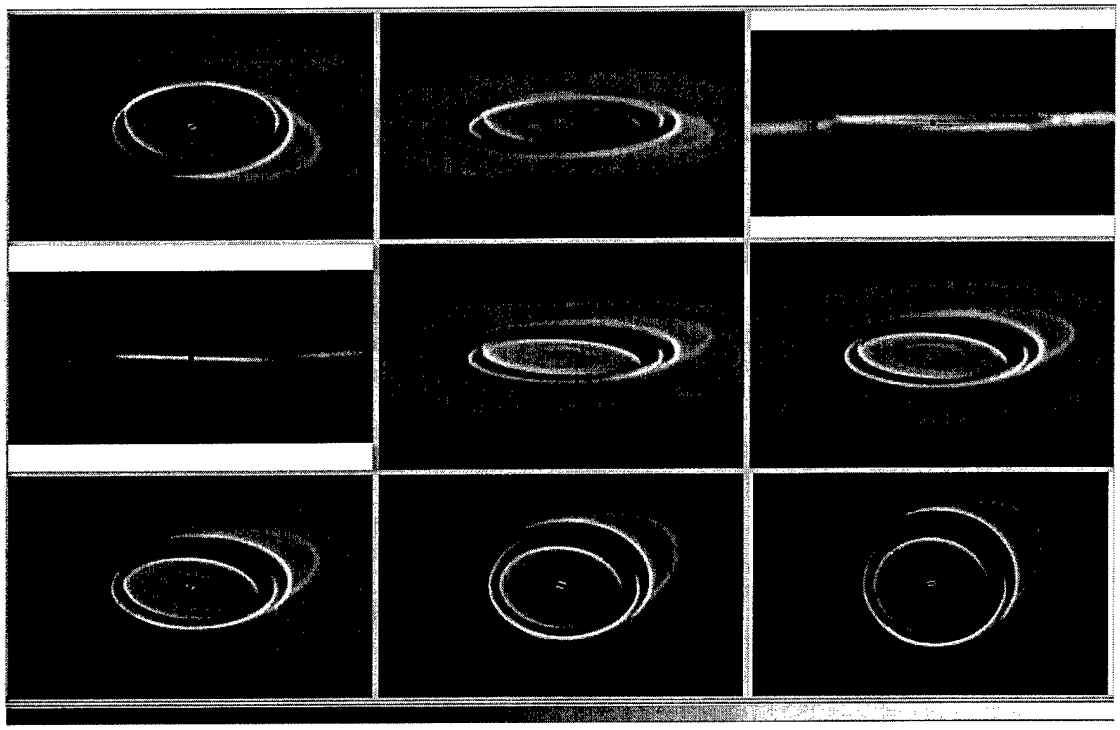

Figure 5–12: Visualization of a SIMUL model representing the distribution of surface area. The upper left frame shows the bottom of the disk, with the disk tilted 30 degrees from edge-on. Going left to right and top to bottom, the tilt angle -15, -3, 0, 15, 20, 30, 45, and 60 degrees. The images clearly show the resulting two disk structure.

As was discussed in chapter 3, secular perturbation theory is a well-developed theory used for analyzing the long-term orbital perturbations in a many-body system. This theoretical framework has been applied extensively to problems within the solar system. In fact, analysis of the secular perturbations arising from Jupiter and Saturn can be shown to create a forced inclination that varies with semi-major axis, a, (see for example Dermott et al. (1984, 1985); Murray and Dermott (1999)). It can also be shown that this variation of forced inclination can produce a warp in a dust disk.

In this chapter it was shown that warps can be simulated by considering the edge-on view of a multi component system in which the components are concentric and have a non-zero mutual inclination. Therefore, any modeling technique utilized must produce results consistent with this effect. In other words, the approach used in this research should ideally reproduce the multi-component system.

One of the tools utilized in this research, which will be discussed in detail later, calculates the distribution of surface area based on the functional form of the orbital parameters with respect to semi-major axis. One such realization is shown in figure 5–12. This image was created using Beta Pictoris with a two planet system. The orbital parameters were those of Jupiter and Saturn, but with the Saturn-like planet pushed out to 20 AU. This image illustrates how the planes of symmetry of a disk model are influenced by secular perturbations associated with planets of relatively low inclination. Furthermore, it illustrates how such a configuration can produce a structure consisting of two disks, one inclined to the other. These results are the same basic results achieved in the other models, but without the less plausible scenario of having a single planet on an orbit inclined the disk from which it formed.

CHAPTER 6
THE MODELING PROCESS

6.1 Introduction

Previous modeling of the Beta Pictoris dust disk consisted primarily of N-body or hydrodynamic analysis. These approaches consist of assuming an initial configuration for the dust particles or their parent bodies, simulating key physical processes, and allowing the system to evolve with time from t_0 to t. The approach taken in this research is different in that the simulation process does not track and record the evolution of the particle orbits or the distribution of particles within a region of space, but instead attempts to directly calculate the overall effect of gravitational perturbations on long timescales. In other words, the modeling described here directly calculates the configuration at time t. This chapter will discuss the simulation process utilized in this research in developing a disk model.

6.2 SIMUL

Dynamic modeling of the dust cloud within the solar system, the zodiacal cloud, has been studied for many years and many tools have been developed to facilitate this research. In particular, a program called SIMUL was developed initially by Dermott and Nicholson (1989) and then by Xu et al. (1993) to construct a three-dimensional numerical model of the solar system dust bands and illustrate their link to the major Hirayama asteroid families.

Key to SIMUL is the idea that a disk is a distribution of many dust particle orbits, along which the dust particles are distributed. The characteristics of an orbit are defined and or influenced by both initial conditions and other perturbing forces. The dust particle orbits are described by the standard orbital elements of semi major axis, eccentricity, longitude of pericenter, inclination, and longitude of ascending node. Furthermore, the observable orbital elements, the *osculating* elements, are associated with two components: the *forced* elements and the *proper* elements.

As stated before, the forced and proper elements can be linked to the perturbing planets or the conditions in which the dust was created. This implies that characteristics of a particle's orbit can be determined by knowing how the dust composing the disk was created and how the orbit is perturbed by massive bodies. Furthermore, these two components are not coupled and can be determined independently. The forced elements are determined by performing the calculations described in chapter 3. The proper elements are determined by making assumptions based on what we know of dust creation within the solar system extrapolated to other environments.

The distribution of the orbits in space is determined by both the distribution of the bodies creating the dust and the way in which the dust is affected by radiation affects. The dust is generally assumed to be created from the destruction of larger bodies. After creation, the dust, depending on the grain size and density, will either stay in the same orbit, be blown out of the system by radiation pressure, or spiral into the star by PR drag. These factors will determine the spatial distribution of dust of a given size as a function of distance from the star.

The primary function of SIMUL is to produce a three dimensional mapping of total surface area associated with dust particles for any specified value of Beta. As input, SIMUL requires either tabulated or functional forms of forced and proper orbital elements. It also requires the radial distribution of dust particle orbits which is influenced by the interaction of the dust with the radiation from the star.

The models produced by SIMUL are based on dividing up the total surface area, a model parameter, among a large number of dust particle orbits. For each orbit, the surface area is distributed evenly in mean anomaly. Orbits are determined by randomly selecting a value for semi-major axis based on a distribution function determined from the expected distribution of dust particle orbits. For the specific value of semi-major axis selected, the corresponding forced and proper elements are selected from input data, and the orbit is mapped out in three dimensional space. The orbit thus defined, contains all characteristics associated with the initial creation of the dust particle and the effects of perturbations over long timescales. This process is repeated any number of times, $\sim 10^6$ in this research, until the disk is adequately populated with enough orbits to reproduce the specified total surface

area. The final spatial distribution is generated by determining where each of the orbits intersects an element of a predefined three dimensional grid.

6.3 Visualization

The final output of SIMUL is a three dimensional array in which each element represents the surface area per volume for a given particle diameter. To transform this result into a simulated dust distribution several steps must be taken. If a mapping of the distribution of surface area is desired, then integration along a line of sight, through the disk described by the three dimensional array output by SIMUL can be done directly after the appropriate rotations are performed. If a model disk is desired, then further input is required.

An actual circumstellar disk will contain dust that is emitting thermal radiation. This dust is heated, primarily by the short wavelength radiation of the star, and emits in the long wavelength region of the spectrum. This makes the mid-IR ideal for observing the dust in circumstellar disks. If a simulation of these emissions is desired, the thermal and optical properties of the dust must be considered. The properties that determine how a particle absorbs light, is heated, and then re-radiates energy is based on the dust's material properties and structure. Coupling assumptions about these properties with the properties of the star allow estimates to be made about the temperature of dust particles as a function of distance from the star and particle size. This in turn produces an estimated flux per unit of surface area for a particular sized particle.

Finally, this flux can be utilized with the surface area model to determine an overall flux distribution for the entire disk. This is done by selecting an observing direction with respect to the disk, and integrating along that line-of-sight. This produces a two-dimensional mapping for which each pixel value is related to the total flux from that location.

6.4 Summary

The approach to using secular perturbation theory to model the warp in a disk like that of Beta Pictoris requires determining the properties of a planetary system that will produce a disk model that has features matching those seen in the observed disk. This requires first choosing a configuration of planets and calculating the forced orbital elements

as a function of semi-major axis. Then, by considering the other physical processes involved in determining the distribution of material in the disk, a model disk can developed. The following chapter illustrates how the characteristics and features quantified in an observation can constrain the input parameters in this process and produce an output that matches the original observation.

A subtle but important point to emphasize about this approach is that the dynamics of the dust particles themselves are *not* being modeled. It is actually the larger and more massive source bodies that are being modeled dynamically. This is necessary as the particles that are generally responsible for the majority of the thermal emissions are measured on the scale of microns. These particles are generally short lived in a system like Beta Pictoris, as they are quickly expelled from the system on parabolic or hyperbolic orbits due to radiation pressure. However, as will be discussed in the following chapter, under the appropriate conditions it is valid to assume that the observed particles trace the larger unseen bodies. This is because the spatial distribution of the small particles, despite being quickly blown out, share many of the characteristics of the spatial distribution of the source bodies from which they were created. This is discussed further in the next chapter.

CHAPTER 7
CHARACTERIZING THE BETA PICTORIS DISK

7.1 Introduction

The recent mid-IR images of Beta Pictoris show with great detail the features and asymmetries of a warped circumstellar disk. Such images allow the unique opportunity to directly observe the effects of dynamical perturbations on the disk material. This research asserts that these unique features and asymmetries are linked to the presence of a multiple planet system.

The goal of the next two chapters is to illustrate how the theory and modeling process presented in previous chapters can be applied in such a way as to reproduce the important characteristics of a warped circumstellar disk such as those determined from the observations of Beta Pictoris. Considering the fact that only a single observing perspective is available, a unique solution cannot be found with the number of free parameters in a system as complex as that of Beta Pictoris. Nevertheless, the next two chapters will develop a logical approach to constrain a proposed system. Furthermore, it will be shown that at least one plausible configuration of planets will produce the same type of interesting features that have been identified in several observations, thus adding validity to the general approach.

In this chapter, the recent observations of Beta Pictoris made in the mid-IR by the University of Florida team (Telesco et al., 2003) will be discussed. Similar observations made by other groups will also be addressed. Highlighted in this discussion will be the identification of the major symmetry planes and the associated relative inclinations. The major symmetry planes are the most well studied feature of the disk and will be the first characterized in the modeling.

The physical conditions in the circumstellar environment place important constraints on the modeling process. The assumptions made about the physical processes specific to

the environment around Beta Pictoris are also discussed in this chapter. This discussion includes analysis on the timescales of the various physical processes that occur within the disk. The link between these processes and environmental properties such as dust grain composition and the estimated optical depth, is also addressed. Finally, the assumptions about the values of the proper orbital elements will be discussed. In chapter 4 the link between the observable characteristics of the disk and the proper orbital elements was discussed. This chapter will discuss the ways in which the observation of Beta Pictoris constrain the values for the proper elements that are used in the models to be presented in chapter 8. These discussions will be used to argue the validity of the model assumptions and the applicability of secular perturbation theory to this problem.

7.2 Recent Mid-IR Observations of Beta Pictoris

The University of Florida's IR group made 10.8 and 18.2 micron observations of the Beta Pictoris disk using the instrument OSCIR on the 8 m Gemini South telescope on Cerro Pachon in Chile (Telesco et al., 2003). The observations made in December of 2001 are shown in figure 7–1. The observations shown in this image represent the highest resolution images (approximately 0.5 arcsec at 18 μm) ever taken at these mid-IR wavelengths.

The images expose emission from the disk extending out to a radius of approximately 100 AU from the central star. The images also reveal several characteristics that hint at the presence of a planetary system. Clearly seen in the 18 μm image is an "S-curve" shape in the southwest extension. This is consistent with the warping seen in other observations. The UF images however indicate the details of the warping in such a way as to expose the complex shape of the disk's mid-plane. This hints at a complex mechanism being responsible for shaping the spatial distribution of circumstellar material.

Also observed in the images are regions in the disk's mid-plane that suggest depletions or enhancements in the dust number density. Consistent with theories of gap creation by large bodies in a circumstellar disk, these voids or gaps will be used later to constrain the locations of the planets used in the model. Identification of these features is discussed later in this chapter.

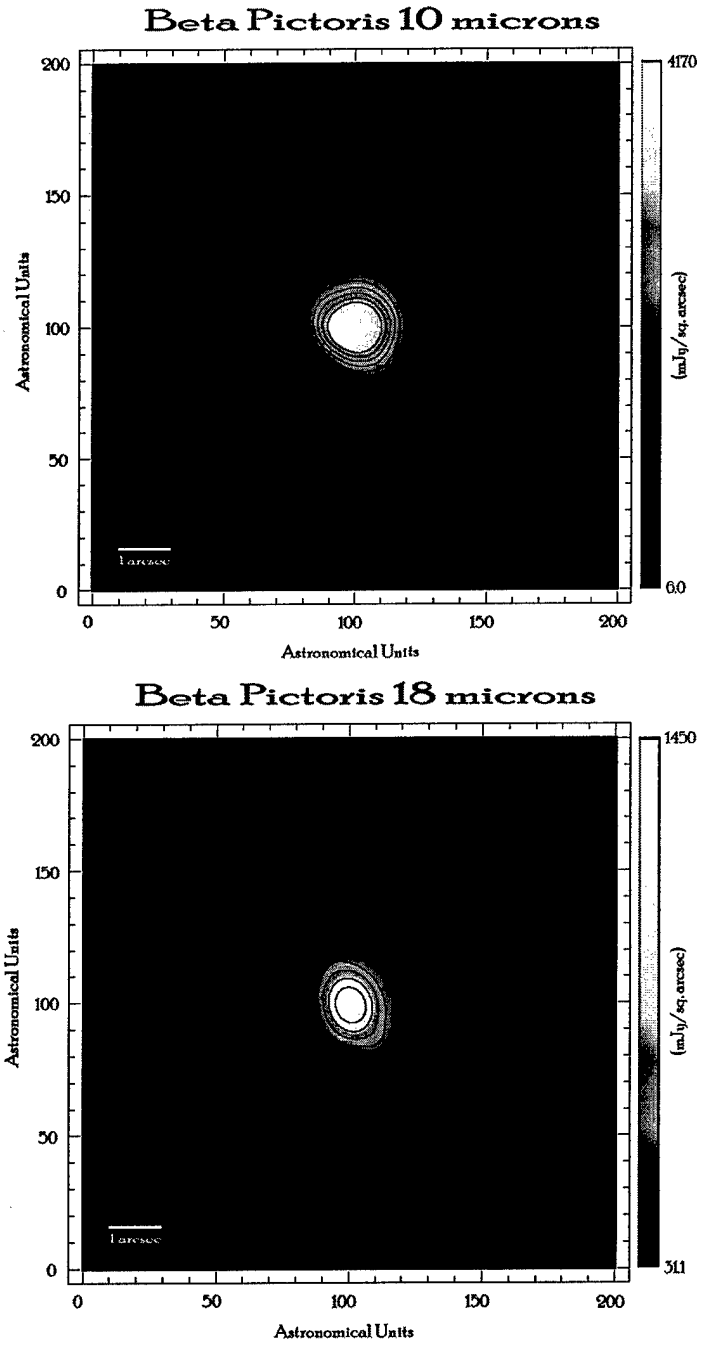

Figure 7–1: Mid-IR images of Beta Pictoris in 10 μm (top) and 18 μm (bottom).

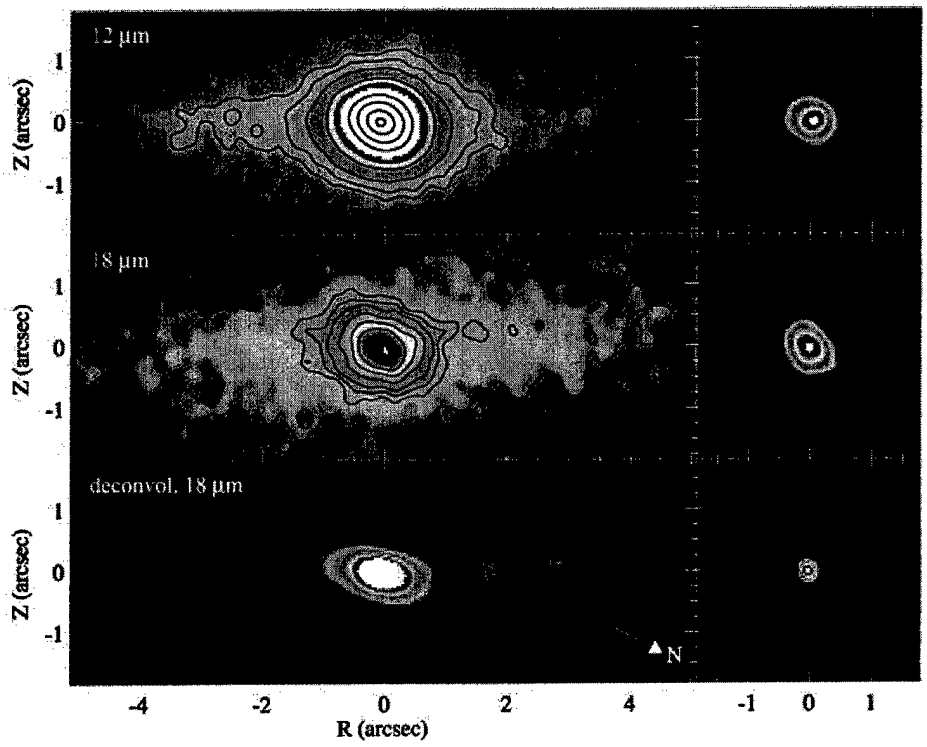

Figure 7–2: Mid-IR images of Beta Pictoris in 12 μm (upper) and 18 μ m (lower) (Weinberger et al., 2003). The images show the inclined plane of the inner disk ($\lesssim$ 1 arcsec) and outer disk ($\sim$ 3 arcsec).

Weinberger et al. (2003) and Wahhaj et al. (2003) also presented mid-IR observations of Beta Pictoris at 11.7 and 17.9 μm and 17.9 μm respectively. Both observations were made using the Keck observatory in Hawaii. These images illustrate the changes in relative inclination angle along the mid-plane. Weinberger et al. identified the inner warp in the disk ($\leq$ 20 AU) as well as the previously identified large scale symmetry planes. Wahhaj et al. not only observed the warping of the mid-plane, but they also identified emission peaks within the disk that they associated with a ring system. The estimated ring radii were 14 $\pm$ 1, 28 $\pm$ 3, 52 $\pm$ 2, and 82 $\pm$ 2 AU. The rings were also argued to have inclinations that alternate in orientation relative to the invariant plane of the disk. The Wahhaj et al. image is consistent with the UF images in the sense that it shows a disk consisting of a ring-like structure but it does show inconsistencies in the locations and inclinations of the rings. However, inconsistencies should not be entirely unexpected as the UF observations were made at significantly lower airmass than that of the Wahhaj observation.

Further analysis of the UF Beta Pictoris images reveals essentially the same symmetry planes as seen in the images of Heap et al. (2000), Weinberger et al. (2003), and Wahhaj et al. (2003). Together these observations create a consistent picture of a distribution of dust with three major symmetry planes. Furthermore, the secondary effects of planets that may be responsible for the large scale warping are seen within the UF images. The modeling of all of these features is saved for the next chapter.

7.3 The Physical Environment

Modeling the Beta Pictoris system in the context of secular perturbation theory required three primary steps. First, the timescales associated with the various processes were determined to ensure that the system has had enough time to fully evolve; i.e. all regions of the observed disk have been influenced by the secular perturbations. Key to understanding the timescales associated with the disk, is a reasonable estimate of the dust properties – composition and typical size. Second, the location of the planets had to be assumed using characteristics of the observed morphology. Finally, the forced elements needed to be calculated and used to simulate a distribution of dust. This section discusses the first step of determining the physical conditions existing within the disk, starting with an analysis of

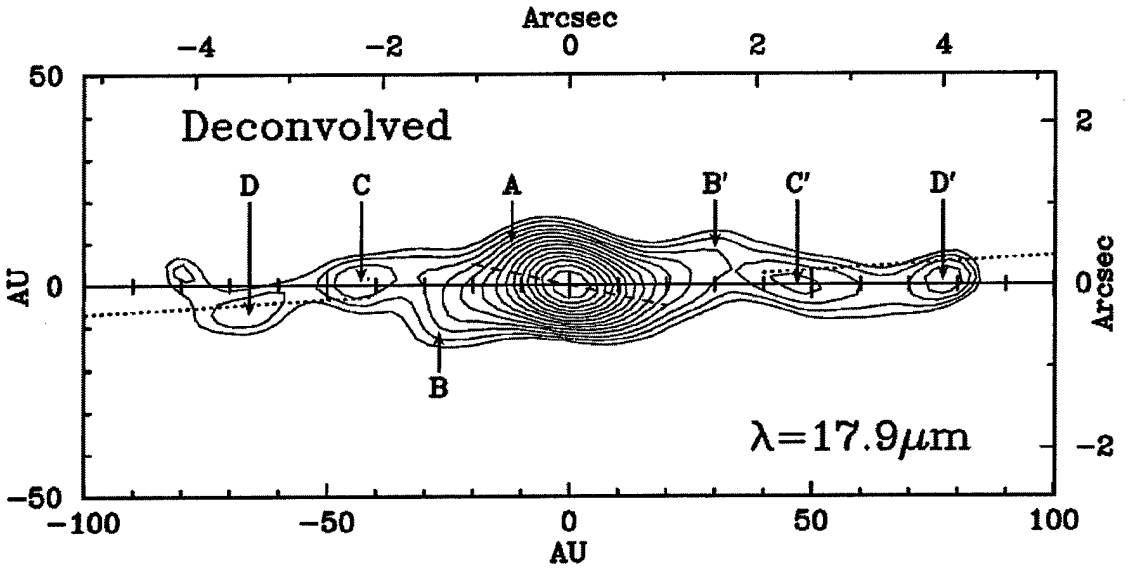

Figure 7–3: Mid-IR images of Beta Pictoris at 17.9 μm (Wahhaj et al., 2003). The image shows the inclined plane of the inner disk ($\lesssim$ 20 AU and outer disk ($\sim$ 60 AU).

the timescales associated with the processes that most affect the morphology of the disk.

7.3.1 Typical Particle Size

The interaction between radiation from the star and the dust particles play an important role in determining the distribution of dust in a disk. For a thorough discussion on the dust particle size distribution that is expected for a circumstellar disk see Wyatt et al (1999) and references within. As a general summary, particles can be grouped into several categories based not strictly on size but on the value of β discussed in chapter 2. Particles for which $\beta > 0.5$ are unbound and quickly leave the system on hyperbolic orbits. These particles are referred to as β meteoroids. Particles that are below but still close to the blow out limit of $\beta = 0.5$ are called β critical particles and have values of β that fall in the range of $0.1 < \beta < 0.5$. These particles are still bound but have their orbits significantly affected by radiation effects. In general the distribution of these particles will extend outwards from that of the bodies that that created them. Particles for which β is very small are generally the larger particles that are relatively unaffected by radiation affects.

Another class of particles is the one in which PR drag plays a significant role. These particles are the ones that, because of PR drag, spiral in towards the star before being

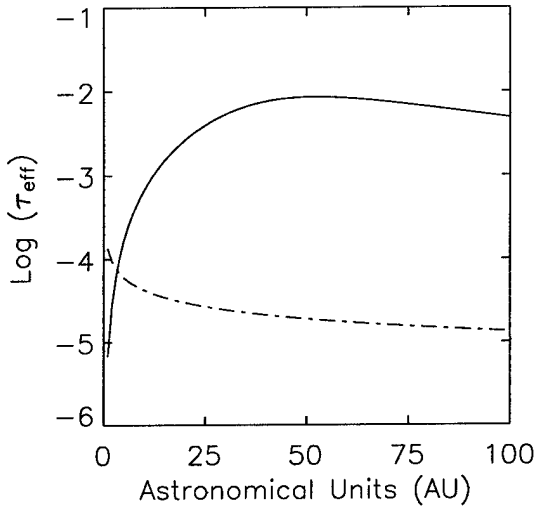

Figure 7–4: The effective optical depth assumed for Beta Pictoris (the solid line) and the threshold value for which evolution due to PR drag becomes insignificant (the dotted dashed line).

destroyed by collisions or evaporation. The value of β for these particles is in the range of $\beta_{PR} < \beta < 0.1$, where β_{PR} is defined as the value of β for which the collisional lifetime is the same as the PR drag lifetime (see chapter 2). This value is expressed as

$$\beta_{PR} = 5000\ \tau_{eff}(r)\sqrt{(M_{\odot}/M_{\star})(r/a_{\oplus})}. \tag{7.1}$$

If the disk has a high enough optical depth, these particles will be destroyed by collisions before they experience significant inward migration which will result in this category not existing in such disks (Wyatt et al., 1999). The threshold value for the effective optical depth is determined by finding where $\beta_{PR} > 0.5$ and is given by

$$\tau_{eff}(r) > 10^{-4}\sqrt{(M_{\star}/M_{\odot})(a_{\oplus}/r)}. \tag{7.2}$$

Artymowicz and Clampin (1997) proposed an analytic form of the normal optical depth in Beta Pictoris based on the observed surface brightness. This expression has the form

$$\tau(r) = 2\tau_m\left[\left(\frac{r}{r_m}\right)^{-p_{inner}} + \left(\frac{r}{r_m}\right)^{p_{outer}}\right]^{-1} \tag{7.3}$$

where τ_m is the maximum normal optical depth which is reached at a distance of r_m. The exponents p_{inner} and p_{outer} represent the slopes of the inner and outer disc. The values of the parameters, as estimated from 12 μm observations, are as follows: $\tau_m = 8.5 \cdot 10^{-3}$, $r_m = 50$ AU, $p_{inner} = 2$ and $p_{outer} = 1.7$.

Plots of the assumed optical depth and the threshold value are shown in figure 7–4. This figure suggests that the scenario described above does apply and that the disk of Beta Pictoris does not possess a significant distribution of PR drag affected particles. In this situation, half of the cross sectional area is thought to come from the β critical particles (Wyatt et al., 1999). Though the value of β is dependent on the material properties of the dust (see figure 2–1 in chapter 2), for the materials considered likely to constitute the dust in Beta Pictoris, the lower limit for the β critical particles corresponds to $D \approx 10\mu$m.

Typical particle sizes determined from past observations and analysis were thought to have a radius of $\approx$ 2 to 3 μm (Artymowicz, 1997). However, this estimate was done prior to the release of the Hipparcos data, which revealed a greater distance to Beta Pictoris than had been previously thought and, consequently, a more luminous star. Another approach used to study the size distribution of dust within the Beta Pictoris system was a theoretical study using a proposed collisional model of dust generation (Krivov et al., 2000). This analysis resulted in an estimate of the dominant particle size to be $\sim$ 10 μm. This was based on the result that showed the largest contributor to cross sectional area was in the range just below the blow out limit.

For the modeling presented in this research, the typical particle size was assumed to take the value of $\sim$10 μm in diameter for dust grains composed of organic refractory material. This corresponds to particles slightly larger than the blow-out limit of $\beta \sim 0.5$. The justification for using the specific material composition is discussed in the next chapter.

As a final note, it is important to keep in mind that though radiation effects play a significant role in the radial distribution of dust, the orbital planes are unaffected. This is important because this research focuses on warping which is directly related to the mean orbital planes of the dust particles and source bodies. Therefore, even if the estimate on

particle size is not completely accurate, only the radial distributions are affected and analysis of the symmetry planes is still arguably valid.

7.3.2 Timescales of Physical Processes in Beta Pictoris

The expressions for timescales associated with each of the primary physical processes within the disk discussed in chapter 2 were applied to Beta Pictoris. Using the parameters taken from observations, the timescales were determined and are plotted as a function of semi-major axis in figure 7–5. These calculations were most dependent on physical characteristics of the disk such as mass/luminosity of the central star, typical particle size, and optical depth.

The mass and luminosity of the central star were taken from the results based on the Hipparcos data (Crifo et al. 1997): $M = 1.8M_{\odot}$ and $L = 8.7L_{\odot}$. As pointed out in chapter 5, the most recent estimate determined by observing the stars constituting the Beta Pictoris moving group suggests an age of ~ 20 Myr (Navascues et al. 1999).

Based on the values of optical depth given earlier, the collisional timescales are much shorter than the PR lifetimes. These calculations are based on dust modeled as particles composed of organic refractory material, and typical particle sizes ranging from 1.0 to 25.0 microns. The associated timescales are plotted in figure 7–5.

Analysis of the different timescales suggests once again that the collisional lifetime is the shortest of the timescales and thus collisional processes dominate over all others. This implies that the observed dust is arguably a direct tracer of the larger, secularly perturbed, bodies. This supports the idea that by modeling the distribution of bodies affected by secular perturbations, the distribution of dust within the system can be reasonably simulated. However, two questions must first be addressed: what is the magnitude of the secular timescale and how does it compare to the estimated age of the disk?

The appropriate timescale associated with the secular perturbations is the proper precessional rate that is determined from calculating both the A and B values of equations 3.7a and 3.7c. These rates can be converted to timescales by using the expression

$$t_{sec} \approx \frac{2\pi}{A}. \tag{7.4}$$

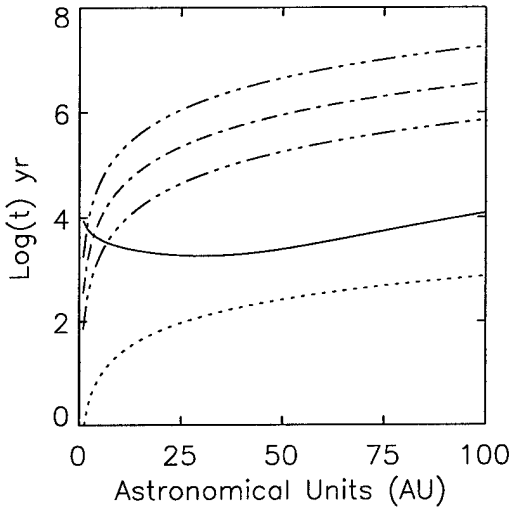

Figure 7–5: The timescales associated with the various physical processes expected within the Beta Pictoris disk. The dotted line represents the Keplerian period. The solid line represents the collisional timescales for the particles in the disk that make up most of the disk's cross sectional area. The three dashed-dotted lines represent, from bottom to top, the PR timescales associated with particles with D=1, 5, 25 microns respectively.

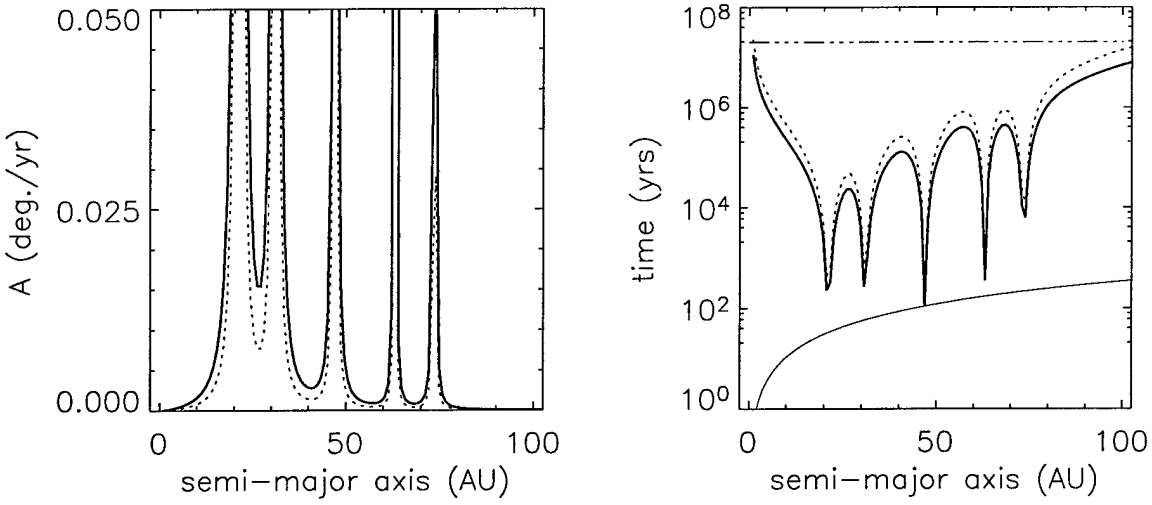

Figure 7–6: Proper precessional rate for a four planet system (left) and the associated timescales (right). The solid line represents the results for one of the systems of planets used in the models discussed in the next chapter. The dotted line represents the same system but with the mass of each planet scaled by 0.5. The dotted dashed line in the left panel represents the age of Beta Pictoris. The solid lines represents the Keplerian period.

Since A is a function of semi-major axis, t is as well. A plot of the variation of secular timescales is shown in figure 7–6 where the A values are associated with one of the planetary configurations used in the modeling. Also shown on the plot for reference is the Keplerian timescale and the estimated age of the Beta Pictoris system. Plotted in these diagrams are the results from the five planet planetary configuration used in the models presented in the next chapter and the results for the same system using a mass scale factor of 0.5 for each of the planets. This figure provides insight into the magnitude of change that would occur in the secular timescales for a far less massive system. The important characteristic of this illustration is that there exists plausible configurations in which secular timescales are in fact shorter than the estimated age of the disk. Furthermore, this statement is fairly robust as the results are not strongly affected by significant changes in the total mass of the planets comprising the system. This answers the question of whether or not the disk has existed long enough to evolve under the influences of the secular perturbations. It should also be noted that the 20 Myr age is an estimate of the *minimum* age of the Beta Pictoris system.

7.3.3 Dust Grain Composition

Prior to 1998, it was generally accepted that the dust grains within the Beta Pictoris disk belonged to one of two populations: within $\sim$ 100 AU the material was considered to likely be silicates while outside $\sim$ 100 AU the material was considered to likely be ice (Artymowicz 1997). Li and Greenberg (1998) studied the material properties in more detail and suggested that the dust particles in the inner region are fluffy aggregates of silicate core/organic refractory mantle grains. In the outer regions these aggregates also possess an ice mantle. A transition in material properties or distribution is suggested in the UF observations by the change in slope of the brightness profile at $\sim$ 80 - 100 AU, as shown in figure 7–7.

The primary goal of the simulations performed in this research were to address the effects of gravitational perturbations on the disk morphology, i.e. the spatial distribution of the dust. Therefore, a simplistic approach was taken in selecting the material composition of the dust particles in the model. This was based on determining which of the dust model candidates produced approximately the same ratios between the 10 and 18 μm emissions

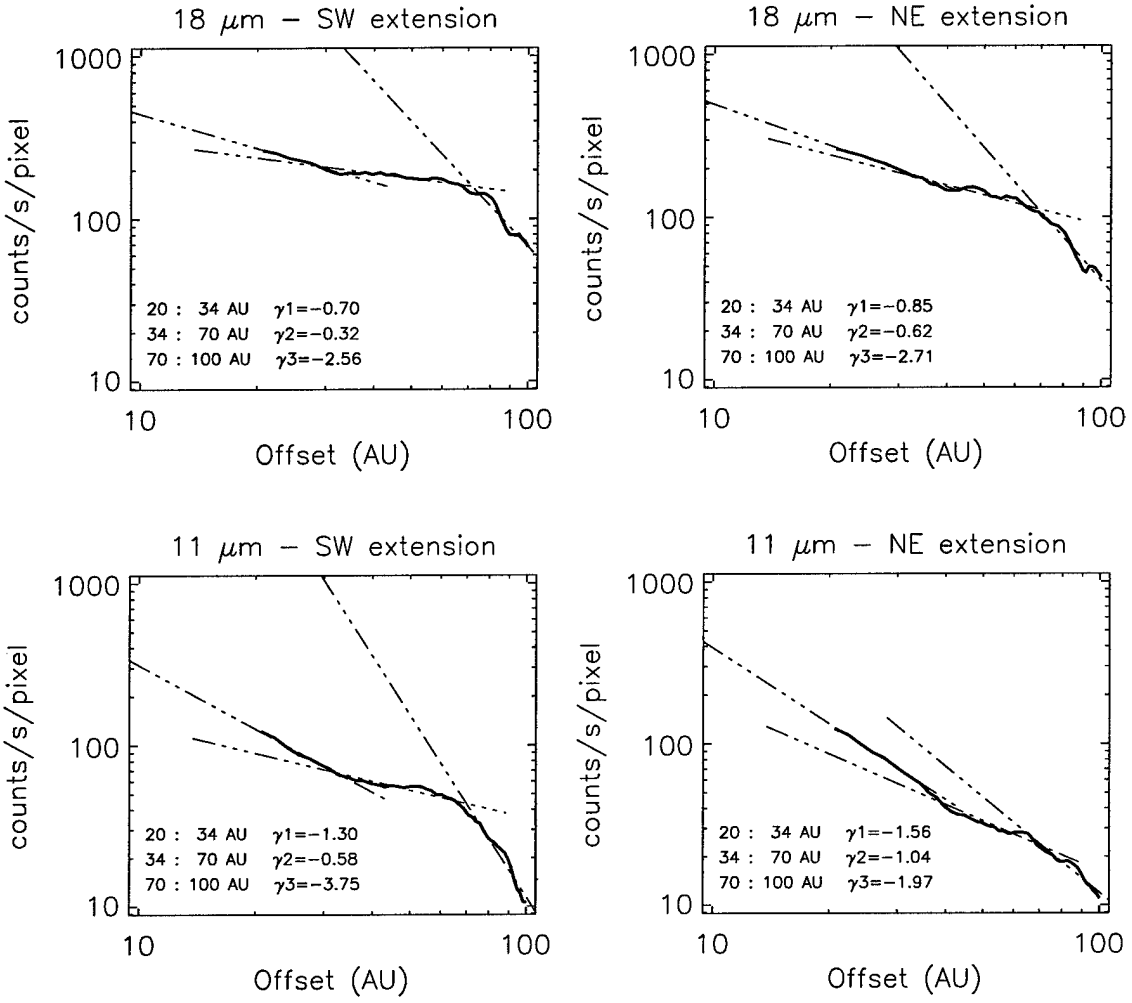

Figure 7–7: The radial brightness profiles along the midplane in a 5 AU swath. This is plotted on a log-log scale to facilitate a linear fit and determine the index for an assumed powerlaw. Three regions were identified for the line fit. The boundaries of the regions and associated power law indices are shown on the plot.

as determined from the observations. Implied in this assumption is that the same particles are responsible for the 10 and 18 μm emissions, over the entire disk.

In a collisional model, the grains are likely to be porous aggregates of silicate core – organic refractory mantle particles with porosity on the order of $\sim$0.5 (Thebault et al., 2003) as opposed to cometary dust that could have porosities $\sim$0.95 (Li and Greenberg, 1998). For comparison, data from dust attributed to the collisional destruction of asteroids in the solar system suggests a porosity of $\sim$ 0.50. If this research focused on an exact reproduction of the brightness distribution, a more thorough analysis would be required. However, since the morphology of the disk, mostly at a single waveband, is the primary concern of the modeling, the analysis considered only homogeneous Mie spheres of astronomical silicates and organic refractories. Though aggregates of silicate core – organic refractory mantles are likely present, they are much more difficult to handle through the simple approach used in this research. In order to handle these composite materials the use of an effective medium theory, such as Maxwell Garnett, is necessary. However, Several important limitations are inherent to this approach. First, Maxwell-Garnett effective medium theory has many limitations that are discussed thoroughly in Gustafson et al (2001). Among these limitations is the necessity of the particles making up the aggregate to be small compared to the wavelength of interest. Though the particles making up an aggregate of 10 μm with a fifty percent porosity may fit this criteria for 11 and 18 μm observations, it still causes concerns when considering the fact that the interaction with the shorter wavelengths is primarily responsible for the heating of the particles. Furthermore, Gustafson et al. showed significant weaknesses when considering regions near the 10 μm silicate feature.

Since a detailed investigation into the potential material composition and structure of the dust grains within the disk was well outside the scope of this research, the simple approach presented here was deemed satisfactory. To reiterate, if a detailed analysis of the brightness distribution was the focus of the research and not disk morphology at a single waveband, a much more rigorous and thorough analysis would be required.

Temperature profile of dust particles

To simulate the emissions from dust particles it is necessary to make an estimate of the temperature of dust grains as a function of distance from the star. The temperature profiles were determined by considering the scattering efficiencies, as determined from Mie theory, for the materials thought to most likely represent the dust grains within the disk. The complex refractive indices and the temperature profiles for the different materials considered are shown in figure 7–8. This diagram lists the optical constants as a function of wavelength and the temperature profiles as a function of distance from the star. The values for the optical constants for the astronomical silicates and organic refractories were taken from Laor and Draine (1993) and Li and Greenberg (1997) respectively. The results for several particle diameters are shown.

To select which profile is appropriate to use in the models, the thermal emissions at 10 and 18 μm were compared to the observations. Figure 7–9 shows the temperature and flux ratios as a function of size for various radial distances from the star. The observed mean flux ratio is shown as a horizontal line and the shaded region shows the one sigma uncertainty. Only the organic refractory material produces reasonable values that are consistent with the previously assumed particle size of $\sim$10 μm.

7.3.4 Mass of the Disk

The total mass of dust within a disk can be estimated from the millimeter flux that is primarily associated with the disk's gas. The fact that the dust material is not detected in these observations is generally accounted for through the use of an estimated gas to dust ratio. Beckwith (1999) gave an expression for disk mass

$$M_{disk} = 0.03\ M_{\odot}\ \frac{F_{\nu}}{1\ \mathrm{Jy}}\left(\frac{D}{100\ \mathrm{pc}}\right)^{2}\left(\frac{\lambda}{1.3\ \mathrm{mm}}\right)^{3}\frac{50\ \mathrm{K}}{<T>}\ \frac{0.02\ \mathrm{cm^{2}g^{-1}}}{\kappa_{1.3\mathrm{mm}}} \qquad (7.5)$$

where F_{ν} is the measured flux density, D is the distance in parsecs, λ is the observational wavelength, $< T >$ is the estimated mean temperature, and κ is the particle mass opacity which is $\sim 0.02(1.3\ \mathrm{mm}/\lambda)\mathrm{cm}^{2}\ \mathrm{G}^{-1}$ (Beckwith, 1999). The millimeter flux density for the Beta Pictoris disk was measured by Liseau et al. (2003) at 24.3 ± 0.3 mJy at 1200 μm. This provides an estimated mass for the disk as $\sim 1M_{\oplus}$. This is consistent with the values

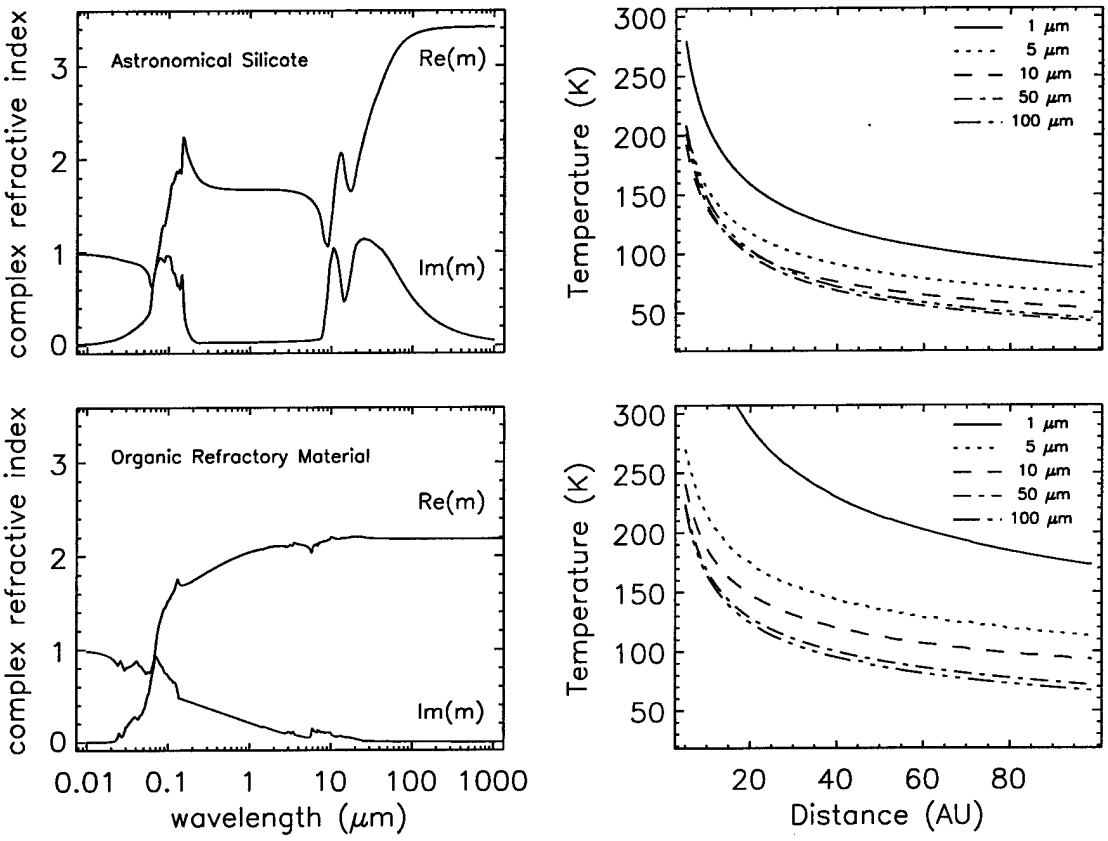

Figure 7–8: Complex index of refraction (left column) for several materials considered likely candidates for the dust in the Beta Pictoris disk. Also shown, is the temperature profile (right column) as a function of distance from the central star.

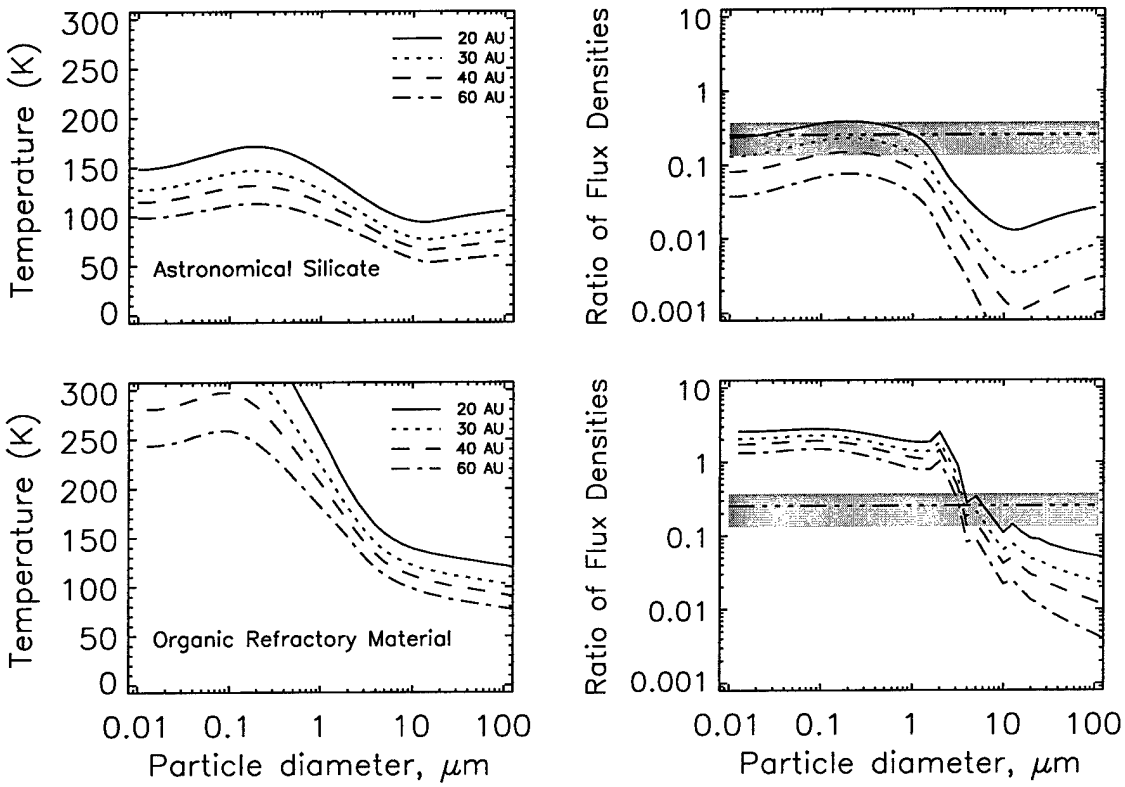

Figure 7–9: Temperataure profile (left column) for dust particles as a function of particle size in the Beta Pictoris system. Also, the ratio of 10 and 18μm flux densities (right column) as a function of particle size. The materials are the same as those considered in figure 7–8. The horizontal line in the plots of flux ratio show the observed mean value and shaded region shows the one sigma uncertainty.

of 0.3 to 0.5 $M_{\oplus}$ for the total mass of dust determined by Li and Greenberg (1998) and Artymowicz (1997).

The mass of the disk is important to consider because of the potential influence of the disk on the other massive bodies and dust. As will be discussed in the following sections, the proposed planetary system consists of planets that have masses comparable to that of Jupiter, $\sim 317\ M_{\oplus}$. This suggests that the mass of the disk, which is spread out over an enormous area, should have little effect on the dynamics when compared to that of the proposed planets. However, it needs to be pointed out that the mass associated with the source bodies is not considered in calculations based on this approach. This could lead to a significant underestimate of the total mass. A further analysis of the potential influence of a massive disk is presented in chapter 9.

7.3.5 Distribution of Dust

As described in the previous chapter, the modeling process requires an estimate of the radial distribution of orbits. This is obtained by using the estimated number density as estimated from observational data. As discussed earlier, it is assumed that the particles primarily responsible for the observed thermal emissions are rather quickly destroyed by collisions before being removed from the system by radiation pressure. This implies that the particles not only need a source for replenishment, but that the observed particles trace the distribution of source bodies. From analysis of optical depth as determined from observations and from theoretical analysis based on a collisional model of Beta Pictoris, an expression for the number density was given by Krivova et al. (2000) and has the form

$$n(r) = n_0 \left[\left(\frac{r}{r_m} \right)^{-p_{inner}} + \left(\frac{r}{r_m} \right)^{p_{outer}} \right]^{-1} \tag{7.6}$$

where the values of p_{inner}, p_{outer}, and r_m were suggested to be roughly 1.0, 2.7, and 60 AU respectively.

The important information provide in this expression is the general shape of the distribution function. The models in this research require, as an input parameter, a normalized distribution function which means that the magnitude of n_0 is unimportant. The actual

values of density are manifested in the modeling process by specifying the total disk surface area, which is a separate model parameter.

7.3.6 The Proper Elements

Necessary for the simulation of a disk are the proper orbital elements; these parameters link the model to the initial conditions associated with the dust at the moment of creation. The values used for the models in this research are based on the unbiased distribution determined for the main-belt asteroids (Xu et al., 1993). This distribution however, was scaled in such a way as to provide mean values consistent with observable quantities of the disk. As discussed in chapter 4, the half-opening angle of the disk is related to the proper inclination. The observed opening angle has been measured to be $\sim$12 degrees (Artymowicz et al., 1989) which implies a mean proper inclination of $\sim$6 degrees. Because of the edge-on view of the Beta Pictoris disk, it is more difficult to make estimates of the proper eccentricity. However, a value for the mean proper eccentricity of 0.1 was chosen in order to maintain the same relationship between the mean proper inclination and mean proper eccentricity as is observed for the main belt asteroids, i.e. $< \sin I > \approx < e >$.

The probability distribution function (pdf) for the main belt asteroids and the modified pdf for the Beta Pictoris disk are shown in figure 7–10. Also shown is the histogram representing the randomly selected values of proper elements based on the modified pdf.

These values were appropriate based on the values for the half-opening angle documented in the literature. However, the next chapter will show that the disk may actually be better represented by smaller mean values. The high resolution images reveal fairly well isolated regions of dust that are suggestive of a mean proper inclination of $\sim$ 3 degrees and a mean proper eccentricity of $\sim$ 0.05. Several models were run with these values and did in fact produce a better visual match to the features of the high resolution images. This will be discussed further in the following chapter.

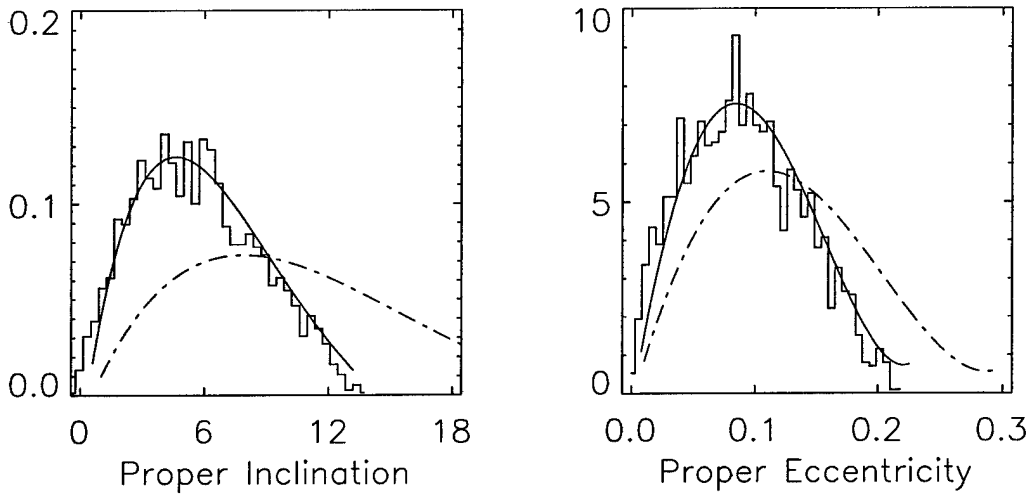

Figure 7–10: Distribution of proper orbital elements used in the simulated disk of Beta Pictoris. The solid line shows the theoretical pdf curve determined by modifying the pdf for the main belt asteroids. The dotted-dashed line shows the pdf for the main-belt asteroids as determined from the distribution of Xu et al. (1993). The histogram shows the distribution of values randomly drawn using the modified pdf (solid curve).

7.4 Summary

This chapter provided the current understanding of the environment around Beta Pictoris to the extent necessary to create adequate models for an investigation into disk morphology. The next chapter will discuss the way in which these characteristics are implemented into the modeling of the morphology of the dust disk surrounding Beta Pictoris.

CHAPTER 8
APPLICATIONS OF SECULAR PERTURBATION THEORY TO BETA PICTORIS

8.1 Introduction

The previous chapter discussed the characteristics of the physical environment surrounding Beta Pictoris. These characteristics provide the boundary conditions needed to develop a reasonable model of the circumstellar disk. However, the important characteristics needed to assess the warping of the midplane of the disk are associated with the details of the orbits of the perturbing planets. Therefore, an approach must be defined to extract information from the observations of a disk that can be used to characterize the orbits of an embedded planetary system.

A system of multiple planets will be utilized to explain the existence and configuration of the major symmetry planes of the disk. However, current theory of planet-disk interaction suggests that these planets will also have secondary effects on the disk, some of which should be observable in the observations. These effects include gap clearing and warping on smaller scales - both of which are suggested by the UF observations. Regions will be depleted through interaction with planets via tidal forces or accretion. Both process can be related to characteristics of the planetary orbits or the masses of the planets themselves. Furthermore, the eccentricity imposed on the dust particles through secular perturbations combined with the particles' inherent eccentricity can cause the dust, not initially in a region cleared by a planet, to enter an orbit that will cause it to enter such a region, and thus be removed from the disk. This potentially results in additional regions in which dust depletion should occur and has implications for the stability of a large disk in a multi-planet system. The small scale warping is also expected for planets with mutual inclinations due to the potentially dramatic behavior of the forced orbital elements, particularly the forced

inclination and node. By probing the small scales, information about the behavior of the forced parameters can be gleaned.

These quantifiable features provide additional constraints on the perturbations from the planets and thus on the planets themselves. The way in which these constraints are determined and then applied is the primary goal of this chapter. Sample models based on the approach proposed here will be presented along with a discussion of the results in the context of the observations.

8.2 Constraints on a Planetary System from Observations

As discussed in the previous chapter, secular perturbation theory predicts that the gravitational influence of a system consisting of multiple planets will define the mean orbital planes of the disk's constituent dust particles. If the planets have a nonzero mutual inclination, the components of the dust particles' orbital elements that arise from the gravitational perturbations, the forced elements, will vary with semi-major axis. Since the forced inclination and longitude of ascending node define the planes about which particles will precess, and since these elements are a function of semi-major axis, warping occurs. This effect can also be considered in terms of angular momentum planes. At radial distances corresponding to the semi-major axis of one of the planets, the dust particles will precess around the same plane as the corresponding planet – the plane perpendicular to the planet's angular momentum vector. This will be the case for each of the planets. Between the planets, the effect, and hence the behavior, is more complicated as the particles are now influenced by multiple masses.

The choice of orbital elements of a proposed system requires adherence to two constraints. First, the chosen planetary configuration must have an associated forced inclination that would produce the large scale warping well documented in the literature. Second, the secondary effects associated with the planets also need to be consistent with the sections of disk identified in the UF images. The observations of Wahhaj et al. (2003), Weinberger et al. (2003), and Telesco et al. (2003) were used to quantify the angle of the inner component that peaked in amplitude at $\sim$20 AU. The observations and analysis of Heap et al. (2000) were used to determine the angle between the intermediate component and the outer

component. Since the UF observations were the highest in quality, they alone were used to study the small scale features.

The following sections describe how the details of the observations are utilized to constrain the characteristics of the proposed planetary system. First, the major symmetry planes are used to constrain the major angular momentum planes within the disk. Second, the additional features observed in the high resolution images are used to further constrain the models by suggesting the likely locations of the planets.

8.2.1 Large Scale Symmetry Planes

Figures 8–1 and 8–2 compare the UF observations with the previously identified major symmetry planes. Figure 8–1 shows a contour plot of both the 18 and 11 μm images. The dashed and dotted lines indicate the major symmetry planes of the inner disk (Weinberger et al., 2003) and the larger scale ridge-line (Heap et al., 2000). Figure 8–2 shows the same data, but each vertical slice has been fit by a gaussian. Contours are shown for the 10% values and the FWHM.

The importance of these two plots is the consistency between the previously identified symmetry planes and the UF data. However, though the images are consistent with the previous assertions, they don't match exactly. The inner disk is only tilted by 8-9 degrees as opposed to the previous estimate of 12 degrees. As discussed in chapter 4, major symmetry planes are associated with primary angular momentum planes within the system. The inner symmetry planes are associated with the angular momentum planes of the planets and the outer large scale symmetry plane is associated with the total system angular momentum plane. These facts provide constraints on the masses and locations of any planets within the system.

These constraints can be assessed by considering the relationships between the masses and semi-major axes of the planets. Figure 8–3 shows the results from a calculation of the inclination of the plane associated with the system's total angular momentum with respect to the plane of the second planet. This calculation was made by assuming an expression for the inclination that was simplified to a function of the mass ratios and the ratio of semi-major axes. To make this simplification, several assumptions were made. First, the

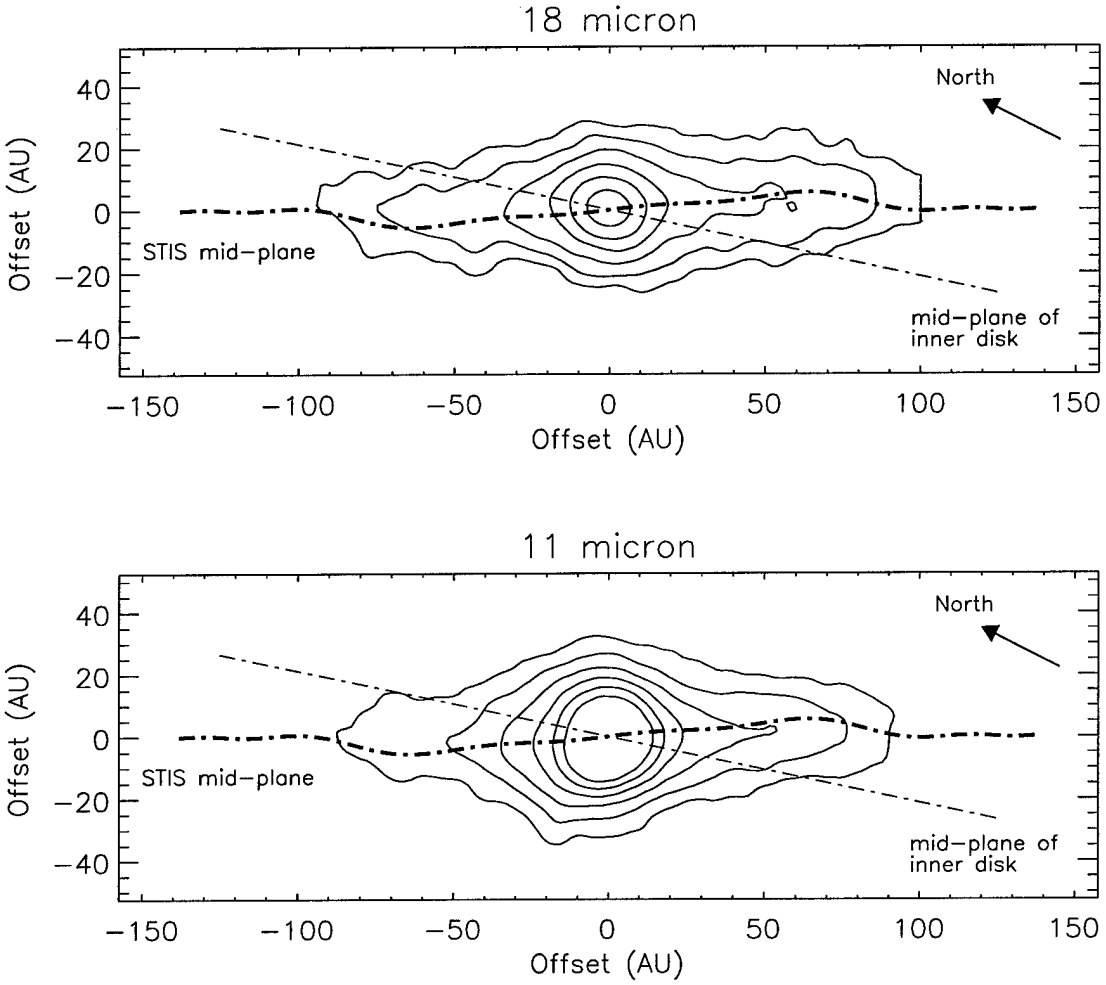

Figure 8–1: Contour plot of the 18 and 11 μm images. Also plotted over the image is the STIS mid-plane (Heap et al., 2000) and the mid-plane of the inner disk as presented by Weinberger et al. (2003).

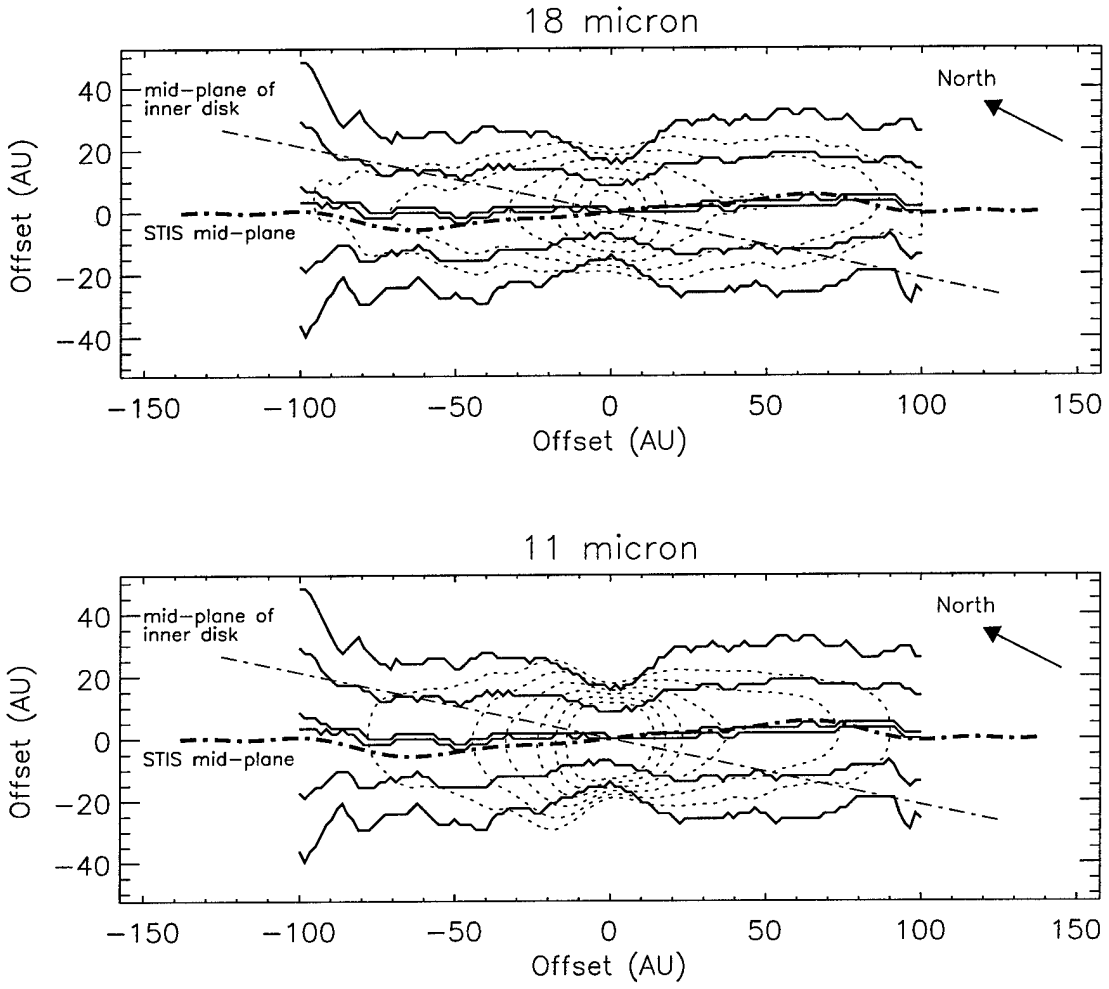

Figure 8–2: Same as figure 8–1 but with each vertical slice normalized to the peak value and fitted by a gaussian. Plotted are the contours representing, for each vertical cut, the $\geq$ 99% brightness, the FWHM, and the 10% values. These are also shown in comparison to the STIS and Weinberger reference planes.

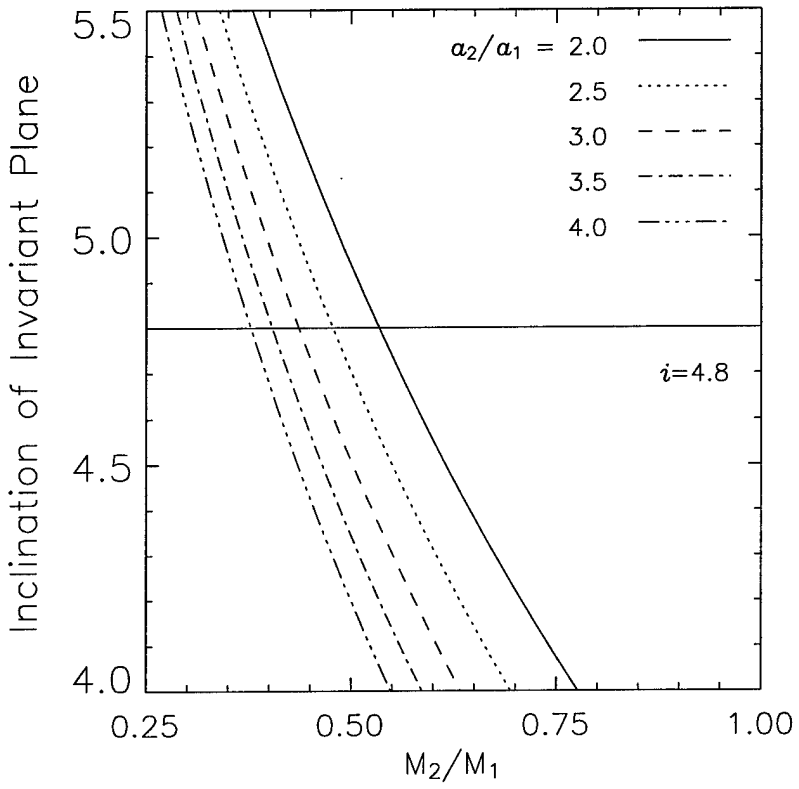

Figure 8–3: Calculated values of the inclination of the plane defined by the total angular momentum of the system as a function of the mass ratios of the two planets assumed to comprise the system. Each curve represents a unique value of the semi-major axis ratio. The observed value for the inclination of the invariant plane is shown. The intersection of this line with the calculated curves defines the acceptable values of semi-major axis and mass ratios. The reference plane is that of the outer planet.

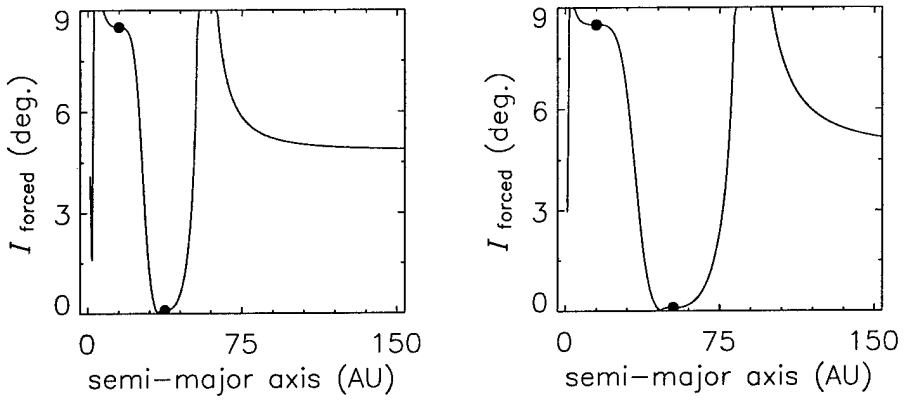

Figure 8–4: The forced inclination for two planets with mass and semi-major axis ratios determined from the plot shown in figure 8–3. The filled circles indicate the inclinations of the planets. The reference plane is that of the outer planet. The figure on the left corresponds to the $a_2/a_1 = 2.5$ and the figure on the right corresponds to case of $a_2/a_1 = 3.5$.

planes were assumed to be a result of just two planets – one associated with each of the inner symmetry planes. Furthermore, the inclinations of each planet were assumed to be the same as the inclinations of the corresponding symmetry planes. The final assumption was that the nodes, including that of the total angular momentum plane, were aligned with the line of sight of the observation.

The curves shown in figure 8–3 shows the inclination of the system's total angular momentum plane as a function of mass ratios of the two planets. Each curve represents a different value for the ratio of semi-major axes. Also plotted is the value for the observed inclination, ~ 4.8 degrees. It is the intersection of this line with the various curves that provide the acceptable value for the mass ratio for a given value of semi-major axis ratio.

The information plotted in figure 8–3 can be used to create a model system with major symmetry planes matching those of Beta Pictoris. Examples of the forced inclinations associated with planetary systems defined by the ratios determined from figure 8–3 are shown in figure 8–4. Also plotted in this figure are the inclinations associated with the planets composing the system – the filled circles. The semi-major axis of the inner planet

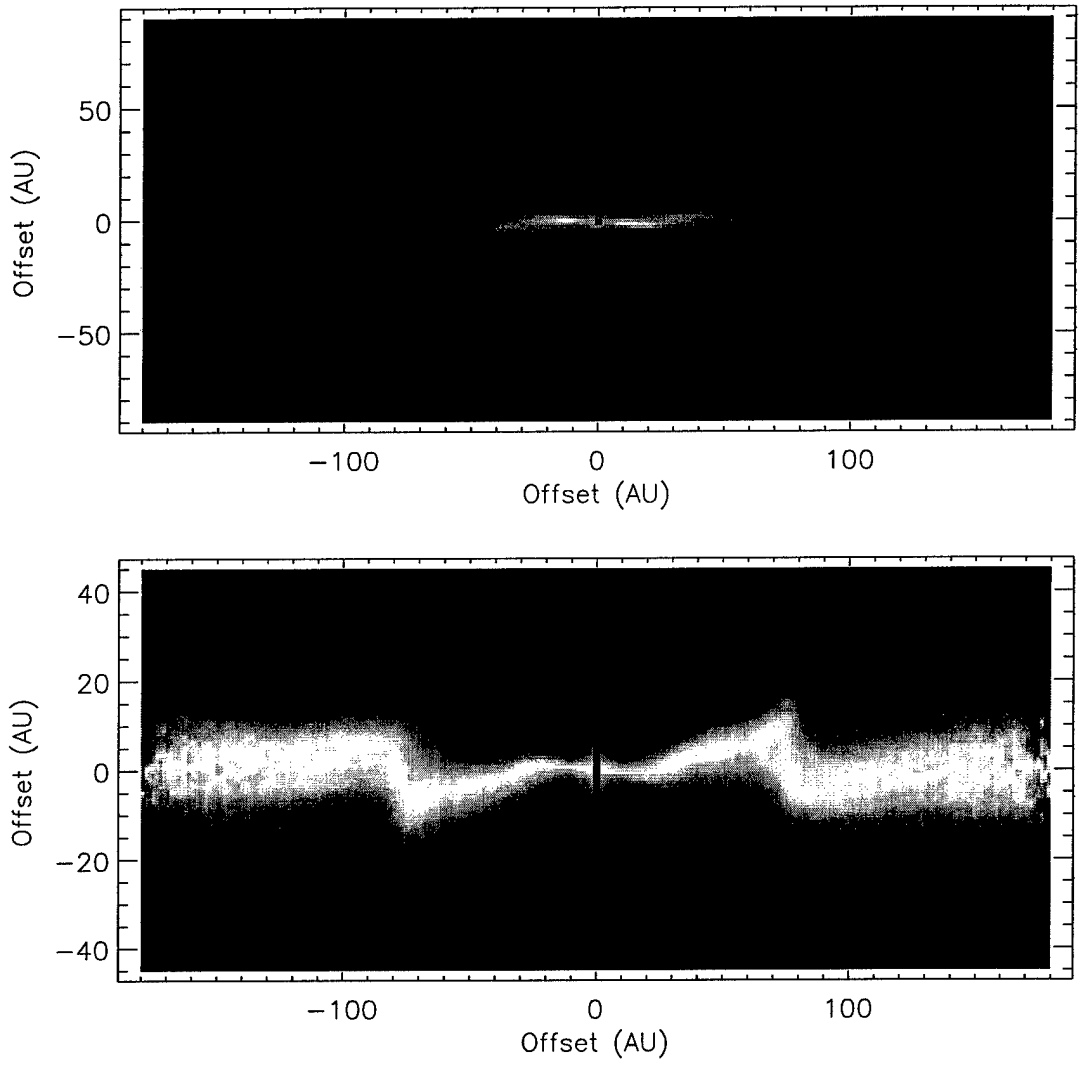

Figure 8–5: A model disk for a two-planet system. The orbital parameters and masses used were determined from the calculation shown in figure 8–3. The planetary system used is the same system that produced the forced inclination shown in the second panel of figure 8–4.

in both plots is 15 AU and corresponds to the estimated radii of the inner hole. The semi-major axis ratio is 2.5 in the first plot and 3.5 in the second plot. The mass ratios in the first and second plots are 0.47 and 0.40 respectively.

Beyond the assumptions already discussed, one additional constraint needed to be considered – the radial extent of the middle or intermediate symmetry plane. Heap et al. (2000) showed the central disk to extend out to about 70 AU which is consistent with the value estimated from the UF observations of about 70-80 AU. This feature corresponds to the region where the forced inclination passes through a significant secular resonance and begins approaching its invariant value. This can be seen in the plots of figure 8–4. For the first configuration, this occurs at approximately 50-60 AU. For the second configuration, this occurs at approximately 80-90 AU. To show how this translates into a disk model, a simple model was developed using the second of the configurations shown in figure 8–4. A visualization of this simple model is shown in figure 8–5. In this diagram, the multiple components can be clearly seen and the relationship between transitional locations and features in the forced inclination are obvious.

It should be noted that with the limited information available this is as far as an analysis of the major symmetry planes can go. Because angular momentum is the key issue, it is only the ratios of mass and semi-major axis that can be constrained by this approach. However, the identification of additional features allows a deeper probing of the system. The way in which this is accomplished is discussed in the next section.

8.2.2 Brightness Enhancements and Voids

A different reduction of the UF data is shown in figure 8–6. This image shows the rotated 18 μm image with irregular contours used to highlight the observed structure. Along the mid-plane of the disk image, multiple brightness enhancements and voids were observed. The voids are arguably logical locations for planets based on current theories describing the accretion/clearing process of planetary formation (Lin and Papaloizou 1993). As was discussed in chapter 2 the region cleared during the process of planet formation is roughly four times the radius of the Hill's sphere. For Beta Pictoris, $M_\star = 1.8 M_\odot$, this corresponds to regions that extend approxiamately $r \approx 0.224\ a\ (m_p/M_J)^{1/3}$. For the values

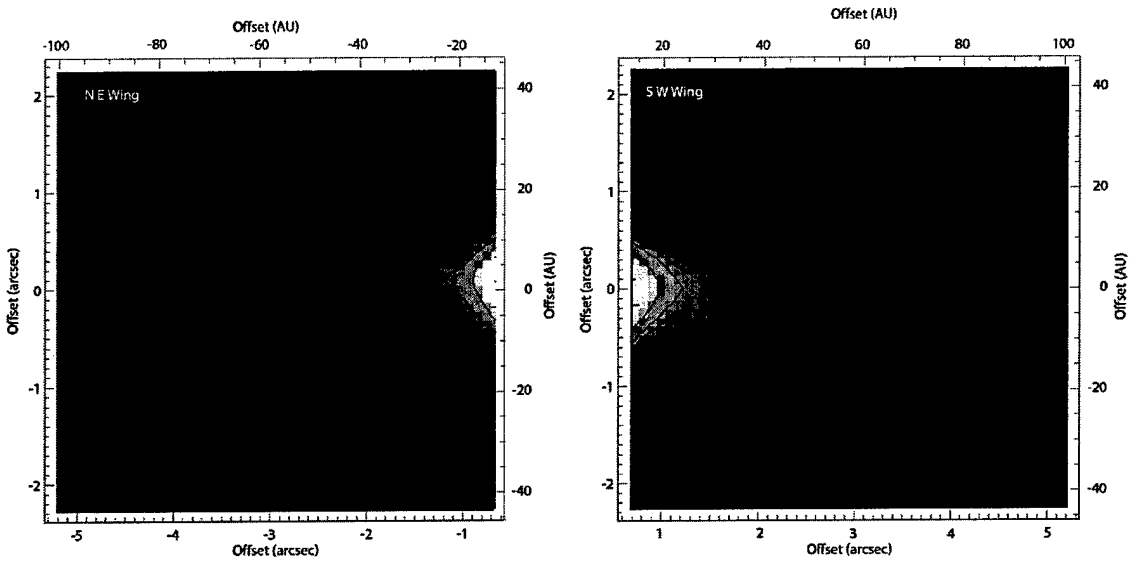

Figure 8–6: (left) 18 μm image of thermal emissions from Beta Pictoris.

of mass and semi-major axis considered in this research, this corresponded to roughly 5-6 AU. These values are consistent with the typical distances between the bright regions which were approximately 6-10 AU.

Gaps are generally attributed to tidal interactions between the planets or protoplanets and the disk. As a result of these interactions, the material interior to the planet's orbit drifts inward and the material exterior to the planet's orbit drifts outward. The inward drift of material is a result of angular momentum being transferred from the disk to the planet and the outward drift of material is a result of angular momentum being transferred from the planet to the disk. Though this work will not investigate the possibility, resonant trapping may also play a significant role in creating regions that appear as bright spots in the observations. As is the case for the asteroid belt, mean motion and/or secular resonances are likely to play roles in defining the boundaries for different reservoirs of asteroid like bodies.

The UF images of Beta Pictoris indicate regions in which gaps within the disk may exist. Brightness enhancements were identified in the observations and are listed in table 8–1. The regions between these bright spots are likely depleted regions and are arguably related to a gap clearing process. Based on the assumption that these potential gaps are a

Table 8–1: Brightness Peaks

NE Wing		SW Wing	
Radial Position	Position Relative to mid-plane	Radial Position	Position Relative to mid-plane
26 AU	North	26 AU	South
32 AU	South	36 AU	North
43 AU	North	42 AU	South
49 AU	South	52 AU	North
58 AU	North	58 AU	South
68 AU	North	68 AU	South
79 AU	North	77 AU	South
93 AU	North	96 AU	South

result of clearing by planetary bodies, the corresponding radii were used as possible ranges for the semi-major axes of the planets constituting the model system.

The gaps may also provide a reasonable means for estimating the eccentricities of the orbits. Based on the analysis done by Sari and Goldreich (2003) there is a symbiotic relationship between the disk and the massive planets within. This relationship provides a connection between the eccentricity of the planets and the gaps which they clear. Sari and Goldreich suggest that once the gap is cleared, the eccentricity of the planet is maintained at a value of $e \approx w/r$, where e is the planet's eccentricity, w is the gap width, and r is the distance from the star. Therefore, the values from the 18 μm image, where the gaps are most clearly observed, provide a constraint to the final model. However, several problems are associated with determining the values of eccentricity with this approach. First, the exact edges of the inferred gaps are difficult to determine. Second, even a conservative estimate of the edge locations suggest extremely large eccentricities for the planets, some as high as $e \sim 0.3$, which are not consistent with estimates based on other considerations such as those presented in the next section. Therefore, the eccentricities determined from this type of analysis of the brightness voids will be used only as an absolute upper limit.

8.2.3 Forced Orbital Elements

The bright spots described in table 8–1 hint at a symmetry in their locations from the central star and in their relative position to the mid-plane of the mid-IR images. Though

not conclusively, this suggests a relationship between regions in the NW extension and in the SW extension. If these regions are related, they can be interpreted as toroidal sections of disk, similar to those described in chapter 4. If this is true, they should have characteristics related to the forced and proper orbital elements as described in that chapter and illustrated in figure 4–6. This implies that the offset of the center of symmetry from the star for each section of disk should relate to the local value of the forced eccentricity. Similarly, the inclination, with respect to a reference plane, should relate to the local value of the forced inclination with respect to the same reference plane.

Extracting the offset and inclination from the observations, for a given value of semi-major axis, allows the development of a tabulated set of forced elements. Though these do not strictly define the form of the forced orbital elements, they do set constraints to which a final form of the orbital elements must adhere.

The way in which the information about the local values of the forced elements was extracted was by reproducing the sections. This was accomplished by reproducing the different sections of disk by defining a set of forced and proper orbital elements for each section. The proper elements were chosen in a way consistent with the relationships discussed in chapter 4: the radial width of the section is $\sim 2ae_p$ and the angular thickness is $\sim 2i_p$. Likewise, the forced elements were chosen in a way consistent with the offset from the center of symmetry being $\sim ae_f$ and the inclination of the section of disk from a reference plane being $\sim i_f$.

Using the parameters that provided the best visual fit, the sections of disk considered were reproduced and are shown in figure 8–7. The figure shows first the sections of disk with no inclination, but with an eccentricity and orientation (longitude of pericenter) capable of reproducing the offsets from the center of symmetry as observed from the observational line-of-sight. It should be emphasized that these two parameters are coupled and cannot be separated with only a single line-of-sight. Second, the same sections are shown but with an inclination and orientation (longitude of ascending node) incorporated that is consistent with the inclination from the reference mid-plane of the mid-IR images. The final two panels show the edge-on view of the system with the final panel only showing the

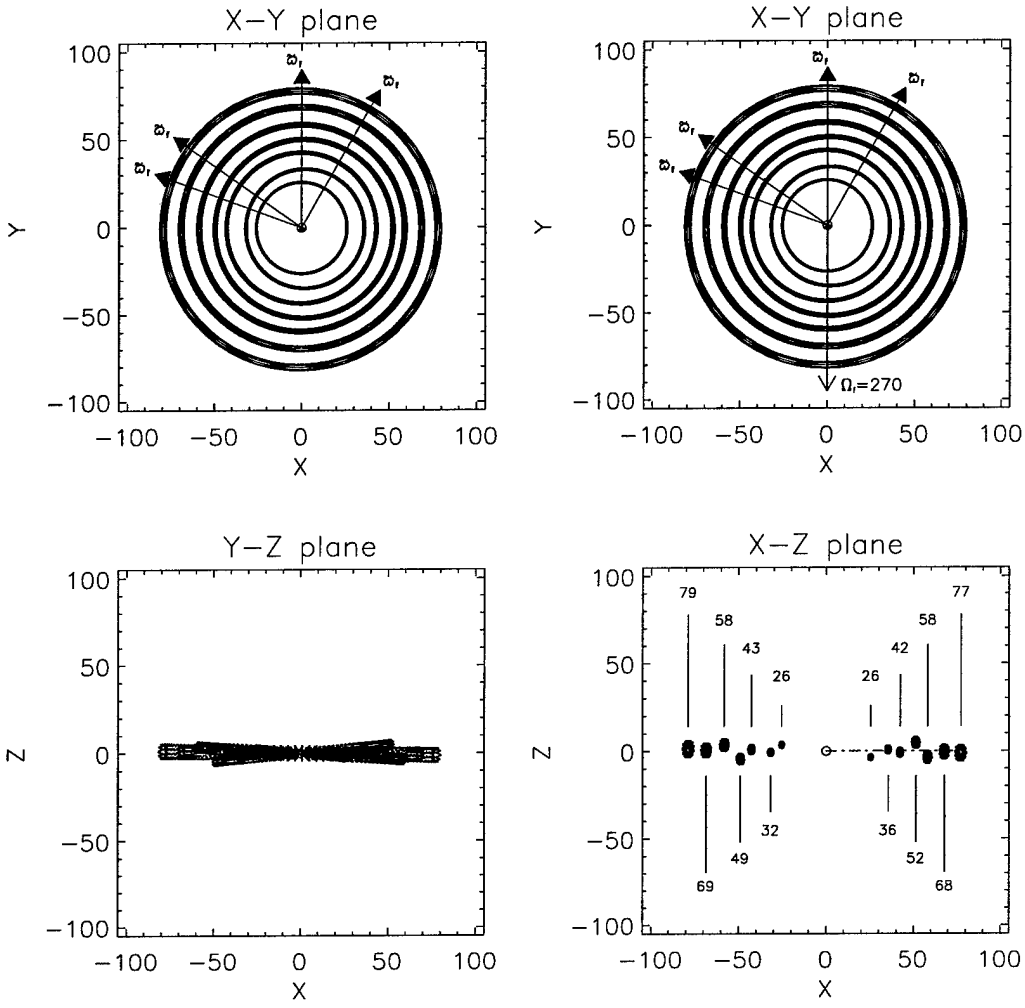

Figure 8–7: Reproduction of the sections of disk possibly identified from the UF observations. a) disk sections with no inclination but with an eccentricity capable of producing the observed offsets in symmetry. b) same as panel a but with a mutual inclination capable of producing the observed positions of the brightness enhancements relative to the mid-plane. c) a side view of the configuration shown in panel b. d) the same as panel c but with only the regions of greatest optical depth shown.

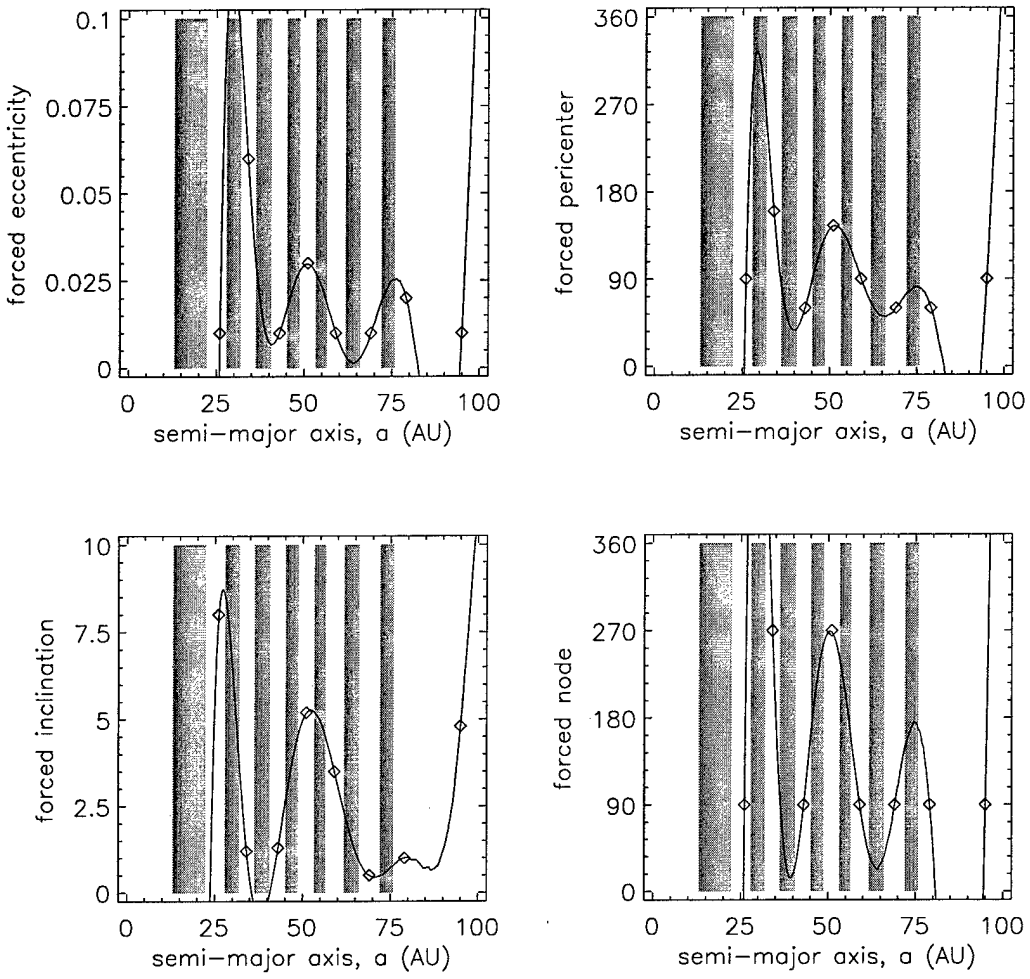

Figure 8–8: A plot of the orbital elements associated with the disk sections shown in figure 8–7. Also shown is a polynomial fit to the points associated with each disk section. Though this does not define the functional form of the forced elements with semi major axis, it does show the constraints to which any solution must conform. The grey areas correspond to the regions in which planets are most likely to be found.

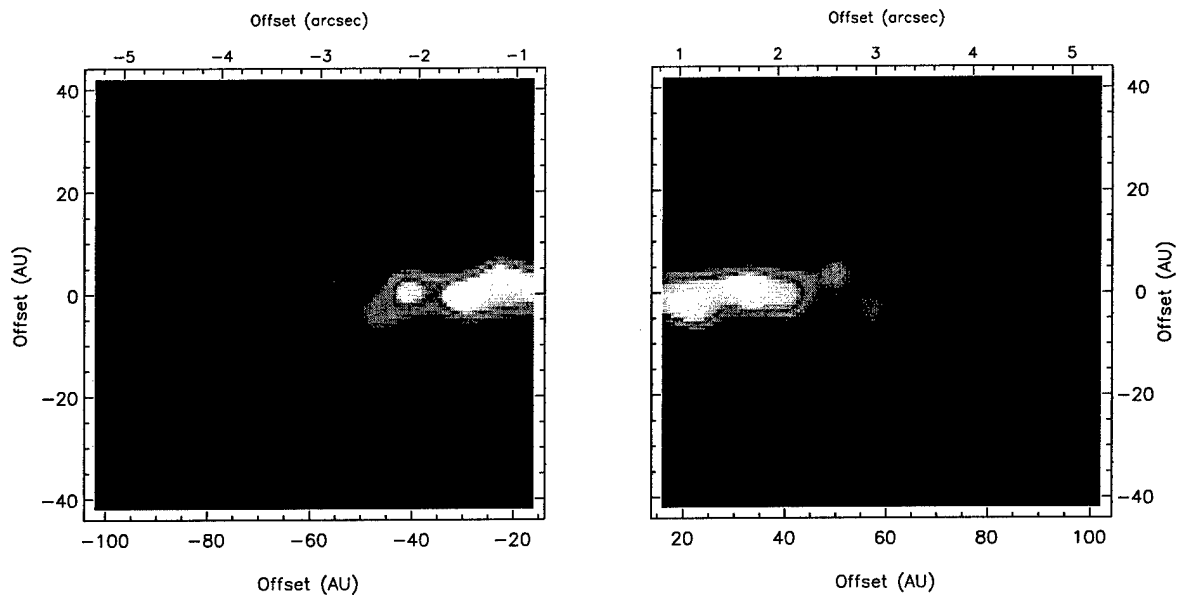

Figure 8–9: Simulated disk based on a set of forced elements extracted from the UF images. The values used for the forced elements are those plotted in figure 8–8.

regions corresponding to those regions with greatest optical depth – the regions that would correspond to the observed bright spots in the observations.

The values for the parameters were found by adjusting the eccentricities and pericenters until the distances from the star to the bright regions, in both extensions, matched those reported in table 8–1. The inclinations and nodes were adjusted until the orientation, with respect to the mid-plane, for each bright spot roughly matched those seen in the image shown in figure 8–6.

The values of the forced parameters that were used to reproduce the locations of the bright spots were tabulated and are shown graphically in figure 8–8. This figure not only shows the complete set of forced orbital parameters, but it also shows the regions in which planets are most likely to be found – the shaded regions in the diagram. This judgment is based on the simple idea that a planet will clear a region of the disk, and thus produce a gap. However, it should be noted that because a planet will create a gap, it cannot be automatically assumed that the apparent presence of a gap is conclusive evidence of a planet. It is also possible that the brightness enhancements are in fact caused by resonant trapping from the gravitational influences from the planets. Secular resonances may also play a role in

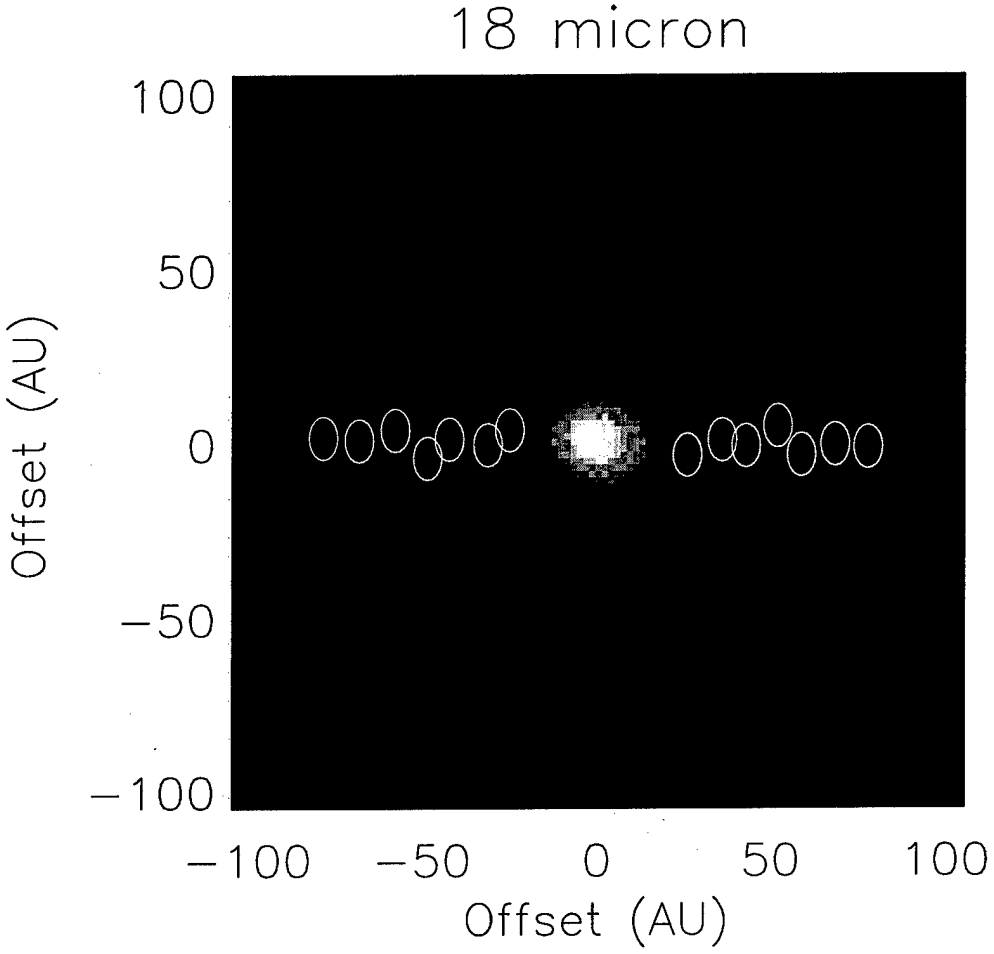

Figure 8–10: Superposition of the estimated brightness locations from figure 8–8 over the 18 μm data.

Table 8–2: Planet Locations and Masses

Planet	a (AU)	Mass (10^{-4} $M_\star$)	Mass (M_{jup})
1	21.2	11.20	2.12
2	31.0	2.50	0.47
3	38.4	1.25	0.24
4	46.0	0.50	0.10
5	55.5	0.30	0.06
6	63.0	0.25	0.05
7	73.5	0.25	0.05

defining the edge of of a distribution of source bodies, much as they due in the asteroid belt of the solar system. However, if it is assumed that the gaps are associated with planets, the brightness enhancements can be logically used to assess the local values of the forced orbital elements. To ensure that a set of orbital elements consistent with these values will in fact reproduce the observed features, a model disk was simulated using the extracted parameters as the forced elements. The result is shown in figure 8–9. This image reproduces the location of the brightness enhancements and more importantly the orientation of each enhancement with respect to the mid-plane. This validates the assumptions made in extracting the estimates of local values for the forced orbital elements from the observations. Figure 8–10 shows a comparison of the locations of the bright spots in figure 8–7 to the 18 μm images of Beta Pictoris.

Once again, it is important to point out that the inclination and node are likely better constraints than the eccentricity and pericenter. Though both are coupled, node to inclination and eccentricity to pericenter, the later set is much more difficult to constrain because of the single line of sight. This fact will be important in the following step of developing a proposed planetary system.

The initial configuration of planets used was based on the assumption that each region identified as a prospective gap corresponded to a plant, and thus set the value for the semi-major axis. Figure 8–11 shows a complete set of forced orbital elements calculated from secular perturbation theory as described in chapter 3. This set is based on seven planets, represented by the filled circles, placed within the regions identified as likely locations for planets (the shaded regions). This model is constrained by the values determined from

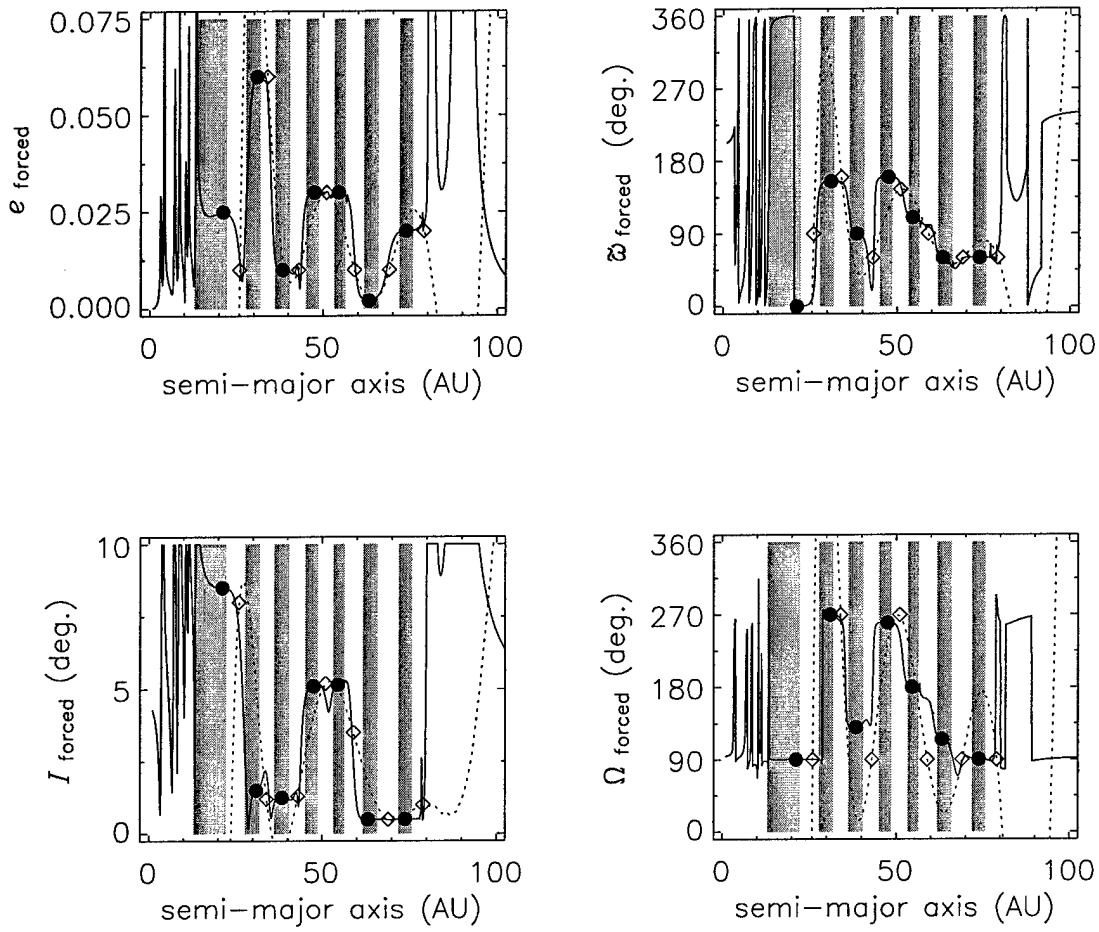

Figure 8–11: A complete set of forced orbital elements as a function of semi-major axis for a seven planet system. The masses associated with the planets are shown in table 8–2.

analysis of the disk sections (shown as diamonds on the plots) and by the large scale symmetry planes.

The approach in selecting a set of orbital elements took two steps. The first step was to investigate whether or not a system of planets located in each of the regions interpreted as gaps could produce a set of forced orbital elements consistent with the constraints extracted from the observations – the observed sections of disk. The secondary goal was to investigate whether or not a fewer number of planets could also produce a set of orbital elements that was consistent with the constraints described above. The absolute minimum number of planets needed was based on the number of major symmetry planes. Since there are three well documented symmetry planes, a minimum of two planets was needed (see discussion in chapter 4). However, it was found through trial and error that the behavior of the forced inclinations, as illustrated in figure 8–8, could not be reproduced without additional masses. Planets were added to the gap locations, one at a time, until the calculated forced elements provided a reasonable match to the constraints extracted from the observations. The locations of the planets were chosen based on the details of the warp. The specific gap locations were chosen by determining where the most dramatic changes occurred between two consecutive regions of disk.

The minimum number of planets is clearly difficult to determine. The number is clearly more than two, but beyond that, the number becomes difficult to constrain. An example of a calculation of forced orbital parameters, highlighting the problem in determining the minimum number of planets, is shown in figure 8–12. This figure shows the forced inclination and node for a two and three planet system. Also shown on the plot are the values extracted from the observations. The two planet system clearly cannot produce the complex structure suggested by the observations. The three planet system, on the other hand, at first inspection hints at the possibility of fitting the observed values of forced inclination. However, when the calculated and observed values for the forced longitude of ascending node are examined, the three planet system clearly is unable to reproduce the necessary values of the forced node. This is significant because it is the value for the forced node that defines the orientation of the observed sections of disk. Through further iterations of placing and moving planets, it was found that a five planet system could also reproduce the

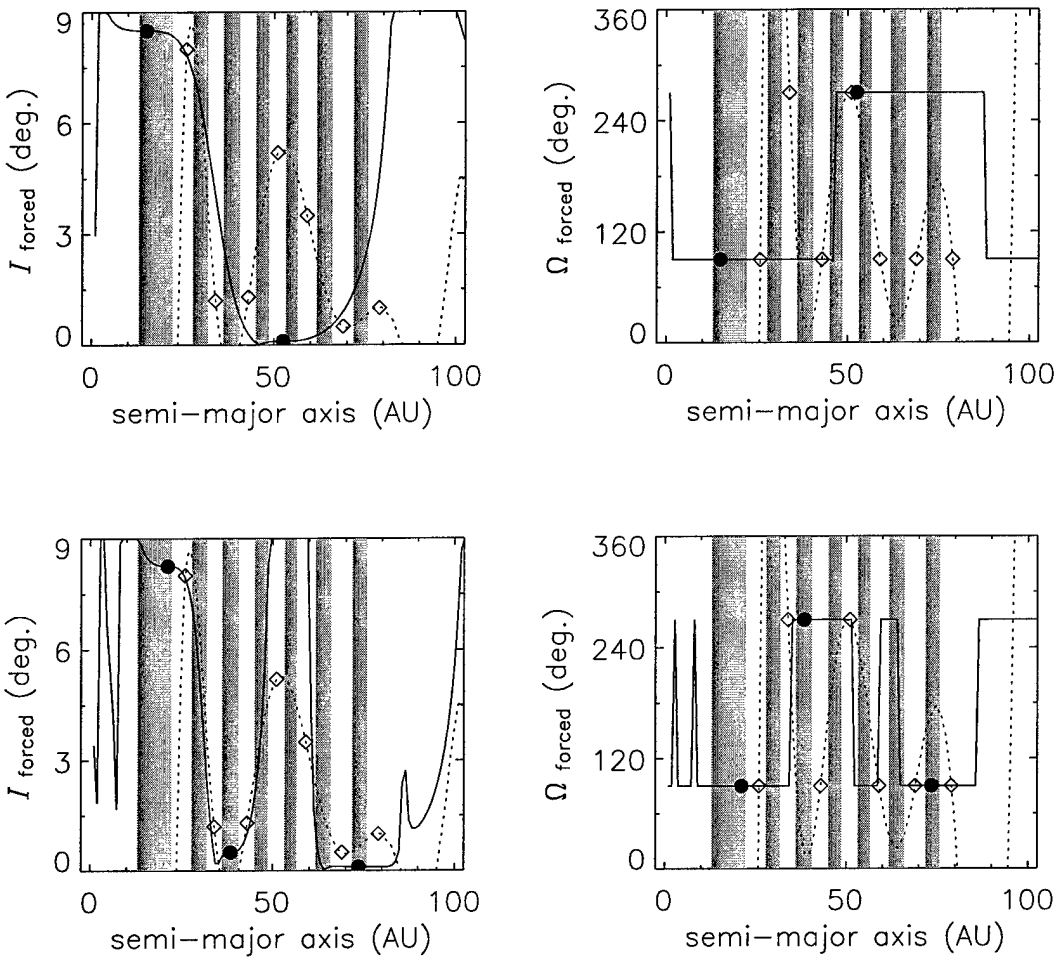

Figure 8–12: The forced inclination and node for a two (top) and three (bottom) planet system. The diamonds correspond to the values extracted from the observational data. The masses for the planets are $M_1 = 0.5M_J$ and $M_2 = 0.2M_J$ in the top set and $M_1 = 0.7M_J$, $M_2 = 0.2M_J$, and $M_3 = 0.2M_J$ in the bottom set.

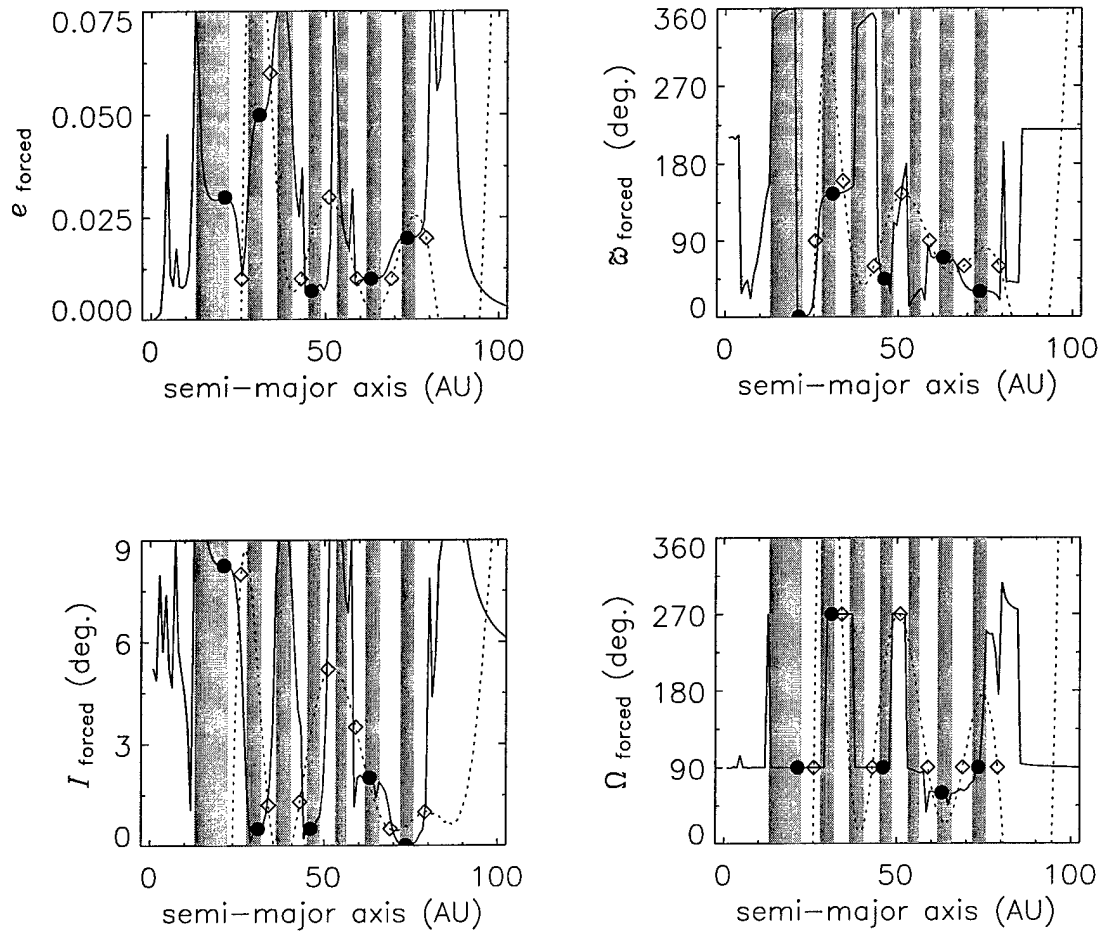

Figure 8–13: A complete set of forced orbital elements as a function of semi-major axis for a five planet system.

necessary forced elements. The forced orbital elements calculated for a five planet system are shown in figure 8–13. This provides a further example of how a multiple planet system is capable of meeting the constraints set by analysis of the observed sections of disk. This type of analysis would therefore suggest that the number of planets is between five and seven.

However, one important characteristic about the form of the forced orbital elements for the five planet system must be made clear. Though the plot of the forced elements passes through the points corresponding to the observed sections of disk, it is the dramatic behavior of the curve that allows this to happen. The case is the same for the six planet

systems. What this implies is that for such a system of planets to produce the type of morphology observed in Beta Pictoris, the high amplitude perturbations are required to play a significant role. The difficulty with this is that a region affected by high amplitude perturbations is likely to not exist for a long period of time and thus not necessarily relate to truly observable features. It is for this reason, that the most likely candidate is the seven planet system.

The values of the resulting forced elements were constrained by the observed disk sections but the masses were primarily constrained by angular momentum considerations. As was discussed earlier, the large scale symmetry planes are related to primary angular momentum planes which are heavily dependent on the planetary masses. Ergo, the masses of the planets were adjusted, after the locations were chosen, until the large scale symmetry planes matched those discussed earlier. Another way of considering this, is that the masses were adjusted until the invariant value of forced inclination matched the inclination of the outer disk. The masses of the planets in units of stellar masses and in units of Jupiter masses are shown in table 8–2

The models associated with the various simulations based on parameters developed in this section are discussed and shown in the following section.

8.3 Model vs. Observations

The most well studied characteristic of the Beta Pictoris disk is the observed warping of the disk's mid-plane. It has been shown in previous analysis that the warp can be considered as an edge-on ($\sim 2-3$ degrees) view of a multi-component disk in which the components have a non-zero mutual inclination. The most recent observations suggest that this multi-component system consists of three primary components.

The first goal of any model simulating the Beta Pictoris disk must reproduce the three major symmetry planes. Per the discussion in chapter 4, the major symmetry planes are likely to be associated with specific angular momentum planes associated with the planetary orbits. To recreate this warping, it is thus necessary to invoke a configuration of planetary orbits corresponding to the observed symmetry planes of the inner disk and whose total angular momentum vector defines the observed large scale symmetry plane. The presence

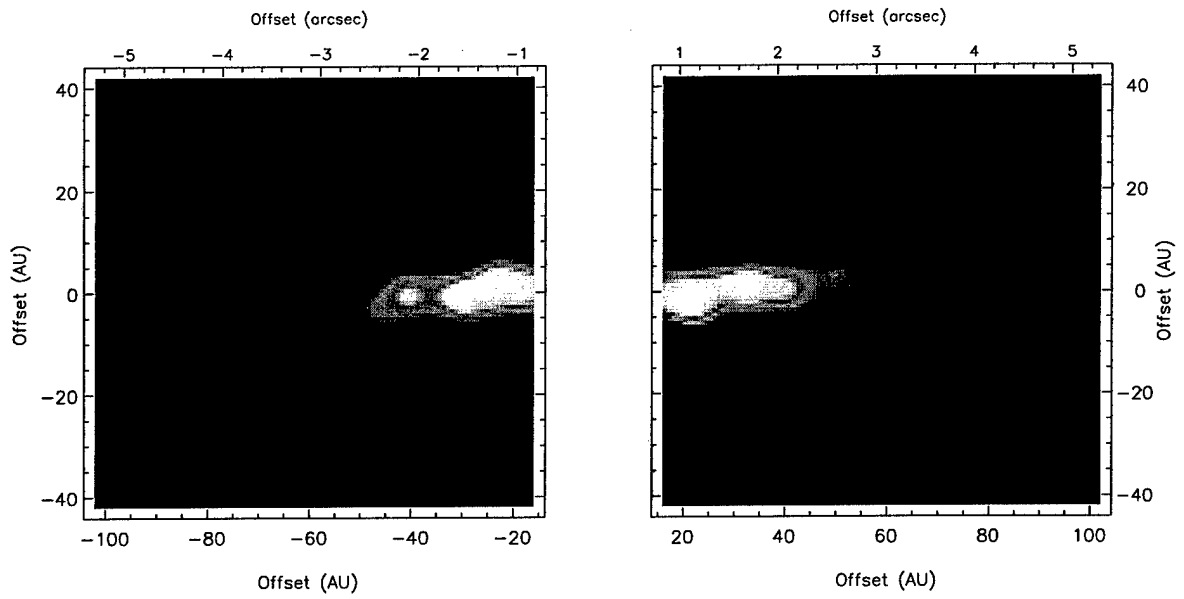

Figure 8–14: Simulated disk based on orbital elements constrained by the UF 18 μm images. The values for the forced orbital elements are those shown in figure 8–11 and the values for the planetary masses are those shown in table 8–2.

of planets, however, must produce additional effects as the planets interact with the circumstellar material. These effects should produce, at the very least, gaps in the circumstellar disks. The final model of the Beta Pictoris disk must therefore reproduce the major symmetry planes, have planetary orbits consistent with the observed gaps, and have forced orbital elements that will shape the disk in such a way as to reproduce the features observed in the high resolution images. Albeit a non-unique solution, one planetary configuration that produces a model satisfying these requirements is presented in this section.

8.3.1 Major Symmetry Planes

The most well documented aspect of the mid-plane warping is the warp first quantified by Heap et al. (2000). This warp shows an inner region that is inclined to the outer region by about 5 degrees and reaches a maximum amplitude of about 1.5 AU at approximately 60 AU from the star. The inner warp has only been observed in several observations as it is more difficult to identify due to the proximity to the star. The UF images shown in figure 8–1 also suggest an inner tilted component. The same is true for the model disk based on

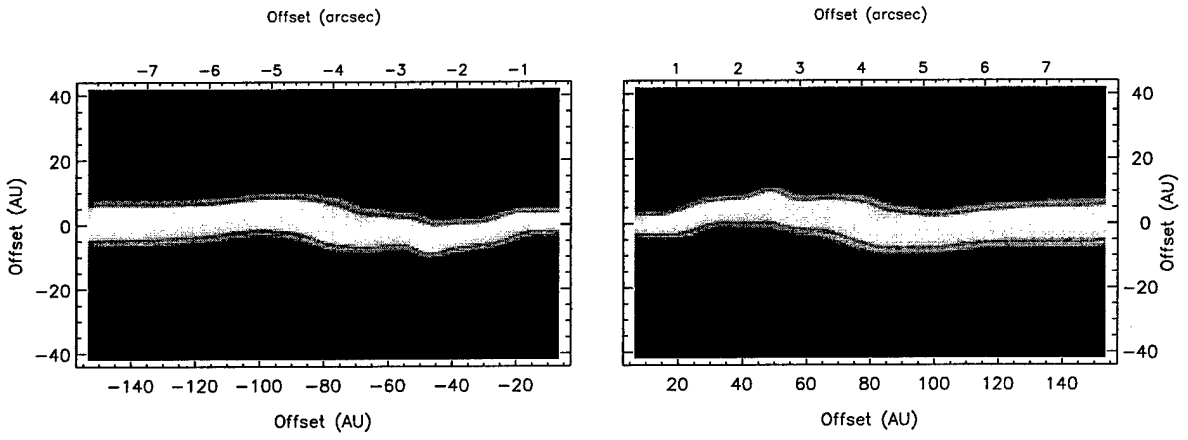

Figure 8–15: The large scale structure of the model disk shown in figure 8–14, but with each vertical slice normalized to the peak value of the slice.

those observations. A plot illustrating the large scale structure of the model disk is shown in figure 8–15. This image is clearly consistent with the outer warp identified by Heap et al., and, to the same extent that the UF images are, is consistent with the inner plane.

The primary symmetry planes are significant as they relate the inner planets to the large scale structure. The inner and intermediate symmetry planes reveal the orientation of the angular momentum planes associated with the planets. The outer or invariant plane of the disk is associated with the system's total angular momentum. These connections are important because they imply that a simple way to make a first approximation of a potential planetary system can be accomplished by simply considering the angular momentum for each planetary orbit in the proposed system. Therefore a matching of major symmetry planes in the model is not a significant accomplishment. To exemplify this point, a simpler model could easily reproduce the major symmetry planes. An approach to modeling the major symmetry planes based on these assumptions was discussed in section 8.2.1. In the case of Beta Pictoris, planets were required to be chosen in a way that the orientation of their orbits matched the inner and intermediate symmetry planes. The masses then needed to be adjusted to provide the necessary total angular momentum and hence the invariant plane associated with the total angular momentum vector.

This implies that if only the three major symmetry planes were desired, this could be accomplished with 2 planets – one for each of the inner symmetry planes. The model can

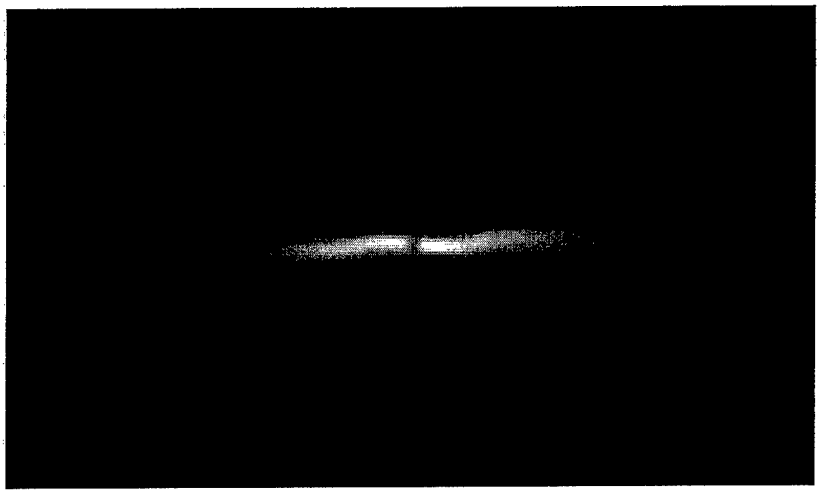

Figure 8–16: A simple model of the distribution of material in a system perturbed by three planets. The inner planes are associated with planes of the perturbing planets and the large scale invariant plane is that associated with the systems total angular momentum vector.

be further tuned by adding additional planets. Such a toy model is shown in figure 8–16, but as discussed above is relatively meaningless. Fortunately, additional constraints exists. The presence of planets will have additional effects; such effects are clearly observed in the UF images. These observable effects include the gaps and small scale structure that are discussed in the next section.

8.3.2 Brightness Enhancements and Voids

A model created using the forced elements matching the constraints extracted from the observed sections of disk is shown in figure 8–14. The model was created by simulating each section of disk observed in the UF images. Each section of disk was influenced by the distribution of proper elements discussed in the previous chapter and the forced elements determined for the seven planet system shown in figure 8–11. As a note, the five planet system was equally capable of producing the features. The distribution of surface area was created by using a superposition of each section of disk where each section was weighted based on the estimated form of the number density radial distribution given in equation 7.6. The final image was created using the flux determined for 10 μm particles.

The resulting model clearly shows the sections of disk observed in the 18 μm images with the same orientation relative to the reference plane. Furthermore, the offset of the

center of symmetry with respect to the star suggested for each section of disk has also been reproduced. The eccentricities associated with each planet also are consistent with the gaps in the model image as well as the observations.

In addition to the gaps created by accretion, it is possible for particles to enter the regions near a planet that could remove the particle form the system. As was discussed in chapter 4, because of the vector relationship between the proper and forced orbital elements particles will reach a maximum eccentricity that may or may not bring them close enough to a planet to be removed and thus cause depletion for a particular section of disk. This is especially true for particles that are in regions influenced by secular perturbations. A calculation to assess this effect is shown in figure 8–17. The top panel shows the forced eccentricity for the seven planet system whose orbital elements are shown in figure 8–11. The middle panel shows the intersections of the regions assumed to be affected by the planets and the maximum excursion by the dust particles. It is at these intersections that depletion is likely to occur. The bottom plot shows the gaps created in the radial number density distribution given in equation 7.6. Further investigation into the consequences of this analysis in terms of disk structure and stability are saved for a later work. Other contributing influences, such as resonnance overlap, are also likely to play a significant role and need to be considered.

8.4 Discussion

In this chapter, it has been shown that the type of mid-plane warping observed in the Beta Pictoris circumstellar disk can be accounted for by the secular perturbations associated with a multiple planet system. Mid-plane warping is clearly a consequence of a distribution of forced orbital elements in which the forced inclination varies with semi-major axis. This is consistent with both theoretical modeling and observed effects within the solar system dust bands.

Many additional factors could be added to the model presented here to add further sophistication to the modeling process. Some of these will be discussed in the following

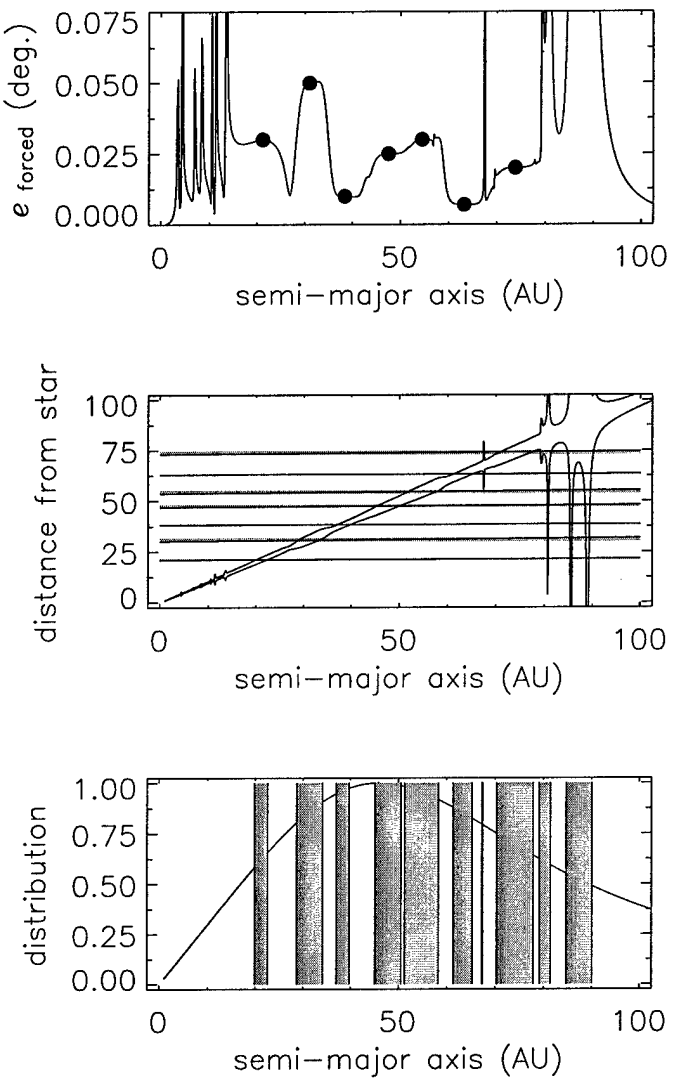

Figure 8–17: A plot describing the potential impacts on the distribution of material as a results of secular perturbations, especially resonances. The top plot shows the forced eccentricity for the seven planet model. The middle plot shows the radii at which regions should be cleared by planets and the maximum and minimum excursions of dust particles. The bottom plot shows the impact of the cleared regions on the assumed radial number density distribution for the disk material.

chapter, however they do not discredit the results and conclusions presented in this research. The basic conclusions of this chapter are the following:

- The environmental factors inferred from observations of the Beta Pictoris disk strongly suggest that the disk is dominated by collisional processes. This implies a reservoir of larger bodies that are subjected to secular perturbations. This creates a view in which the morphology of the disk is dominated by the dynamics of the larger bodies despite the observations being dominated by the smaller, shorter lived, dust particles.

- The age of the Beta Pictoris disk, based primarily on the Hipparcos data, provides strong support for the assertion that the Beta Pictoris disk has had enough time to fully evolve under the influences of the secular perturbations associated with the planetary systems used in the models presented within this chapter.

- Secular perturbations of a multiple planet system produce a distribution of forced inclinations that vary with semi-major axis and thus produce a warped mid-plane.

- The secondary effects associated with the presence of planets and suggested by the observations, are consistent with the expected effects of the planets used to create the large scale warping.

CHAPTER 9
FURTHER CONSIDERATIONS

The model presented within this dissertation, though based on reasonable assumptions, is somewhat idealized. A more complex model could be investigated by considering a more sophisticated use of the disturbing function. Two examples are briefly discussed in this chapter and involve the consideration of the effects of a massive disks and the likely non-spherical shape of the central star. Both effects are easily handled within the theory presented in earlier chapters simply by adding either more perturbing masses or by adding additional terms to the disturbing function.

9.1 Massive Disks

It was asserted earlier that the mass of the dust within the disk of the Beta Pictoris model is insignificant compared to the combined mass of the planets. However, this is based on many assumptions, one of which is the assumed value of the dust to gas ratio which has significant uncertainty. Furthermore, estimated values of the disk mass based the sub-mm measurements discussed earlier ignore the contribution from the more massive bodies like asteroids.

Therefore, it is reasonable to consider the effects on the forced orbital parameters when the mass of the disk becomes comparable to that of the combined mass of the planets. Figure 9–1 illustrates the result of one such calculation. This figure shows the forced inclination calculated for a massless test particle presumably within a disk that is disturbed by three massive bodies on a similar scale and with similar values of inclination as those used in the Beta Pictoris model. The filled circles of zero-inclination correspond to masses that were used to simulate the distribution of mass within the disk by equally distributing the assumed disk mass among masses. The three different realizations allowed for different values of total disk mass. The top panel shows the result when the mass of the disk is

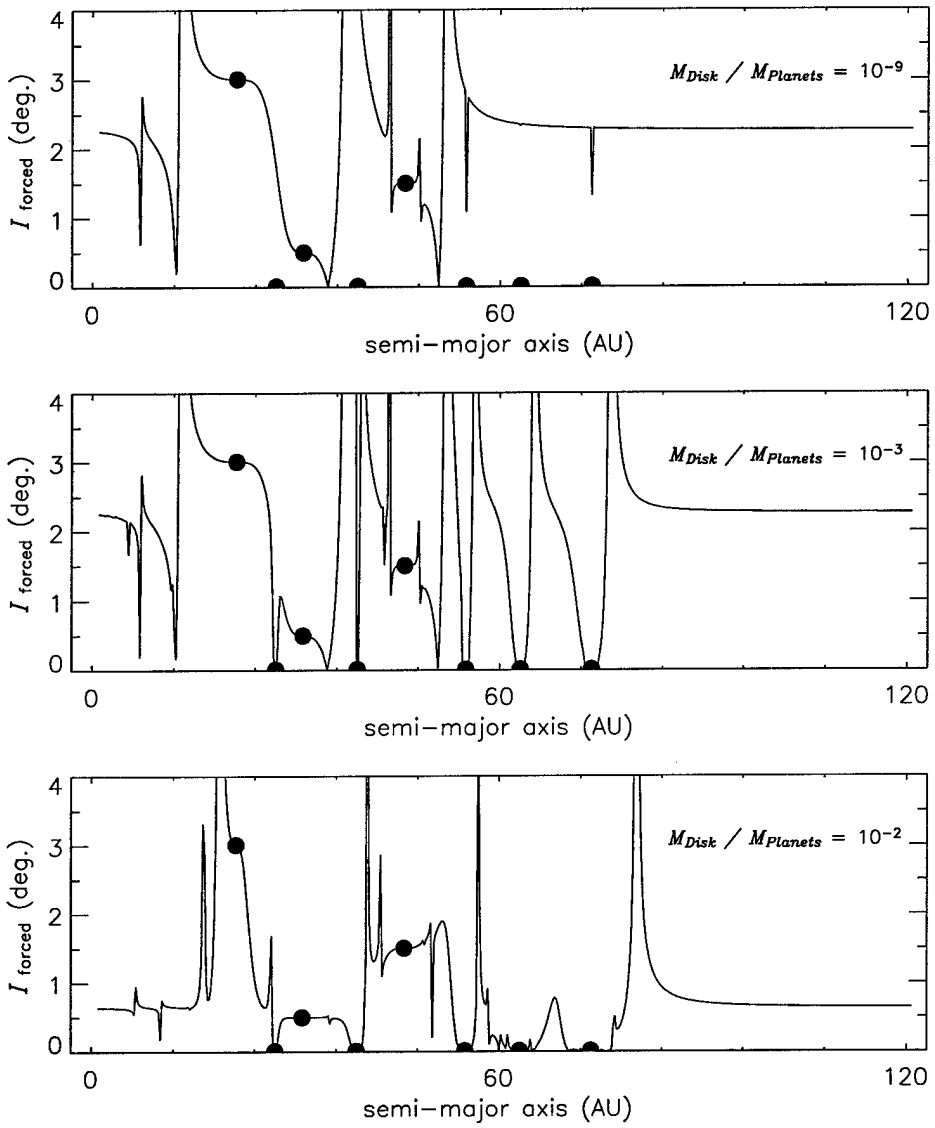

Figure 9–1: The forced inclination for a test particle perturbed by a three planet system; the planets are shown by the filled circles with non-zero values of inclination. The mass of the disk is simulated by adding additional bodies (the zero inclination objects). The top panel shows the result when the combined mass of the disk is equal to 10^{-9} that of the combined mass of the planets. The middle panel shows the same for a mass ratio of 10^{-3} and the bottom shows the same for a mass ratio of 10^{-2}.

arguably insignificant to that of the planets; mass ratio of $\sim 10^{-9}$. The middle panel shows the same system but with the mass ratio increased to 10^{-3}. The bottom panel shows the result when the mass ratio is about 10^{-2}. As a reference, this research assumes an upper value of $M_{disk}/M_{planets} \sim 10^{-5} - 10^{-4}$, which is based on the estimate of the total Beta Pictoris disk mass of $\sim 0.1 - 1.0\ M_{\oplus}$. Though this value neglects the potential contribution from asteroids and other massive bodies within the disk, a significant enough margin of error exists such that the results obtained are reasonably valid.

The results shown in figure 9–1 show the characteristics that should be expected based on discussions in previous chapters. First, for a common semi-major axis the forced orbital elements for the test particle are equal to the osculating orbital elements of the massive bodies. Second, the region around which the massive bodies impose their orbital elements on the test particles is a strong function of mass. Therefore, as the mass of the disk increases, the influence of the disk becomes comparable to that of the planets. This causes the forced elements to match not only the planets, but the disk as well.

The net results of the massive disk is to dampen the effects of the planets. This is seen by the fact that the regions over which the planets exert their influence becomes more spatially limited as the disk mass increases. Another effect is that the invariant plane of the disk, defined by the asymptotic value of forced inclination, approaches a value closer to that of the disk. This would cause large scale warping to become less obvious in external observations. When coupled, these two effects, dampening of the structure created by the planetary perturbations and forcing the invariant plane of the system and the plane of the disk to become coplanar, would serve to diminish the observable characteristics of planets existing within a disk. This suggests that the there may be an ideal epoch over which the observations of structure within a circumstellar can be used to identify the dynamical signatures of planets.

Though this example shows some of the important effects of a massive disk on the observable characteristics of a circumstellar disk, it is still overly simplified. A model based on additional masses spread over a larger region would better simulate a realistic distribution of dust material.

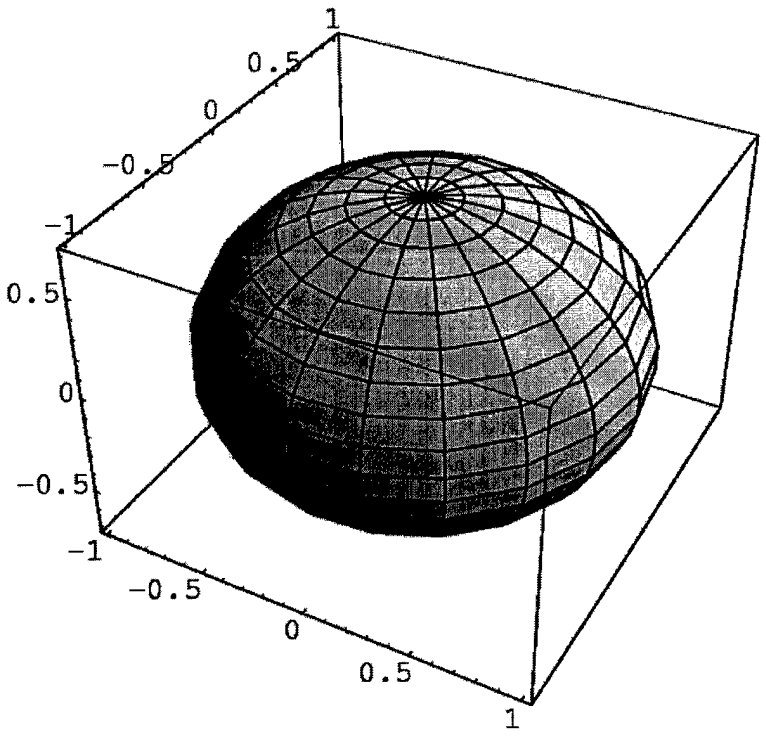

Figure 9–2: An oblate spheroid with an oblateness of 0.25.

9.2 Oblateness of the Central Star

The calculations performed in this research are based on the assumption that the central mass is perfectly spherical. However, a rotating non-rigid body will flatten to an oblate spheroid. This is seen in the sun and the planets within the solar system. An oblate spheroid is generally defined as a spherical object in which the equatorial radius is greater than the polar radius. An example is shown in figure 9–2.

The oblateness of a central star will induce changes in a gravitational potential from one based on a spherical central object. In the context of this research, the oblateness effects are manifested as an addition to the disturbing function (Murray and Dermott, 1999). For particle j, the part of the disturbing function describing the effects of oblateness can be

expressed as

$$\begin{aligned}\langle \mathcal{R}_j^{(obl)} \rangle \;=\; & \\ & \frac{1}{2} n_j^2 a_j^2 \Big[\frac{3}{2} J_2 \Big(\frac{R_c}{a_j} \Big)^2 - \frac{9}{8} J_2^2 \Big(\frac{R_c}{a_j} \Big)^4 - \frac{15}{4} J_4 \Big(\frac{R_c}{a_j} \Big)^4 \Big] e_j^2 \\ & - \frac{1}{2} n_j^2 a_j^2 \Big[\frac{3}{2} J_2 \Big(\frac{R_c}{a_j} \Big)^2 - \frac{27}{8} J_2^2 \Big(\frac{R_c}{a_j} \Big)^4 - \frac{15}{4} J_4 \Big(\frac{R_c}{a_j} \Big)^4 \Big] I_j^2 \end{aligned} \tag{9.1}$$

where R_c is the radius of the star and a_j is the semi-major axis of the particle. The J terms are the gravitational moments. These terms can be expressed as functions of the oblateness, $\epsilon = (a - c)/a$, and the oblateness constant, $q = r^3\omega^2/(GM)$. Typical solar values for oblateness are thought to lie between $5.0\pm\ 0.7\times10^{-5}$ (Dicke and Goldenberg 1967) and $9.6\pm6.5\ \times10^{-6}$ (Hill and Stebbins 1975). Values for q are typically one or more orders of magnitude smaller. Though Beta Pictoris may have values significantly different from the sun because of the difference in mass ($\sim 1.8 M_\odot$) and a different rotation rate, these values should give an idea of the general magnitude.

Based on the model parameters considered in this research, oblateness should have minor effects on the results. The J terms are likely to be in the realm of $\sim 10^{-5}$. The minimum value of semi-major axis considered for particles within the disk was $\sim$ 20 AU and the the radius of Beta Pictoris, if comparable to the sun, is $\sim 10^{-3}$ AU. This implies that the the terms $J_i^n (R_c/a)^m$ are $\sim (10^{-5})^n (10^{-4})^m$. When compared to the other terms in the disturbing function, these are clearly negligible.

The appropriate terms to consider in making the comparison are the elements of the A and B matrices associated with the secular part of the disturbing function.

$$\begin{aligned}\langle \mathcal{R}_j^{(sec)} \rangle \;=\; & n_j a_j^2 \Big\{ \frac{1}{2} A_{jj} e_j^2 + \frac{1}{2} B_{jj} I_j^2 \\ & + \sum_{k=1, k\neq j}^{N} A_{jk} e_k e_j \cos(\varpi_j - \varpi_k) + \sum_{k=1, k\neq j}^{N} B_{jk} I_k I_j \cos(\Omega_j - \Omega_k) \Big\} \end{aligned} \tag{9.2}$$

where the values of A and B are functions of mass and semi-major axis only, and are given by

$$A_{jj} = -n_j \frac{1}{4} \sum_{k=1,k\neq j}^{N} \frac{m_k}{m_c + m_j} \alpha_{jk} \bar{\alpha}_{jk} b_{3/2}^{(2)}(\alpha_{jk}) \tag{9.3a}$$

$$A_{jk} = -n_j \frac{1}{4} \frac{m_k}{m_c + m_j} \alpha_{jk} \bar{\alpha}_{jk} b_{3/2}^{(2)}(\alpha_{jk}) \tag{9.3b}$$

$$B_{jj} = -n_j \frac{1}{4} \sum_{k=1,k\neq j}^{N} \frac{m_k}{m_c + m_j} \alpha_{jk} \bar{\alpha}_{jk} b_{3/2}^{(1)}(\alpha_{jk}) \tag{9.3c}$$

$$B_{jk} = -n_j \frac{1}{4} \frac{m_k}{m_c + m_j} \alpha_{jk} \bar{\alpha}_{jk} b_{3/2}^{(1)}(\alpha_{jk}) \tag{9.3d}$$

These values can be thought of as constant matrix elements and have typical values of $\sim 10^{-3}$, for the type of configuration of planets used in the final models. These values are significantly larger than those associated with the oblateness. This suggests that for the conditions and scales considered in this research, oblateness plays a small or insignificant role.

Though oblateness may not play a role in Beta Pictoris, the effects of a significantly oblate, rapidly rotating star on the accompanying circumstellar disk could prove to be an interesting problem to study.

CHAPTER 10
CONCLUSIONS

The research presented in this dissertation was an investigation into the phenomenon of mid-plane warping in circumstellar disks. This particular effort was inspired by the observations made by the UF mid-IR team of the circumstellar disk of Beta Pictoris. These observations provided images that showed with unprecedented clarity the features of the disks mid-plane. Within the images, was clear evidence of a complex morphology. Furthermore, analysis of the brightness distribution suggested regions in which the dust was depleted. Both of these characteristics strongly suggest the presence of planets.

The basic circumstellar environment was modeled using values for input parameters taken from the extensive coverage of Beta Pictoris found in the literature. These parameters included the dust grain material properties, the radial number density distribution, and the proper orbital elements. Also taken from the literature was the data necessary to estimate the timescales associated with different physical processes and in turn validate the applicability of a secular analysis.

Using secular perturbation theory, a circumstellar disk perturbed by a system of planets was simulated. The planets considered were constrained by observable features of the disk. These features included both large scale and small scale features. The large scale features were the major symmetry planes of the system with transitions at $\sim$20 and 80 AU and have been documented in multiple sources. The small scale features were clearly visible only in the UF images and consisted of brightness enhancements and small scale warping.

The large scale symmetry planes were addressed first. Analysis of these planes provided insight into the dominating angular momentum planes as well as the system's total angular momentum plane. The inner symmetry planes constrained the orientation of the planetary orbits and the outer, invariant plane of the disk constrained the relative masses of the planets by constraining the total system angular momentum.

The small scale features constrain the disk in two ways. First, the regions corresponding to potential gaps were likely to be related to the location of the planets. Based on the observed enhancements in brightness and the interpretation that the enhancements were visible sections of disk, the potential gap regions were isolated. The radial width of these regions were an upper limit to the expected gap width associated with a planet, $w \sim re$. These gap regions also provided a constraint to the masses through the assessment of the accretion zones. The accretion zones are related to the Hill sphere associated with the corresponding planet. The radius of the sphere is determined by the planetary mass and the distance from the star. Therefore the gaps also provides an upper limit to the mass a planet presumed to be located in that particular gap. The second constraint, was associated with the locations of the brightness enhancements with respect to the reference mid-plane. The inclination and orientation of a disk section with respect to the mid-plane of the disk is related to the local value of the forced inclination and longitude of ascending node respectively. This constraint on the forced inclination and node is a constraint on the magnitude of the perturbation and hence a constraint on the inclinations and orientation of orbits of the perturbing planets.

This research suggests that the quantifiable characteristics of the features observed in a circumstellar disk can be used to extract information that will constrain the characteristics of a perturbing planetary system. This means that high resolution images of circumstellar disks can offer not only an alternative to methods like stellar radial velocity measurements as a means to detect exosolar planets, but can actually provide solid constraints on the characteristics of what are likely to be very complex dynamical systems.

APPENDIX:
PLANETARY ORBITAL ELEMENTS

Throughout this research comparisons have been made between proposed planetary systems and the solar system. The following table provides the orbital elements associated with each planet in the solar system (excluding Pluto) (Murray and Dermott, 1999).

Planet	a_0 (AU)	m (10^{24}kg)	e_0	I_0 (deg.)	ϖ_0 (deg.)	Ω_0 (deg.)
Mercury	0.38709893	0.3302	0.20563069	7.00487	77.45645	48.33167
Venus	0.72333199	4.8685	0.00677323	3.39471	131.53298	76.68069
Earth	1.00000011	5.9736	0.01671022	0.00005	102.94719	348.73936
Mars	1.52366231	0.64185	0.09341233	1.85061	336.04084	49.57854
Jupiter	5.20336301	1898.6	0.04839266	1.30530	14.75385	100.55615
Saturn	9.53797932	568.46	0.05415060	2.48446	92.42194	113.71504
Uranus	19.19126393	86.832	0.04716771	0.76986	170.96424	74.22988
Neptune	30.06896348	102.43	0.00858587	1.76917	44.97135	131.72169

The above orbital elements are for the epoch of J2000 with respect to the mean ecliptic and the equinox of J2000.

REFERENCES

Aitken, D. K., Moore, T. J. T., Roche, P. F., Smith, C. H., and Wright, C. M. 1993, MNRAS, 265, L41

Alekseeva, G. A., et al. 1996, Baltic Astron., 5, 603

Armitage, P.J. and Pringle, J.E. 1997, ApJ, 488, L47

Artymowicz, P. 1997, Ann. Rev. Earth Planet Sci., 25, 175

Artymowicz, P., 1999, in *Space Science Reviews*, 92, 69-86

Artymowicz, P., Burrows, C., Paresce, F. 1989,ApJ, 337, 494

Artymowicz, P., and Clampin, M. 1997, ApJ, 490, 863

Aumann, H. H. 1984, BAAS, 16, 483

Aumann, H. H. 1985, PASP, 109, 301

Aumann, H. H., Gillett, F. C., Beichmann, C. A., de Jong, T., Houck, J. R., Low, F. J., Neugebauer, G., Walker, R. G., and Wesselius, P. R. 1984b, ApJ, 278, L23

Augereau, J. C., Nelson, R. P., Lagrange, A.M., Papaloizou, J. C. B., and Mouillet, D. 2001, A&A, 370, 447

Backman, D.E., Gillett, F. C., and Witteborn, F.C. 1992, ApJ, 385, 670

Crifo, F., Vidal-Madjar, A., Lallement, R., Ferlet, R., and Gerbaldi, M. 1997, A&A, 320, L29

Beckwith, S.V.W. 1999, in *The Origin of Stars and Planetary Systems*, eds C. J. Lada and N. D. Kylafis, Kluwer, Boston, 579

Blitz, L. and Willaims, J. P., 1999, in *The Origin of Stars and Planetary Systems*, eds C. J. Lada and N. D. Kylafis, Kluwer, Boston, 3

Burns, J. A., Lamy, P. L., and Soter, S. 1979, Icarus, 40, 1

Crifo,F., Vidal-Madjar,A., Lallement,R., Ferlet,R., and Gerbaldi,M., 1997, A&A, 320L, 29

Dermott, S. F., Gomes, R. S., Durda, D. D., Gustafson, B., Jayaraman, S., Xu, Y. L., Nicholson, P. D. 1992, in *Chaos, Resonance, and Collective Dynamical Phenomena in the Solar System: Proceedings of the 152nd Symposium of the International Astronomical Union held in Angra dos Reis, Brazil, 15-19 July, 1991.* Edited by Sylvio Ferraz-Mello, IAU Symposium, 152, 333

Dermott, S. F., Grogan, K., Holmes, E. K., and Wyatt, M. C. 1998, in Exozodiacal Dust Workshop Conference Proceedings, ed. D. E. Backman et al. (NASA CP-10155), 59

Dermott, S. F., Grogan, K., Durda, D., Jayaraman, S., Kehoe, T. J. J., Kortenkamp, S. J., Wyatt, M. C. 2001, in *Interplanetary Dust*, ed. E. Grun, B. Gustafson, S. Dermott, H. and Fechtig, Springer, New York, 569

Dermott, S. F., Malhorta, R., and Murray, C. D. 1988, Icarus, 76, 295

Dermott, S. F., Nicholson, P. D., Burns, J. A., and Houck, J. R. 1984, Nature, 312, 5994, 505

Dermott, S. F., Nicholson, P. D., Burns, J. A., and Houck, J. R. 1985, in *Properties and Interactions of Dust*, Reidel Publishing Company, Dordrecht

Dermott, S. F. and Nicholson, P. D., 1989, in *Highlights of Astronomy 8*, 259

Draine, B. T., and Lee, H. M., 1984, ApJ, 285, 89

Golimowski, D. A., Durrance, S. T., and Clampin, M. 1993, ApJ, 411, L41

Gustafson, B., 1994, Annu. Rev. Earth Planet. Sci., 22, 552

Gustafson, B., Greenberg, J., Kolokolova, L., Xu, Y., and Stognienko, R., 2001, in *Interplanetary Dust*, ed. Grun, E., Gustafson, B., Dermott, S., and Fechtig, H., Springer, New York, 509

Heap R. S., Lindler, D. J., Lanz, M. T., Cornett, R. H., Hubeny, I., Maran, S. P., and Woodgate, B. 2000, ApJ, 539, 435

Kalas, P. and Jewitt, D., 1995, AJ, 110, 794

Kalas, P., Larwood, J., Smith, B. A., and Schultz, A. 2000, ApJ, 530, L133

Karmann, C., Beust, H., and Klinger, J. 2001, A&A, 372, 616

Kenyon, S.J., 1999, in *The Origin of Stars and Planetary Systems*, eds C.J. Lada and N.D. Kylafis, Kluwer, Boston, 613

Knacke, R. F., Fajardo-Acosta, S.B., Telesco, C. M., Hackwell, J. A., Lynch, D. K., and Russell, R. W. 1993, ApJ, 418, 440

Krivova,N.A., Krivov,A.V., and Mann,I., 2000, ApJ, 539, 424

Krivov, A. V., Mann, I., Krivova, N. A. 2000, A&A, 326, 1127

Lagage, P. O. and Pantin, E. 1994, Nature, 369, 628

Lagrange, A. M., Plazy, F., Beust, H., Deleuil, M., Ferlet, R., Spyromilio, J., Vidal-Madjar, A., Tobin, W., Hearnshaw, J. B., Clark, M., and Thomas, K. W. 1996, A&A, 310, 547

Laor, A., and Draine, B. T., 1993, ApJ, 402, 441

Larwood, J. D. and Papaloizou, J.C.B. 2001, MNRAS, 285, 288

Larwood, J. D. and Kalas, P.G. 2001, MNRAS, 323, 402

Lecavalier des Estangs, A., Deleuil, M., Vidal-Madjar, A., Ferlet, R., Nitschelm, C., Nicolet, B., Lagrange-Henri, A. M. 1995, A&A, 299, 557L

Lecavalier des Estangs., A., 1993, ApJ, 109, 301

Li, A. and Greenberg, J., 1997, A&A, 323, 566

Li, A. and Greenberg, J., 1998, A&A, 331, 291

Liseau, R. and Artymowicz, P., 1997, in *Infrared Space Interferometry : Astrophysics and the Study of Earth-Like Planets.* Edited by C. Eiroa et al., Kluwer Academic, Dordrecht

Liseau, R., Brandeker, A., Fridlund, M., Olofsson, G., Takeuchi, T., Artymowicz, P. 2003, A&A, 402, 183L

Lissauer, J. J., 1993, Ann. Rev. Astron., 31, 129

Mouillet, D., Lagrange, A. M., Beuzit, J.L., and Renaud, N. 1997, A&A, 324, 1083

Mouillet, D., Larwood, J. D., Papaloizou, J. C. B., and Lagrange, A. M. 1997, MNRAS, 292, 896

Murray, C. D., Dermott, S. F. 1999, *Solar System Dynamics*, Cambridge University Press

Navasues, D. B., Stauffer, J. R., Song, I., and Caillault, J. P. 1987, ApJ, 520, L123

Nicholson, P. D. and Dermott, S. F., 1988, Bulletin of the Astronomical Society, 20, 862

Pantin, E., Lagae, P. O., and Artimowicz, P. 1997, A&A, 327, 1123

Panzera, M. R., Tagliaferri, G., Pasinetti, L., Antonello, E. 1999, A&A, 348, 161

Parsce, F. and Burrows, C. 1987, ApJ, 319, L23

Perryman M., 2000, Rep. on Progress in Phys., 63, 1209, *Updated August 2002*

Ruden, S. P., 1999, in *The Origin of Stars and Planetary Systems*, eds C. J. Lada and N. D. Kylafis, Kluwer, Boston, 643

Schneider, J., 2002, in *Extrasolar Planets Encyclopedia*, Observatoire de Paris, http://www.obspm.fr/planets

Shu, F. H., Adams, F. C., and Lizano, S., 1987, ARA&A, 25, 23

Shu, F. H., Allen, A., Shang, H., Ostriker, E. C., and Li, Z., 1999, in *The origins of Stars and Planetary Systems*, eds Lada, C.J. and Kylafis, N.D., NATO Science Series, C, 193

Smith, B. A. and Terrile, R. J. 1984, Science, 226, 1421

Telesco, C. M. and Knacke, R. F.1991, ApJ, 372, L29

Telesco, C., Becklin, E., Wolstencroft, R. D., and Drecher, R. 1988, Nature, 335, 51

Telesco, C., Fisher, R., Pina, R., Knacke, R., Dermott, S., Wyatt M., Grogan, K., Holmes, E., Chez, A., Prato, L., Hartmann, L., and Jayawardhana, R. 2000, ApJ, 530, 329

Telesco, C., Marinas, N., Fisher, R., Novotny, S., Dermott, S., Radomski, J., and Hayward, T., 2003, *in preperation*

Thebault, P., Augereau, J., and Beust, H. 2003, A&A, 408, 775

Wahhaj, Z., Koerner, D., Ressler, M., Werner, M., Backman, D., and Sargent, A., 2003, ApJ, 584L, 27

Weinberger, A., Becklin, E., and Zuckerman, B. 2003 ApJ, 584L, 33

Wyatt M. C., Dermott, S. F., Telesco, C. M., Fisher, R. S., Grogan, K., Holmes, E. K., and Pina, R. K. 1999, ApJ, 527, 918

Xu, Y. L., Dermott, S., Gustafson, B., Liou, J., 1993, LPICo, 810, 317

Yulsman, T., 2003, *Origins: The Quest for our Cosmic Roots*, Bristol, IOP Publishing

I certify that I have read this study and that in my opinion it conforms to acceptable standards of scholarly presentation and is fully adequate, in scope and quality, as a dissertation for the degree of Doctor of Philosophy.

Stanley F. Dermott, Chair
Professor of Astronomy

I certify that I have read this study and that in my opinion it conforms to acceptable standards of scholarly presentation and is fully adequate, in scope and quality, as a dissertation for the degree of Doctor of Philosophy.

Charles Telesco
Professor of Astronomy

I certify that I have read this study and that in my opinion it conforms to acceptable standards of scholarly presentation and is fully adequate, in scope and quality, as a dissertation for the degree of Doctor of Philosophy.

Bo Gustafson
Professor of Astronomy

I certify that I have read this study and that in my opinion it conforms to acceptable standards of scholarly presentation and is fully adequate, in scope and quality, as a dissertation for the degree of Doctor of Philosophy.

James Dufty
Professor of Physics

I certify that I have read this study and that in my opinion it conforms to acceptable standards of scholarly presentation and is fully adequate, in scope and quality, as a dissertation for the degree of Doctor of Philosophy.

Ludmilla Kolokolova
Associate Scientist of Astronomy